

Lawrence Berkeley National Laboratory

Recent Work

Title

ON THE ANNEALING OF STACKENG-FAULT TETRAHEDRA AND FRANK DISLOCATION LOOPS
IN SILVER

Permalink

<https://escholarship.org/uc/item/2zh4j3gk>

Author

Astrup, Thorvald

Publication Date

1974-05-01

RECEIVED
LAWRENCE
RADIATION LABORATORY

LBL-1172
c.)

JUN 26 1974

LIBRARY AND
DOCUMENTS SECTION

ON THE ANNEALING OF STACKING-FAULT TETRAHEDRA
AND FRANK DISLOCATION LOOPS IN SILVER

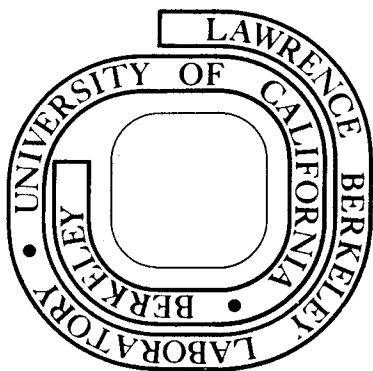
Thorvald Astrup
(Ph.D. thesis)

May 1974

Prepared for the U. S. Atomic Energy Commission
under Contract W-7405-ENG-48

For Reference

Not to be taken from this room



LBL-1172
c.)

DISCLAIMER

This document was prepared as an account of work sponsored by the United States Government. While this document is believed to contain correct information, neither the United States Government nor any agency thereof, nor the Regents of the University of California, nor any of their employees, makes any warranty, express or implied, or assumes any legal responsibility for the accuracy, completeness, or usefulness of any information, apparatus, product, or process disclosed, or represents that its use would not infringe privately owned rights. Reference herein to any specific commercial product, process, or service by its trade name, trademark, manufacturer, or otherwise, does not necessarily constitute or imply its endorsement, recommendation, or favoring by the United States Government or any agency thereof, or the Regents of the University of California. The views and opinions of authors expressed herein do not necessarily state or reflect those of the United States Government or any agency thereof or the Regents of the University of California.

ON THE ANNEALING OF STACKING-FAULT TETRAHEDRA AND FRANK DISLOCATION
LOOPS IN SILVER

Thorvald Astrup

Inorganic Materials Research Division, Lawrence Berkeley Laboratory and
Department of Materials Science and Engineering, College of Engineering;
University of California, Berkeley, California

ABSTRACT

Direct observation of quenched-in stacking-fault tetrahedra (SFT) and Frank dislocation loops in 99.999% silver during annealing were made by hot stage transmission electron microscopy.

The defects produced by quenching from a few degrees below the melting point, had a range of edge sizes L up to 2000\AA for the SFT, and from 650\AA to 1350\AA for the triangular loops. The smaller SFT, $L < 600\text{\AA}$, were found either to shrink or to completely anneal out above 600°C . One large SFT, $L \approx 2000\text{\AA}$, was directly observed to collapse into a loop at 300°C . Shrinkage of loops taking place from one corner were detected.

Existing theories concerning collapse and/or shrinkage of SFT and loops are reviewed and discussed in detail. Calculations show that the quenched-in defects are in the expected size-range. It is shown that the ledge-mechanisms can be the mechanisms responsible for thermally activated shrinkage of SFT. It is further shown that the nucleation energy of a Shockley loop near a SFT-corner is considerably less than that for the loop in the middle of the SFT-face, thus allowing for collapse. The influence of the anisotropy and the temperature on the stacking-fault energy is also discussed, as well as the limitations in the energy calculations due to configurations of core dimensions.

The modified nucleation theory proposed by Escaig is found not to be correct.

PREFACE

The experimental work for this thesis was done in the period from April 1969 to June 1972, after a brief encounter with defects in gold during my first year in Berkeley in 1968 and 1969. Both materials are great for making jewelery, but more of a frustrating experience when it comes to making foils for transmission electron microscopy. Most of the experiments have been done utilizing the Hitachi 650 kV electron microscope in Berkeley. Some initial experiments were done with the Hitachi 125 kV EM, and a few experiments have been run in the Philips 300 EM (100 kV) at the University of Oslo, Norway.

Some few comments regarding the composition of this thesis: A broad theoretical review is given, both as a background for the experiments, and in view of the following extensive discussions of the existing theories. To keep the main body of the thesis as short as possible, a wide use of appendices has been preferred. As a detailed coverage of extended dislocations and jogs in connection with stacking-fault tetrahedra (SFT) and Frank loops and their annihilation could not be found, the detailed models are deduced from Hirth and Lothe (1968) and Appendix 1. In Appendix 2, calculations of the energies of the SFT, loops, and intermediate configurations have been done for the case of silver. To differentiate between the different defects, SFT, extended and unextended loops by use of transmission electron microscopy, a method is described in Appendix 3. Escaig's (1960 a,b) modified nucleation theory is critically examined in Appendix 4. Finally, equations for the calculation of energies for SFT collapse mechanisms are deduced in Appendix 5.

In this thesis, there might seem to be an inconsistency in the use of symbols for energies, but this is only due to consistently citing references without changing given symbols. This is especially evident in the use of U and E , which apparently should be defined as internal and free energy respectively in the cited cases, and W which is the elastic strain-energy. Gibb's free energy is taken as G .

ON THE ANNEALING OF STACKING-FAULT TETRAHEDRA AND FRANK DISLOCATION
LOOPS IN SILVER

Contents

Abstract	iii
Preface	v
I. Introduction	1
II. Theoretical Review	4
A. Dislocation Climb	4
B. Energy of Truncated Stacking-Fault Tetrahedra	6
C. Formation and Growth of FT's and SFT	11
D. Shrinkage and Annihilation of SFT and FT's	12
Summary	22
III. Experimental	23
A. Specimen Preparation	23
B. Thin Foil Preparation	23
C. Transmission Electron Microscopy Technique	24
IV. Observations	25
A. Quenched-In Defects	25
B. Annealing	32
Summary	45
V. Discussion	46
Summary	67
VI. Conclusions	68
Acknowledgements	70

Appendix 1. Extended Dislocations and Jogs	71
Appendix 2. Energies of Faulted Defects in Ag	94
Appendix 3. Contrast from Faulted Defects	105
Appendix 4. Disproof of Escaig's Modified Nucleation Theory . .	109
Appendix 5. Energies for SFT Collapse Mechanisms	121
References	126

"A triangle is the only structurally stable polygon. A tetrahedron the minimum omnitriangulated, omnistructural system. A tetrahedron is the most fundamental of all structures. It is a basic system because it stably and symmetrically subdivides the universe into two parts; all of the universe inside and all of the universe outside its system."

R. Buckminster Fuller
Utopia or Oblivion

I. INTRODUCTION

Due to vacancy condensation, quenching of a low stacking-fault energy fcc metal (and alloy) leads to the formation of faulted, extended Frank sessile loops and stacking-fault tetrahedra (SFT). SFT were first observed in quenched gold by Silcox and Hirsch (1959) through the use of transmission electron microscopy (TEM). Since then considerable effort has been spent investigating the behavior of these faulted defects, both experimentally and theoretically. Smallman et al. (1959) observed SFT in deformed silver. In quenched silver they were first detected by Clarebrough et al. (1966).

During anneal at elevated temperatures, conditions can favor disappearance of SFT. Collapse and/or shrinkage of SFT, and shrinkage of loops (extended Frank loops) in gold during anneal have been observed by: G. Brun (1966), Yokota and Washburn (1967), Yokota (1968), Washburn and Yokota (1969), Johnston et al. (1971), and Fraser et al. (1971). With the exception of Brun's hot stage TEM work, they all used TEM observing specimens annealed outside the microscope. Indirect observations by use of resistivity measurements have been done by Meshii and Kauffman (1959), and de Jong and Koehler (1963) among others.

In silver, only loops have been seen to anneal out, above 600°C, using TEM on outside annealed specimens (Clarebrough et al. 1966, Smallman et al. 1968).

Generally, high temperature anneals are required for the faulted defects in Au and Ag to anneal out. Jössang and Hirth (1966) and Humble et al. (1967) did theoretical calculations of the energies of the loops, SFT, and the intermediate configurations involving a glide mechanism. These calculations led to the determination of the stacking fault energies of Au and Ag, (and Cu), based on the sizes of loops and SFT deformation. Their calculations also yielded a too high energy barrier for the mechanism to work during anneal. A glide-mechanism proposed by Meshii and Kauffman (1960) also gives a too high energy barrier. The non-conservation mechanism for which Escaig (1970b) calculated the energy explains the observations by Yokota (1968) in Au, but cannot explain the loop shrinkage in Ag. Energetically the nonconservative mechanism proposed by Kuhlmann-Wilsdorf (1965) allows shrinkage of SFT in Au, observed by Brun (1966). Finally Escaig (1970 a,b) introduces a modified nucleation theory explaining the collapse and shrinkage of SFT and loops in silver during annealing.

Escaig's suggestions nucleated the present work: investigating the annealing behavior of SFT in silver to verify eventual collapse and/or shrinkage of SFT in Ag.

Due to the very low stacking fault energy of silver, the lowest known for a pure fcc metal at room temperature, a study of the annealing behavior of an extended loop could yield valuable insight into the mechanisms of extended jog-formation and -motion. The mechanisms are

important in dealing with climb, and with interactions of dissociated dislocations which determines the strength of the low stacking fault energy metals and alloys, and concern part of the dislocation theory not yet verified.

II. THEORETICAL REVIEW

A. Dislocation Climb

A dislocation can move by glide, a conservative motion, or by climb, a nonconservative motion. The nonconservative motion involves the diffusion of point defects to and from the dislocation. The concept of glide is fairly simple, while the concept of climb needs a more detailed coverage.

Generally a dislocation climbs by jog-motion, the jog moving along the dislocation line with v_j perpendicular to the motion of the dislocation, \bar{v} (Fig. II-1). At A a double jog is nucleated by the creation of a

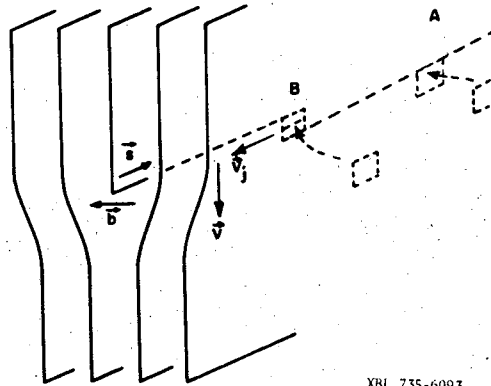
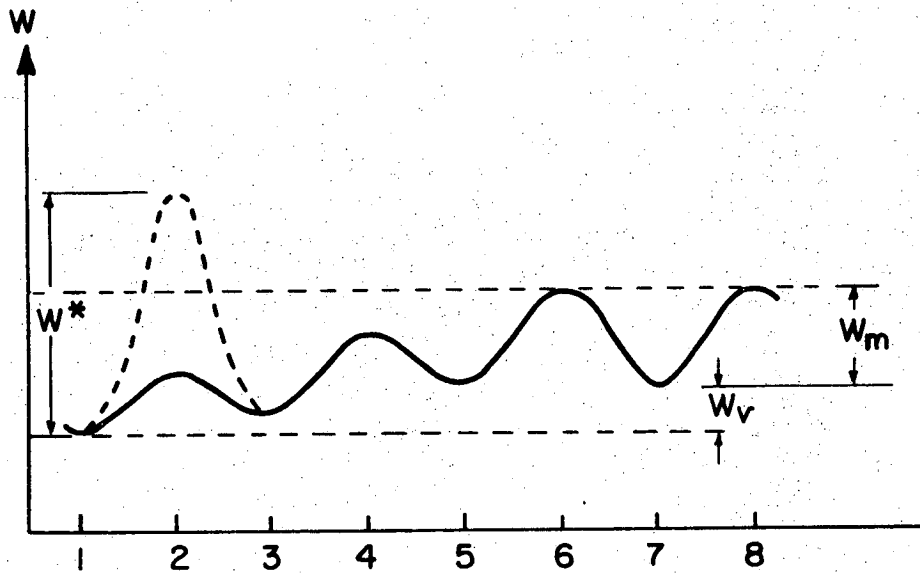


Fig. II-1. Schematic cut through a crystal lattice with an edge-dislocation \vec{b} with sense s , climbing \bar{v} .

core interstitial by motion of a vacancy from A (Hirth and Lothe, 1968). At B the jog would move with \bar{v}_j by emitting a vacancy with no apparent change in the energy of the dislocation. The creation of a vacancy at a jog and its motion into the bulk-lattice entails a series of energy jumps such as those in Fig. II-2 (Hirth and Lothe, 1968, p. 528).



XBL 735-6105

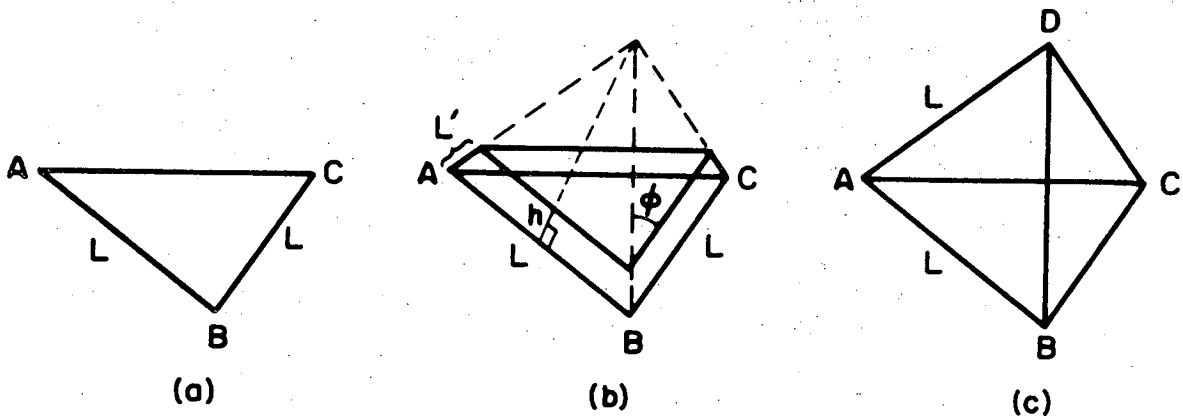
Fig. II-2. Energy-displacement curve for a vacancy at a jog site (1) and in successive positions removed from the jog into the bulk lattice. The dashed line W^* represents a case involving an energy barrier, W^* , for creation of a vacancy at a jog. W_v and W_m are the formation energy and energy of motion for a vacancy, respectively. In the case shown in Fig. II-2, vacancies at 3 are in quasi-equilibrium with the jog and the vacancy at 5 in quasi-equilibrium with the vacancy at 3. We then have a diffusion-controlled process as opposed to the barrier-controlled process shown by the dashed line.

In the case of metals with low stacking-fault energies, the dislocations will be extended with jogs extended into jog-lines (Appendix 1). The creation of a vacancy here could very well involve an energy-barrier W^* due to dislocation reactions and changes in the area of the fault. The energy barrier would appear in the initial stage of combining the vacancy with the partial dislocation.

Extended dislocations and jogs are described in Appendix 1.

B. Energy of Truncated Stacking-Fault Tetrahedra

The geometry and composition of the Stacking Fault Tetrahedra (SFT) and the Frank Triangular loop (FT), are described in detail in Appendix 1. Between these two complete configurations we can have a number of intermediate configurations. The truncated SFT shown in Fig. II-3b represents one such intermediate phase.



XBL 735-6109

Fig. II-3. (a) A Frank Triangular loop.
(b) A dissociated Frank loop or a truncated SFT.
(c) SFT.

Jössang and Hirth (1966) have calculated the total energies of intermediate truncated SFT in the case of gold; their energy formulas are given in Appendix 2 (A2-2 to A2-4). The energies are calculated as functions of $x = L' / L$ as a measure of the degree of truncation for different values of L and the results are schematically shown in Fig. II-4. The curve for $L = 5800\text{Å}$ have later been corrected as calculations show an energy barrier for all L (Clarebrough et al., 1967 and Jössang, 1968). This energy diagram gives the stability ranges for a complete or near-complete SFT vs a dissociated Frank triangle in terms of size L . For $L < L_c$ we would have the SFT as the only stable form. For $L_c < L < L_E$, the SFT is stable with respect to the dissociated FT, but, due to the energy barrier between these two configurations, the dissociated FT is metastable. At $L = L_E$ the energies are equal and for $L > L_E$ the SFT is the metastable configuration, while the dissociated Frank triangle is the stable form. There is always an activation barrier between the SFT and the dissociated FT.

Jössang and Hirth (1966) used $\phi = 60^\circ$ (Fig. II-3). Humble (1966) used an extra parameter in describing the corner configuration without altering the results much. Escaig (1970 b) recalculated the energies using a ϕ varying from 120° for an almost complete SFT to 60° for a dissociated FT. He thus reports an activation barrier between SFT and FT lowered by 15-20% in gold. The activation energies in silver would be considerably higher in any case (see Appendix 2).

So far, the energies of the truncated SFT have been calculated with three Shockley partial dislocations gliding from one corner.

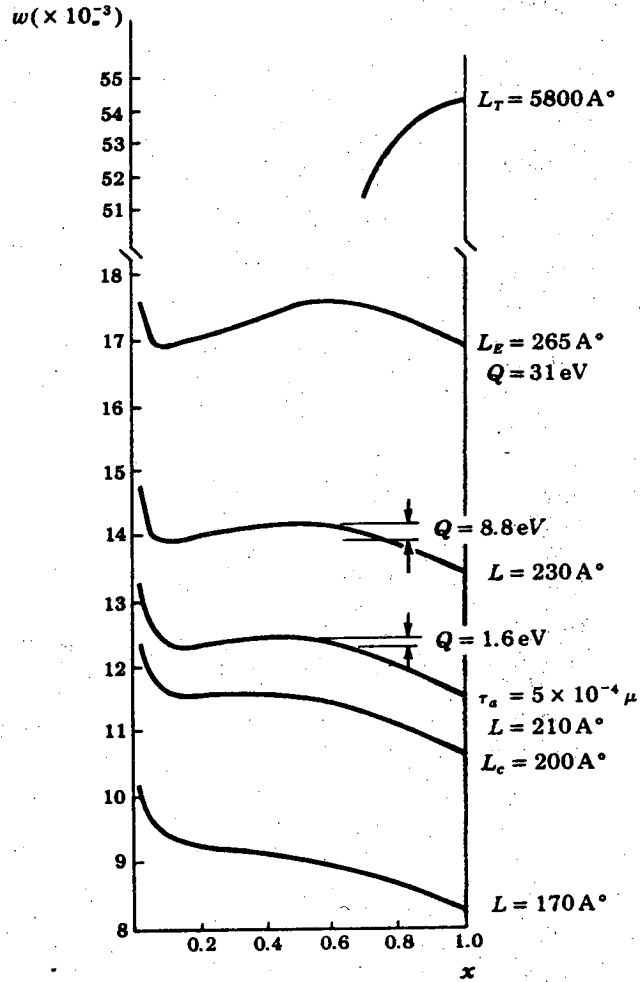
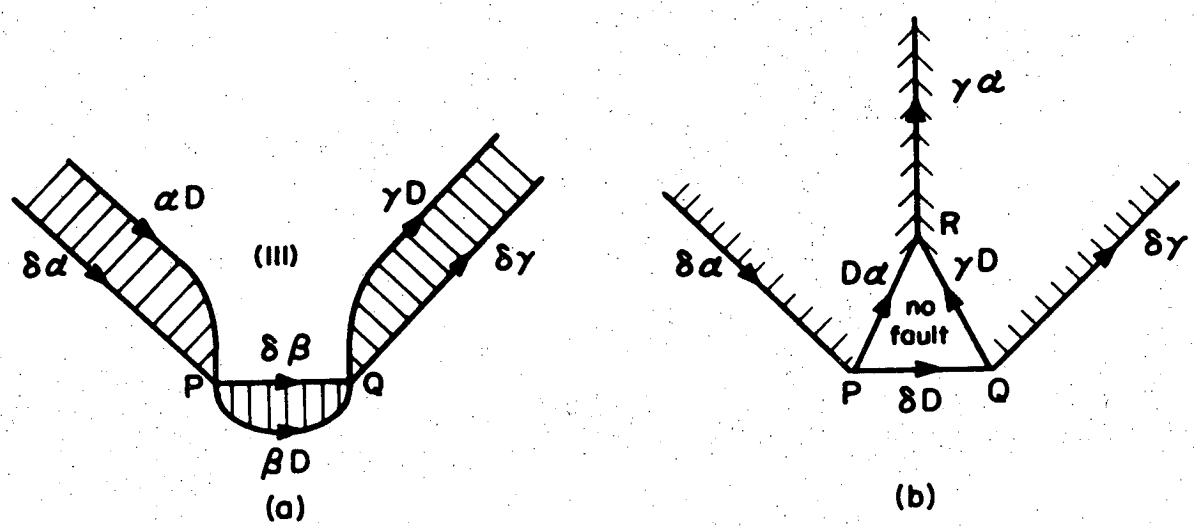


Fig. II-4. The reduced energy w vs x for various sizes of tetrahedra. For curves with maxima and minima, $Q = W_{\max} - W_{\min}$ is shown, together with the minimum resolved shear stress τ_a required to force the Shockley partials over the energy barrier. Note scale change at top. (Hirth, Lothe, 1968).

Escaig (1970) has shown that the energy of the SFT or the dissociated Frank triangle is lowered if the corners are blunted by removing a few vacancies from each corner (Fig. II-5).

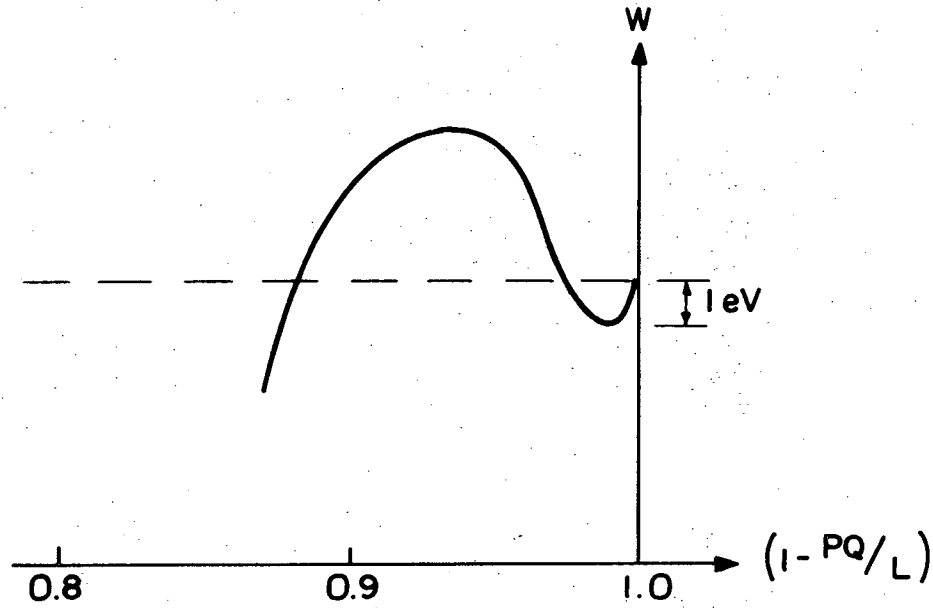
The blunting of one corner lowers the energy by about 1 eV in both cases (see Fig. II-6), and it represents a nonconservative process in that some vacancies must be removed to blunt the corner while the truncated corner mentioned earlier represents a conservative process with three glissile dislocations (δD or $\beta D + \delta \beta$ are sessile Frank dislocations).

For the case of gold or metals with higher stacking-fault energy γ , the energy would decrease with increasing PQ without any activation barrier as in Fig. II-6. For a low γ as in the case with silver, PQ must reach a critical length PQ in order to grow further on. Escaig (1970)



XBL 735-6108

Fig. II-5. (a) A blunted corner (120° corner) on a Frank triangle. (b) A blunted corner on a SFT. The arrows represent the senses of the dislocations. Burgers vectors given in the Thompson notation.



XBL 735-6099

Fig. II-6. The energy of a SFT or FT during growth of one 120° corner shown schematically for Ag.

has calculated the activation energy needed to reach PQ^* to be about 23 eV for silver.

C. Formation and Growth of FT's and SFT

The dislocation reactions generally involved in the formation and growth, and in the shrinkage and annihilation of Frank triangles and stacking fault tetrahedra are quite extensively covered in Appendix 1; they will not be gone into detail here.

SFT can be created by dislocation glide (Hirsch 1962, 1963, Loretto et al., 1965). Frank triangles form directly by the cross-slip of extended dislocations at superjogs. By this mechanism one should be able to get SFT of a maximum size and FT of a minimum size according to the energy diagram, Fig. II-4.

The two other most commonly recognized processes are both caused by vacancy migration and clustering. The supersaturation of vacancies needed are created by quenching and we get quenched-in FT's and SFT.

They can be formed by direct vacancy-clustering (de Jong and Koehler, 1963; Kimura et al., 1963; Cotterill and Doyama, 1964; Kuhlmann-Wilsdorf et al., 1964; Kuhlmann-Wilsdorf, 1965). Thereby a tetra-vacancy acts as a nucleus which grows into a SFT by the adsorption of vacancies at joglines on the tetrahedron face.

The other mechanism is by vacancy clustering and dislocation glide (Silcox and Hirsch, 1959). Vacancy discs nucleate and collapse to form dislocation loops of Frank partials ($\bar{b} = \frac{a}{3} \langle 111 \rangle$) bounding an intrinsic stacking fault on a $\{111\}$ -plane. In fcc metals with a low stacking fault energy, these loops will lower their energy by dissociation

into an extended (dissociated) Frank triangle (Fig. II-3b) or polygons, with edges in the $\langle 110 \rangle$ directions as a sign of the dissociation on $\{111\}$ -faces. The SFT can then be formed by glide of the Shockley partials (Appendix 1) if this is energetically favorable (Fig. II-4). Further growth of the SFT can take place by absorption of vacancies at joglines. Kuhlmann-Wilsdorf (1965) discusses the growth and shrinkage of SFT by the migration of joglines. See also Hirth and Lothe (1968, p. 581). This mechanism is covered in the next paragraph and also in Appendix 1.

D. Shrinkage and Annihilation of SFT and FT's

Generally we would say that the same mechanisms that operate during SFT-growth should operate during shrinkage too. However, the choice of mechanism depends very much on the conditions; i.e., mechanical stress, high or low supersaturation of point defects (quench or anneal) and so on.

We have already seen that above a certain size L_E , the FT is more stable than the SFT. Below the size L_C , the SFT is the only stable configuration. For SFT in a size range where the FT is the more stable form we could expect the SFT to collapse into a FT and then shrink.

If the collapse into a FT is not preferable, the SFT can shrink as such, by migration of joglines (Kuhlmann-Wilsdorf, 1965) or by climb from blunted corners (Escaig, 1970).

In Table II-1 a,b, the different mechanisms for collapse and/or shrinkage of SFT and FT's are described schematically. We see that

Table II-1a. Different mechanisms for collapse and/or shrinkage of SFT and Frank Triangles (loops)(FT). Reference in Table II-1b.

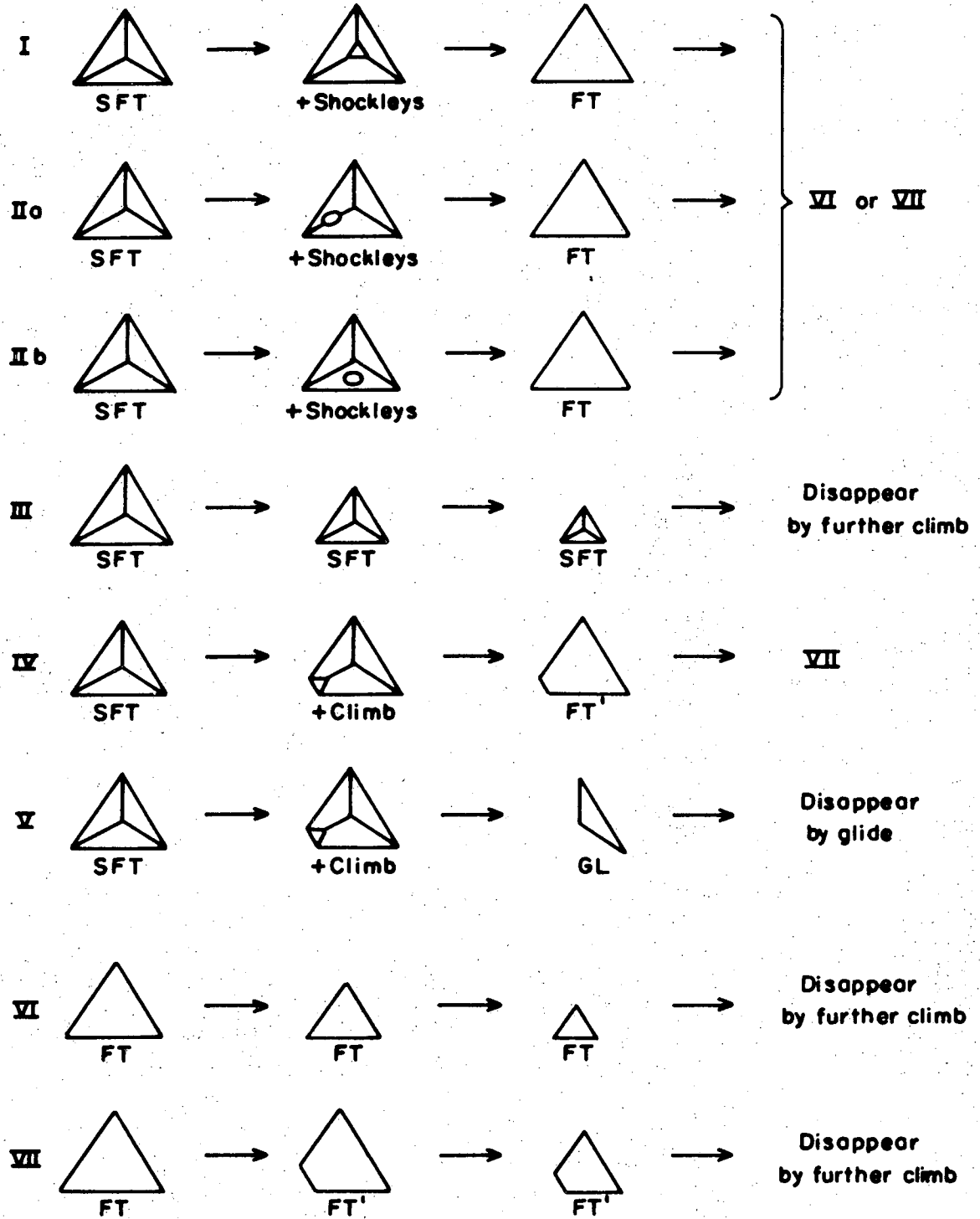


Table II-1b. Description of the different mechanisms for collapse and/or shrinkage of SFT and Frank Triangles (FT) which are shown in Table II-1a. Values of the activation energies are also given. * denotes the use of the "modified nucleation theory" (Escaig 1970).

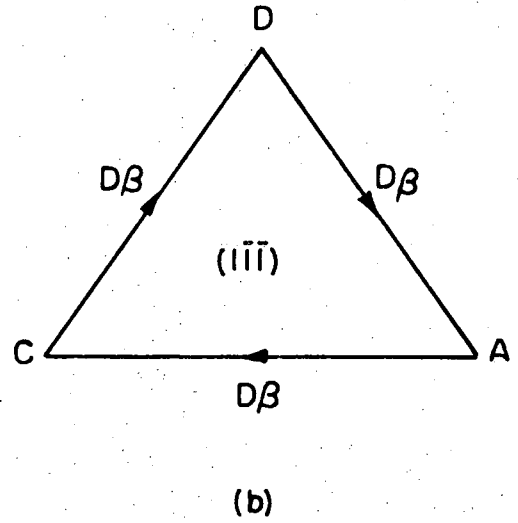
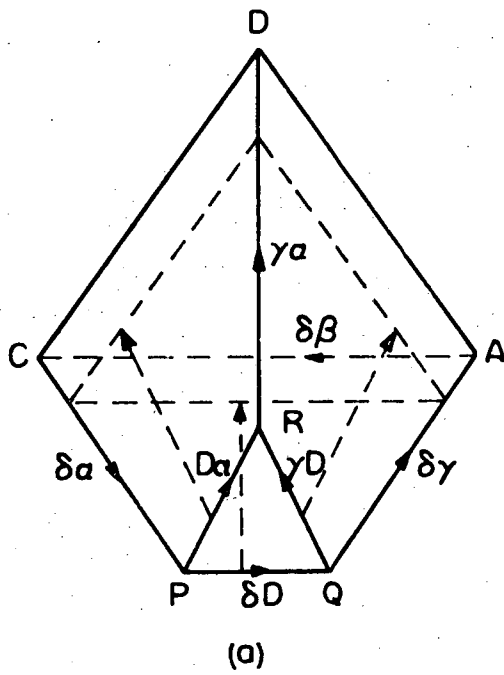
MECHANISM			ACTIVATION ENERGY
I	Conserv. collapse	Glide of 3 Shockleys from one corner of the SFT to form a FT. (Kuhlman-W.65)	170eV Ag 30eV Au (Jøssang & Hirth, 1966) 15eV Au (Escaig 1970) 70eV Ag (Escaig 1970)
IIa	Conserv. collapse	Glide of 2 Shockleys from one edge of the SFT to form a FT.	
IIb	Conserv. collapse	Glide of a Shockley loop from one face of the SFT to form a FT. (Meshii & Kauffman 1960)	6.6eV Au theor. (M & K. 1960) 4.7eV Au exp. (— " —)
III	Non-conserv. shrinkage	Climb by jog-lines. (The ledge mechanism.) The SFT shrink as a SFT. (Jong & Koehler 1963)	15eV Au (Yokota 1968)
IV	Non-conserv. collapse	Climb to make a critical 120' corner on the SFT, then glide to form a FT. (Escaig 1970)	2.8eV Au (Escaig 1970) 25 eV Ag (— " —) 2.7eV Ag (— " —)*
V	Non-conserv. collapse	Climb to make a critical 120' corner on the SFT and then a glideloop that disappears. (Escaig 1970)	———— " —————
VI	Non-conserv. shrinkage	Shrinkage by climb along the edges of the FT.	U_d (act. energy of selfdiff.)
VII	Non-conserv. shrinkage	Climb to make a critical 120' corner and further shrinkage by climb. (escaig 1970)	U_d Au (Escaig 1970) 5-6eV Ag (— " —) 2.7eV Ag (— " —)*

collapse can be conservative or non-conservative, while shrinkage must involve climb.

Mechanism I represents the case for which Jössang and Hirth (1966) calculated the energies of the intermediate truncated SFT (Fig. II-3 and Fig. II-4). Instead of nucleating Shockleys at a corner, Shockleys can be nucleated at an edge or in the form of a Shockley loop on one face (Meshii and Kauffman, 1960). They calculated the nucleation energy for a loop to be 6.6 eV in gold. The activation energy for nucleation at an edge should be slightly smaller (Yokota, 1968). The result of the collapse in all these cases are Frank triangles (extended). The total energies of the intermediate forms between SFT and FT for mechanisms IIa and IIb have not been calculated.

A mechanism for non-conservative collapse has been introduced by Escaig (1970) involving climb of the Frank segment of the blunted corner (Fig. II-5b) with an activation energy (Fig. II-6) to reach a critical length (PQ)*. Depending on the size L, i.e., where in the stability range L is, mechanism IV or V operates. In the first case we get collapse to a blunted (PQ)* dissociated Frank triangle (Fig. II-5a) by glide of the Shockleys PR and QR after (PQ)* is reached. Mechanism V leads to collapse into a glide loop that annihilates by further climb of the Frank segment PQ after (PQ)* is reached (Fig. II-7). The operation of these mechanisms is supported by the observations by Yokota (1968) in gold.

The SFT can shrink as a SFT (mechanism III) by vacancy emission at joglines (Kuhlmann-Wilsdorf, 1965), the mechanism of climb of extended



XBL736-6251

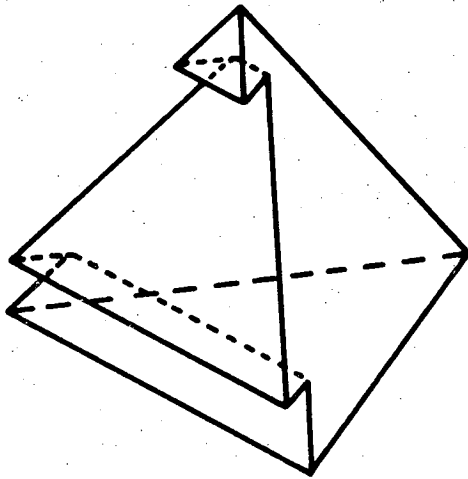
Fig. II-7. (a) Collapse by climb of PQ to combine with CA and glide rearrangement $PR + CD$ and $QR + AD$ to make a glide loop.
(b) $b = D\beta$ in the $(\bar{1}\bar{1}\bar{1})$ plane.

dislocations (Appendix 1). There are two main types of joglines or ledges (Fig. II-8), namely acute superjogs or joglines (Hirth and Lothe, 1968) and obtuse superjogs or joglines. Kuhlmann-Wilsdorf (1965) names the acute jogline V-ledge, resembling a row of 1/3 vacancies and the obtuse joglines I-ledge, resembling a row of 1/3 interstitials. As seen in Appendix 1, this is a special case. Nucleation and migration of an acute jogline from an edge, or of an obtuse jogline from a corner is necessary in order to get shrinkage. Conversely, growth will occur by the formation and traversing from an acute jogline from a corner or an obtuse jogline from an edge. The I-ledge (obtuse) is believed to have 2.5 times the energy of a V-ledge (acute) pr atomic plane; $U_{L*}^I \sim 2.5 \cdot U_{L*}^V$ (Kuhlmann-Wilsdorf, 1965). Thus she argues that the SFT can shrink by V-ledges nucleated at edges during anneal in gold with $U_{L*}^V \sim 0.05$ eV, while Yokota finds an activation energy of about 15 eV for gold.

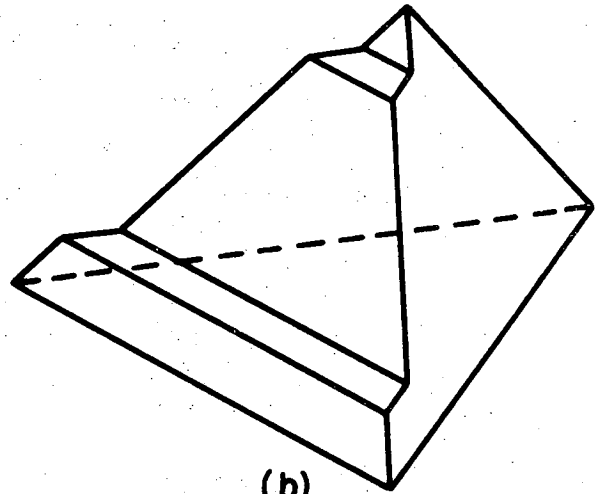
Hirth and Lothe (1968, p. 582) have proposed another type of jogline nucleated at a corner, being a partial acute jogline at a corner (Fig. II-9). This might represent a critical nucleation configuration of less energy than for nucleation of a ledge along an edge.

Extended or dissociated Frank loops can climb by a jogline mechanism (Appendix 1) where the loop is locally shifted (in planes).

An undissociated loop will quite easily shrink (or expand) by the emission (absorption) of vacancies at jogs. Due to the dissociation of the Frank dislocation along the edges, this jog mechanism is more difficult to operate. It is believed that a constriction must be formed in order to create a jog. Such constrictions will naturally



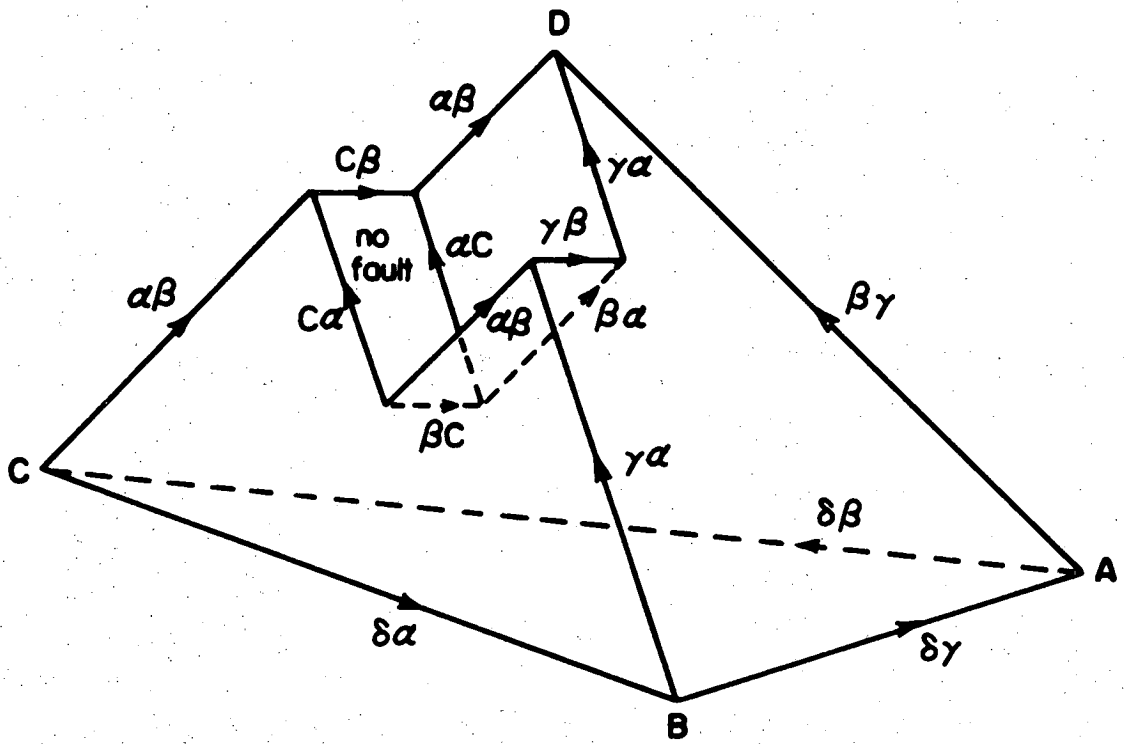
(a)



(b)

XBL 735-6100

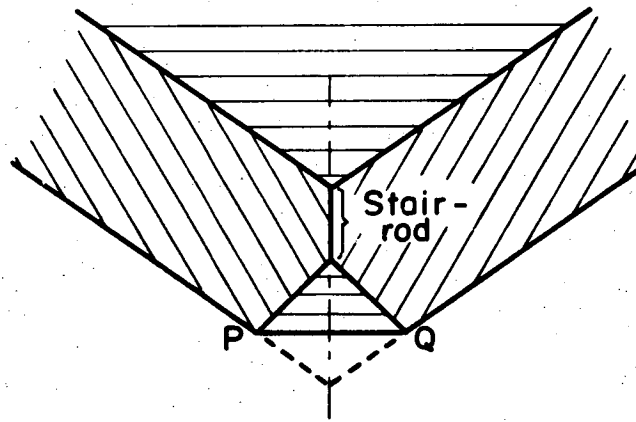
Fig. II-8. Joglines or ledges on one face of a SFT.
(a) Acute joglines.
(b) Obtuse joglines.



XBL 735-6101

Fig. II-9. Nucleation of a partial acute jogline at corner D. Motion towards C is glide. Motion toward B is climb.

exist at so-called 120° corners (Escaig, 1970; Yokota, 1968) or blunted corners (Fig. II-5). Escaig (1970) has shown that this is a stable configuration. The size of these corners, however, are very small, just a few vacancies emitted, so for the climb to proceed, an "unzipping" of the stable corner configuration with the stairrod is necessary (Fig. II-10).



XBL 735-6102

Fig. II-10. Detail of 120° corner of a Frank loop (extended).

Escaig (1970) calculates an activation energy in silver needed to reach a critical length PQ^* , finding about 5-6 eV for the FT against 23 eV for the SFT. His calculations for Au and Cu yield no activation barrier.

Eventually, Escaig (1970 a,b) proposed a modified nucleation theory with the result of lowering the activation barriers for SFT collapse and FT shrinkage to $U_D + 0.8$ eV for both. Escaig's theory is covered in Appendix 4.

SUMMARY

In this chapter we have mainly dealt with the thermally activated mechanisms for creation and annihilation of SFT and loops. For creation the most widely accepted mechanisms are by vacancy-condensation, forming a Frank loop which might extend into a SFT. SFT formed this way can grow by ledges into the metastable size range. SFT can also form by direct nucleation, and grow as SFT by the ledge mechanism.

Loops and SFT can also form by mechanical processes (Loretto et al., 1965), involving dislocation interactions during stress. This creates faults within their respective stable size ranges. The faults can also annihilate by applying an external stress (Yokota, 1968).

The thermally activated mechanisms for annihilation, in which we are mainly interested, are less established and the possibilities are listed in Table II-1. The least probable mechanism seems to be the unfolding of the SFT, the reverse of the extension of the loop into a SFT.

III. EXPERIMENTAL

A. Specimen Preparation

The Ag-specimens suitable for quenching were prepared from 6 mil (150 μ) thick sheets of high purity silver 99.999% + (5N+) received from the Braun Metallurgical Chemical Co., Philadelphia. The specimens were cleaned and preliminarily thinned down to 4 mil by using a chemical etchant consisting of 50% NH₄OH and 50% H₂O₂ (30%).

Due to the oxidation behavior of silver (Ag oxidizes easily below 300-400°C and reduces above this range), the heat treatment must be done in an oxygen-free atmosphere. Heat treatments in vacuum and occasionally in argon led to formation of blisters in the silver foils. The best heating environment has been found to be high purity helium atmosphere.

The specimens were quenched from high temperatures in the range 900°C to 960°C, 960.8°C being the melting point of silver, by dropping them into a container of silicone oil at 20°C.

B. Thin Foil Preparation

Two methods for making thin foil samples suitable for observations in the transmission electron-microscope have been used.

At an early stage of the experiments, the window electropolishing technique (Nicholson et al., 1958) was applied. We did not succeed in getting good foils by previously reported electrolytes, but had to modify the polishing solution of 9% KCN in H₂O at 8 V and 1.8 A/cm², <20°C used by Smallman et al. (1960). This electrolyte worked too fast and we found that 2% KCN in H₂O at 10°C with 2.5 V and 0.25 A/cm² gave satisfactory results. The solution must be freshly mixed and slowly stirred during polishing down to 1 μ .

Using the jet electropolishing technique (Hirsch et al., 1965) has several advantages; the specimen containing the thin area is disc shaped to fit in the E.M. holder without using grids. The disc also tends to be more rigid and easier to handle. Finally, more thin foil specimens can be cut from one quenched sheet than is the case with the window technique. We found that an electrolyte consisting of 30% HNO_3 in 70% methanol was suitable for use with the jet polisher. The temperature is kept at room temperature (or a little higher), the voltage at about 3 V and the current density at about 0.4 A/cm^2 . It is important that the electrolyte be freshly mixed.

C. Transmission Electron Microscopy Technique

The thinned down silver foils were examined in a high voltage 650 kV Hitachi Transmission Electron Microscope with the use of a hot stage specimen holder. The temperature was controlled indirectly by fixing the power input to the furnace-type heater of the hot stage specimen holder. Calibration of the hot stage was performed several times.

Due to the oxidation and reduction properties of silver and its sensitivity to contamination, the HVEM was preferred due to a much better vacuum in this microscope than in the 100 kV-125 kV instruments.

Preliminary experiments utilizing the Siemens IA, Hitachi 125 and the Philips 300 EM showed that the contamination problems were very serious with these instruments and the specimens were virtually destroyed by heating already around 300°C .

Kodak Electron Image Plates were used for the recording of the images.

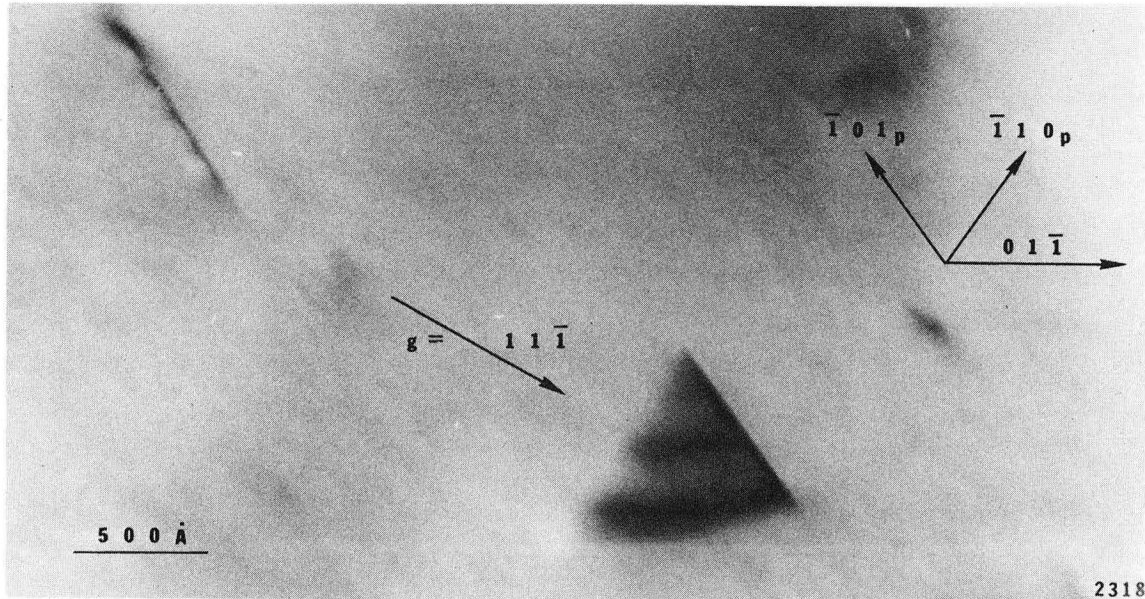
IV. OBSERVATIONS

A. Quenched-In Defects

Figure IV-1 is a micrograph of a SFT, $L \approx 920\text{\AA}$, in silver quenched from 960°C . Due to the preferred orientation in our foils, namely the $\{110\}$ -orientations, the geometrical projections of the Frank-triangles and the SFT can be the same. Thus we had to find a way of differentiating between the two types of defects (see Appendix 3). The foil in Fig. IV-1 is a little off the (110) -orientation and the wedge shaped contrast along BC is the projection of the face nearly normal to the foil surface, and is typical of SFT.

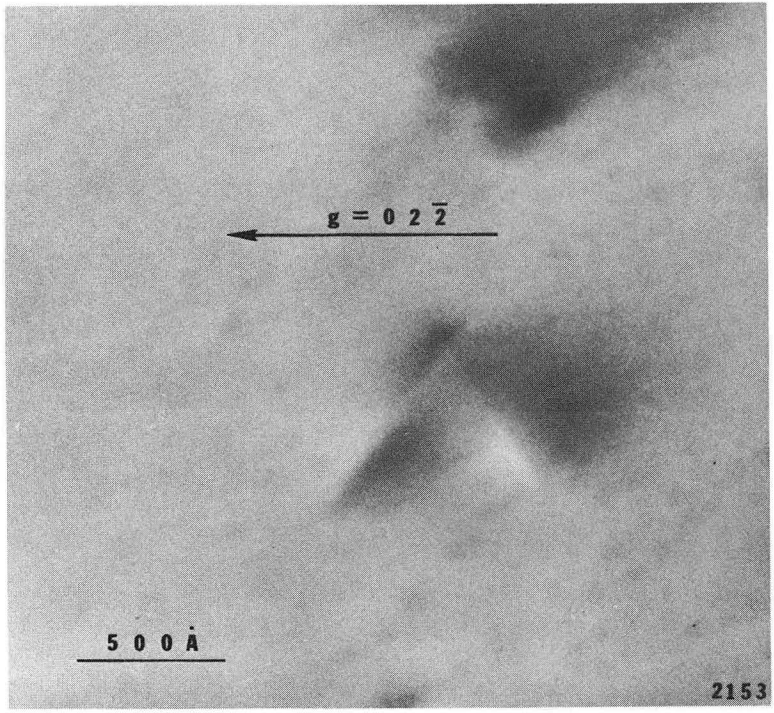
Figure IV-2 shows a SFT, $L \approx 820\text{\AA}$, formed by quench from 910°C . The contrast here is due to the dynamical contrast effect of a SFT discussed by Chik (1966). The same defect is shown in the series of Fig. IV-3 giving the contrast from a SFT for different diffraction conditions. An example of a Frank triangle (dissociated) is shown in Fig. IV-4a. This FT, $L \approx 900\text{\AA}$, is formed in a silver foil quenched from 825°C . SFT in the same foil are shown in Fig. IV-4b. The difference in contrast is clearly demonstrated by looking at the side normal to the reflecting vector \vec{g} . This side does not show any contrast for a SFT, but is clearly in contrast for a FT. Figure IV-5 shows SFT and FT's in a foil quenched from 910°C and Fig. IV-6 gives the details of one of the defects, a SFT in the foil tilted from $[110]$ towards $[111]$.

In silver foils quenched from elevated temperatures, $T > 800^\circ\text{C}$ stacking fault tetrahedra were found ranging in sizes, L , up to 2000\AA with $L \approx 100\text{\AA}$ as the smallest defect clearly identified. SFT in the size range below 700\AA were the most frequently found. Larger SFT



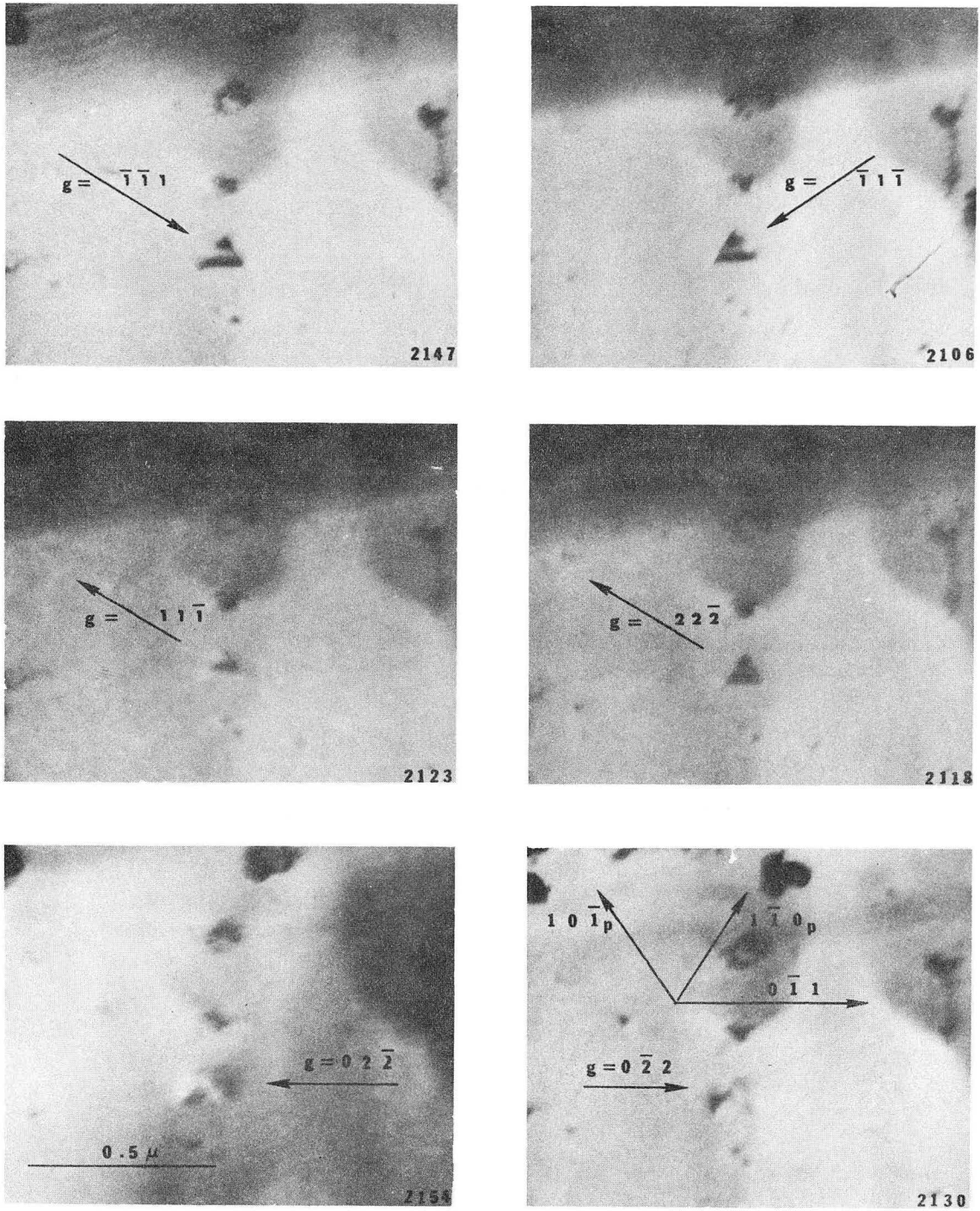
XBB 735-3112

Fig. IV-1. Transmission electron micrograph showing a SFT, $L \approx 920 \text{ \AA}$, in silver quenched from 960°C . The orientation of the foil is slightly off (011) . The indices p indicates traces.



XBB 735-3110

Fig. IV-2. TE micrograph showing a SFT, $L \approx 820\text{\AA}$, formed by quench from 910°C in silver. Foil-orientation (011). p indicates traces.



XBB 735-3104

Fig. IV-3. Contrast from a SFT under different diffracting conditions in a (011)-foil. Same SFT as in Fig. IV-2.

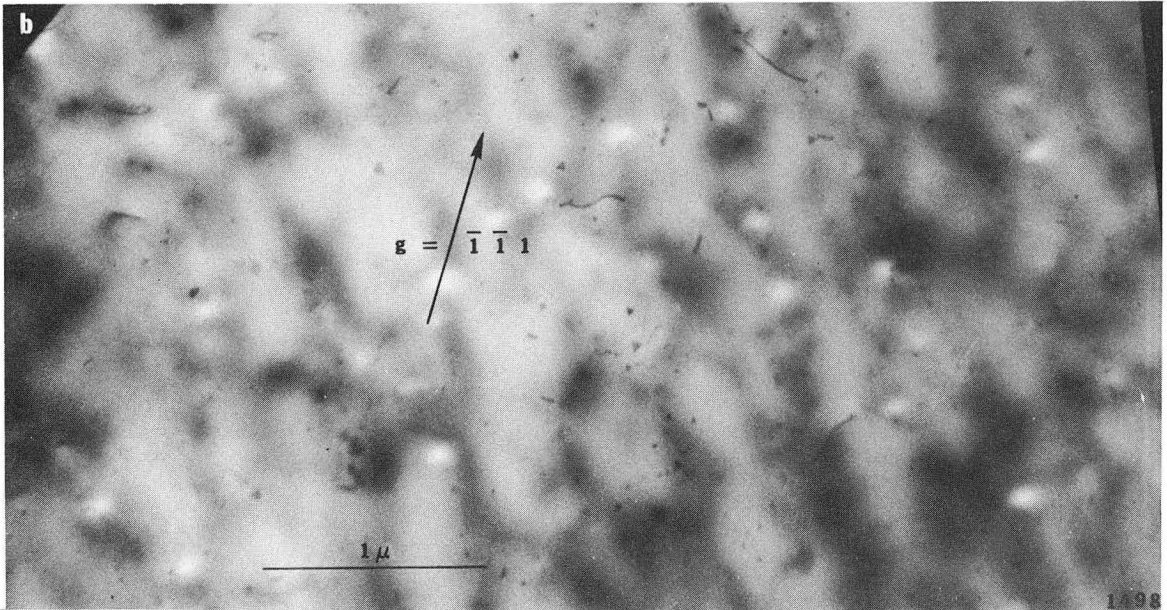
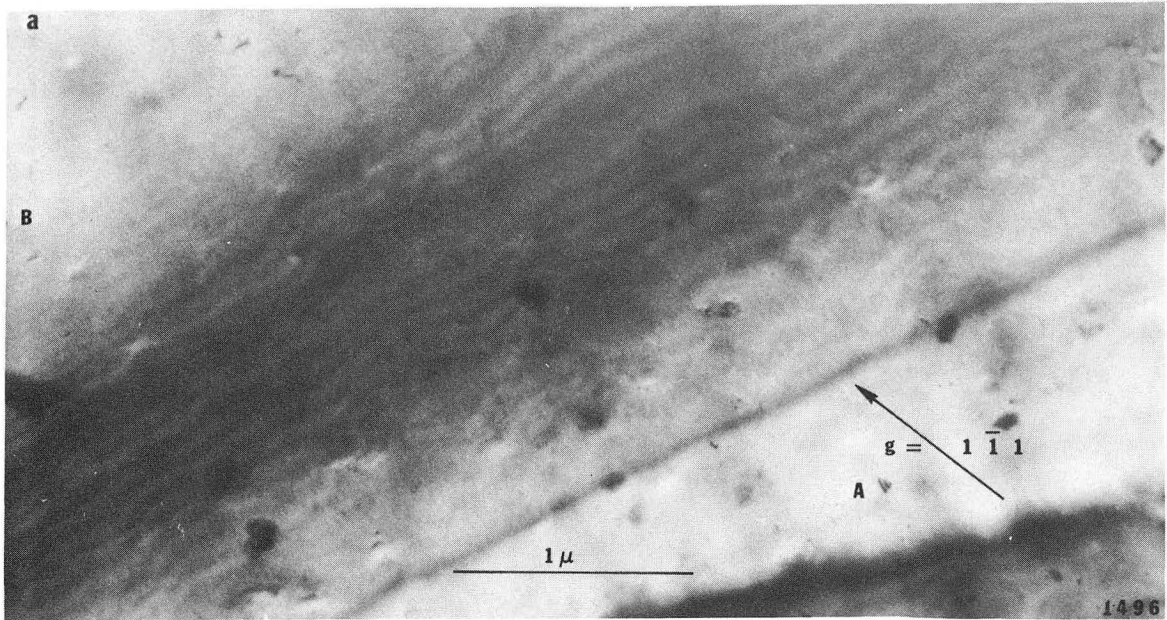


Fig. IV-4. (a) Ag quenched from 825°C in vacuum. Faults at A and B. (b) Same foil as (a). Relatively great density of triangular shaped faults. Foil orientation is (011).

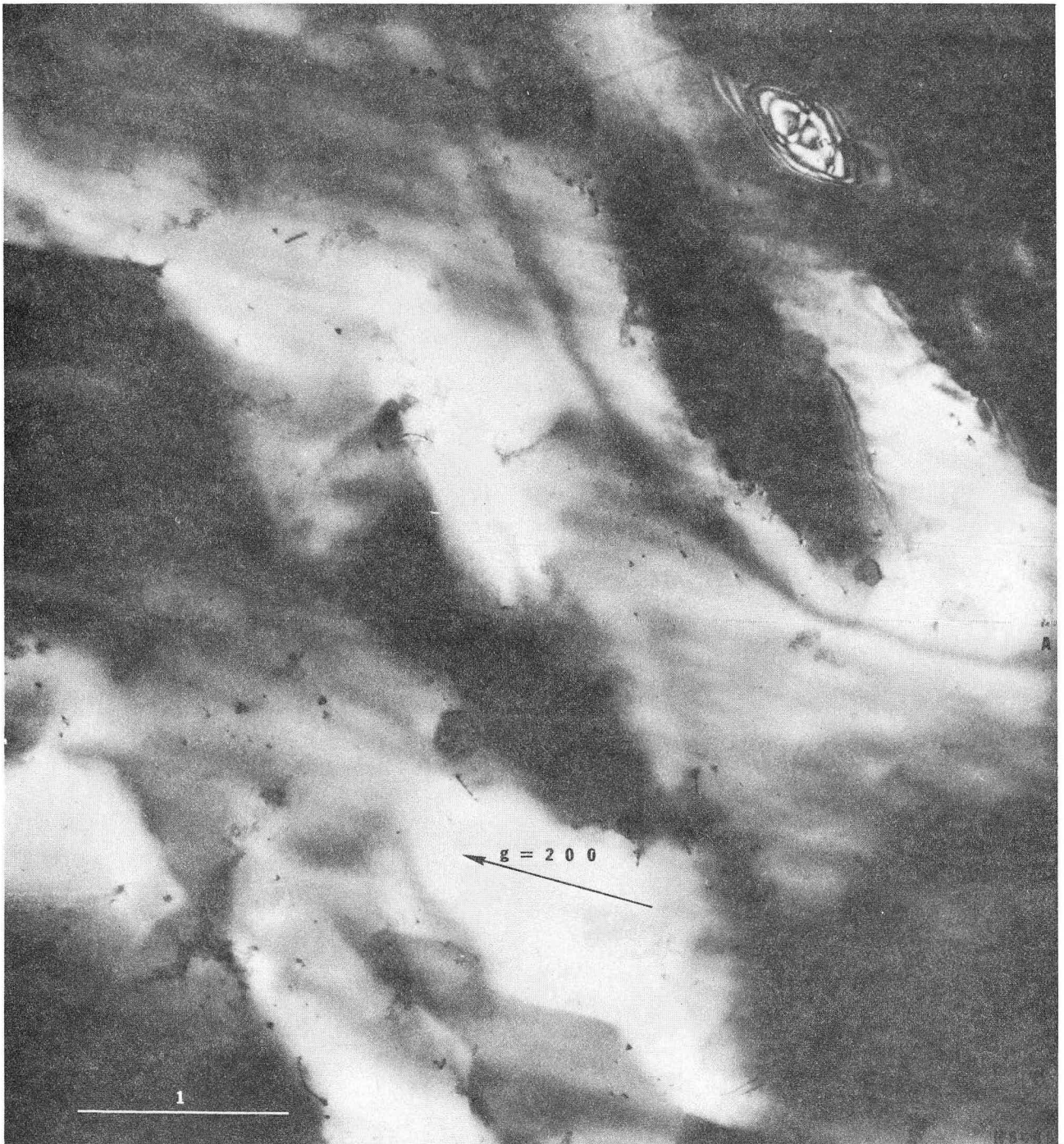
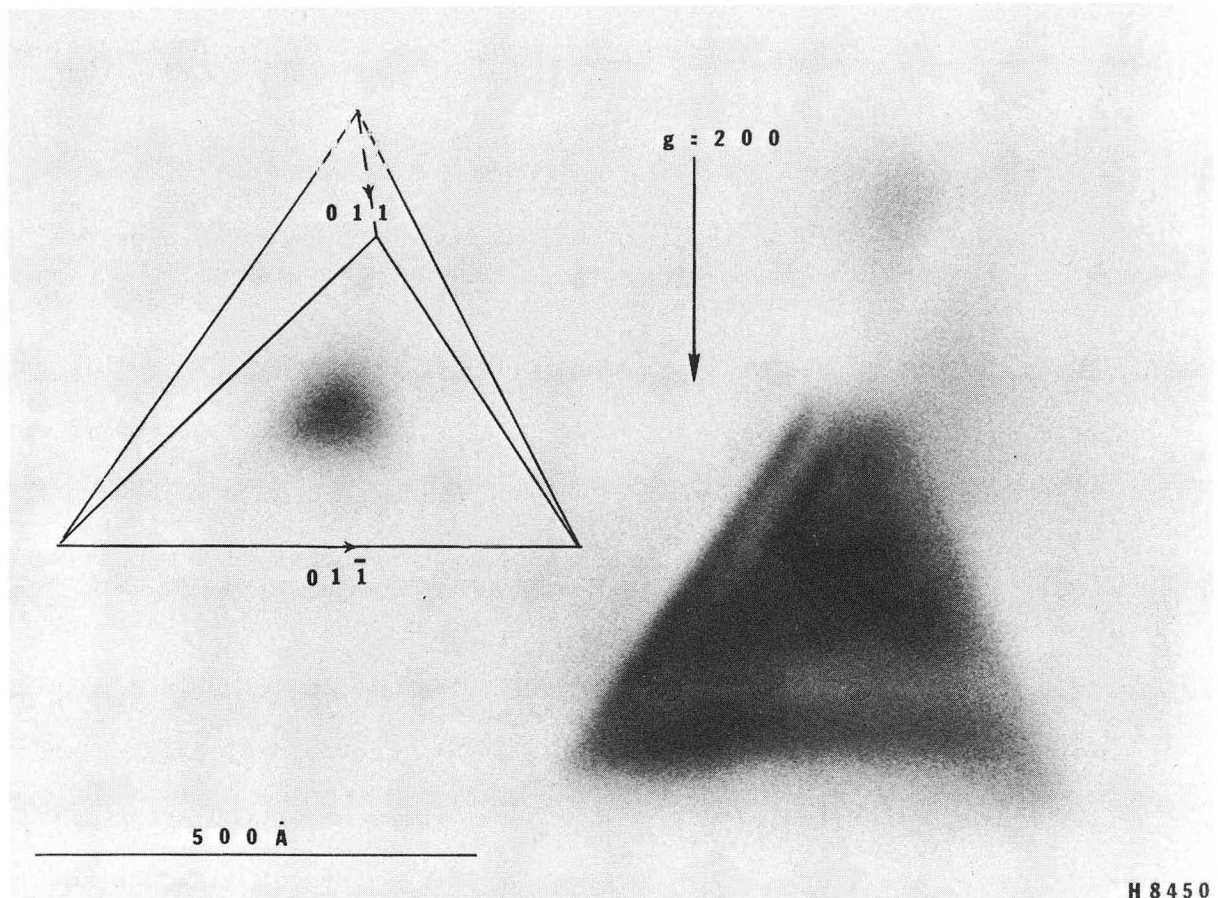


Fig. IV-5. Silver quenched from 910°C. The triangular shaped defects are SFT and Frank loops. Foil orientation is (011). The scale is 1 μ .



XBB 735-3140

Fig. IV-6. Enlargement of the large SFT at A in Fig. IV-5. $\&$ = loops, t = SFT. Scale is $0.1\ \mu:500\ \text{kV}$.

rarely occurred. Loops, identified as extended Frank triangles, FT, were not frequently observed, but appeared in sizes, L, ranging from about 670Å to about 1350Å.

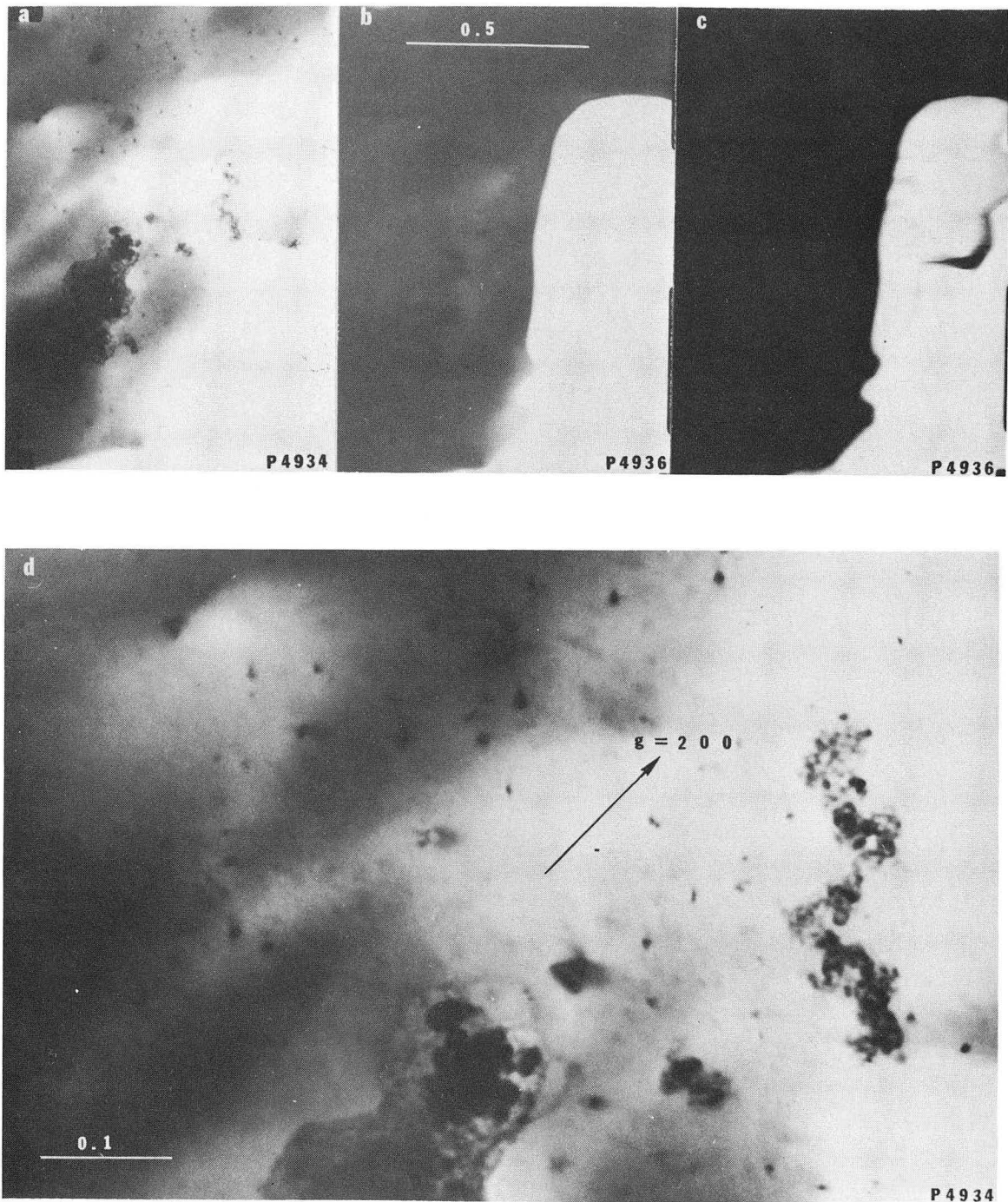
B. Annealing

Experimentally it is a problem to discover the defects on the fluorescent screen and most defects were first found after analyzing the photographic plates. After suitable areas were found in this manner, we could proceed with the hot-stage work. Using hot-stage experiments instead of anneals outside the microscope leads to direct observations, "in situ", but with less accuracy in the temperature determinations.

As mentioned in Chapter III, contamination proved to be a problem. In the annealing sequence shown in Fig. IV-7 we can clearly see this. Parts of the foil disappear, leaving a thin contamination layer and thick non-transparent areas of the metal foil. Selected area diffraction (SAD) from the contaminated layers gave ring-patterns, although not sufficient to analyze the layer. The series shown in Fig. IV-7 shows the contamination being a serious problem at 400°C, even in the 100 kV EM's with the best vacuum.

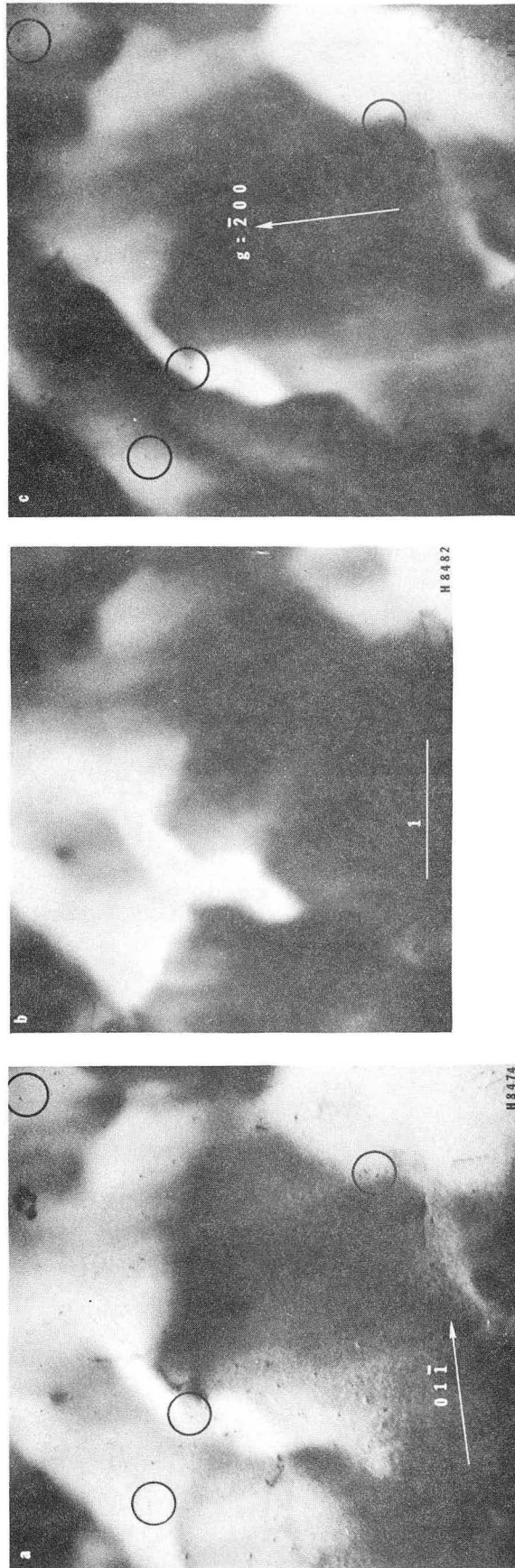
Contamination and motion of the foil during the heat treatment makes it difficult to record the same area during the whole experiment. Figure IV-8 shows an annealing sequence yielding no apparent change of the relatively small SFT, $L \approx 300\text{Å}$, after 1/2 hr at 650°C. Dirt marks proved to be very helpful to identify the areas.

Shrinkage and disappearance of SFT smaller than $L = 600\text{Å}$ after 15 min at 650°C are shown in Fig. IV-9. The defects at a, b, d and e disappear and the defects at c and k have been shrinking. At the top



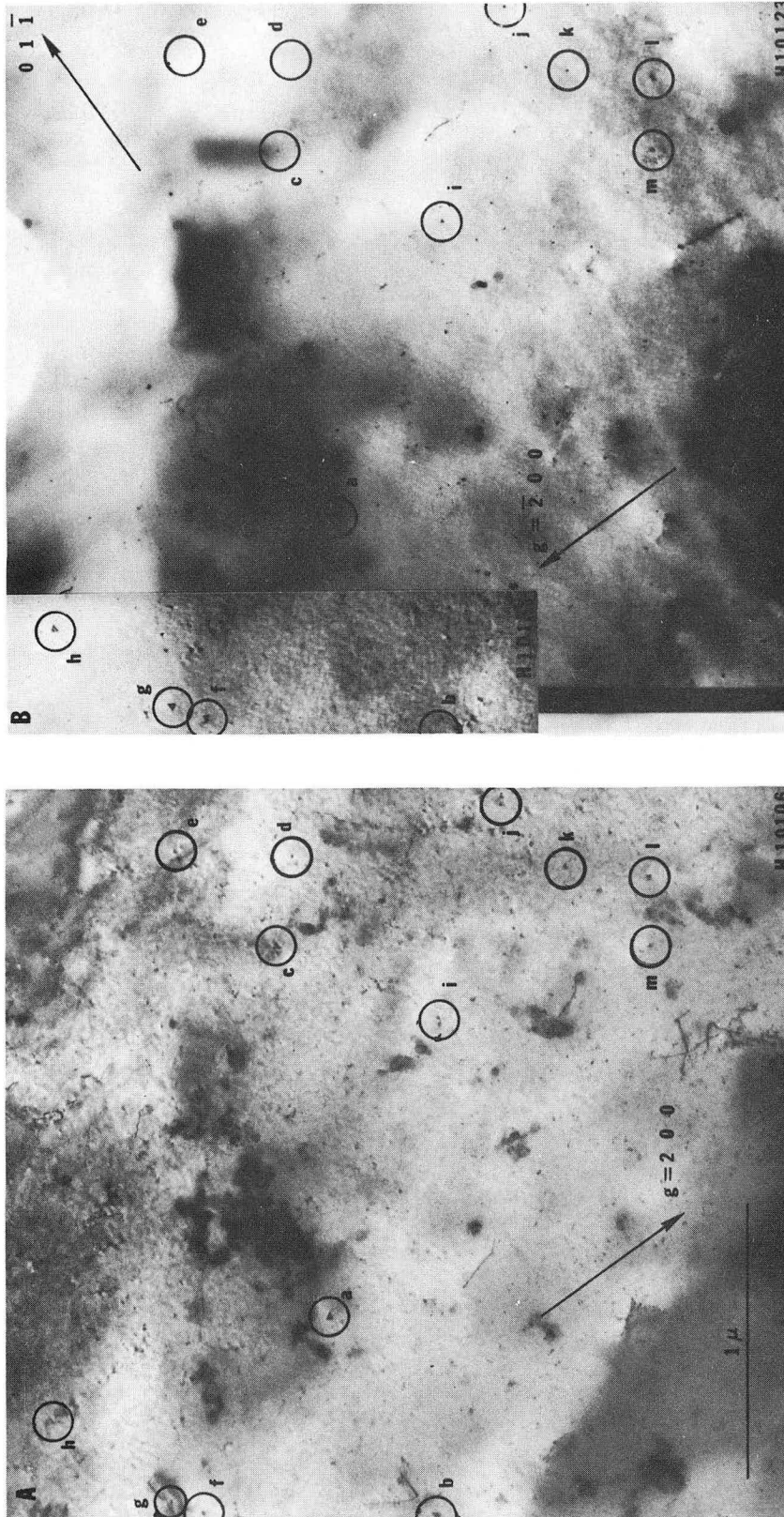
XBB 735-3109

Fig. IV-7. TE micrographs of the same area of a silver-foil during heating "in situ" in a Philips 300 EM, 100 kV. (a) At 200°C. (b) and (c) at 400°C. (d) Detail of (a). A SFT can be seen. (011)-foil. The scales are 0.5 μ and 0.1 μ .



XBB 735-3107

Fig. IV-8. Annealing sequence of a quenched silver foil. The foil has already been annealed once. (a) Before heating. (b) At about 650°C. (c) After cooling (after about 1/2 hr at 650°C). The area shown on the TE micrographs are identical, and the magnifications equal. Encircled are SFT seen before and after the anneal. \bar{g} is the same in all cases and the foil orientation is near (011). 500 kV. The scale is 1μ .



XBB 735-3105

Fig. IV-9. Shrinkage and disappearance of SPT in silver by annealing in the HVEM at 650 kV. (A) is a micrograph of the foil before the anneal. The size of the SFT are 600 Å or less. (B) is a micrograph of the same area after an anneal at 650°C for 15 min. The markings refer to the defects before and after. (011) foil.

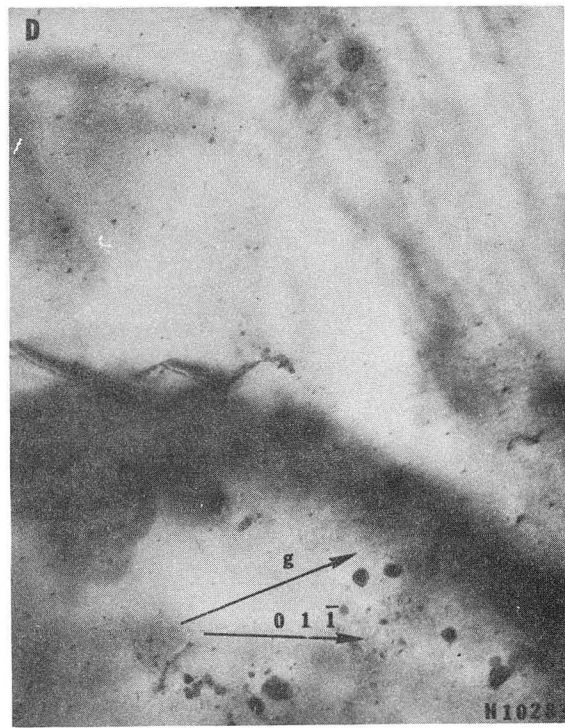
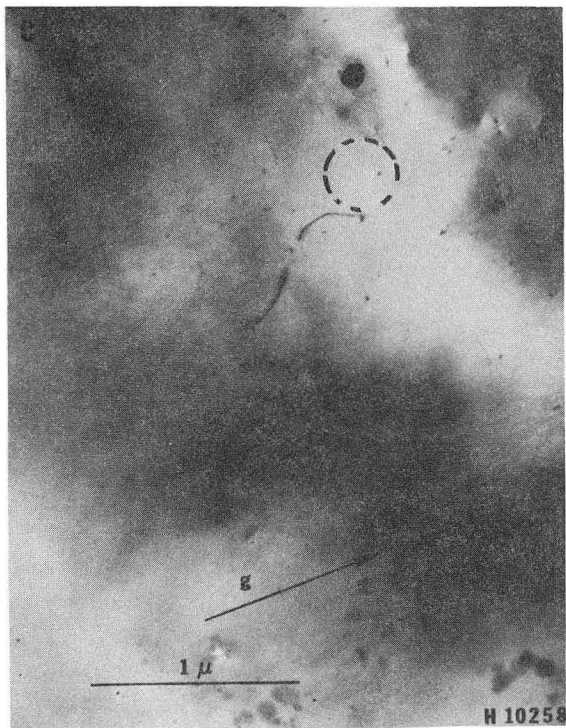
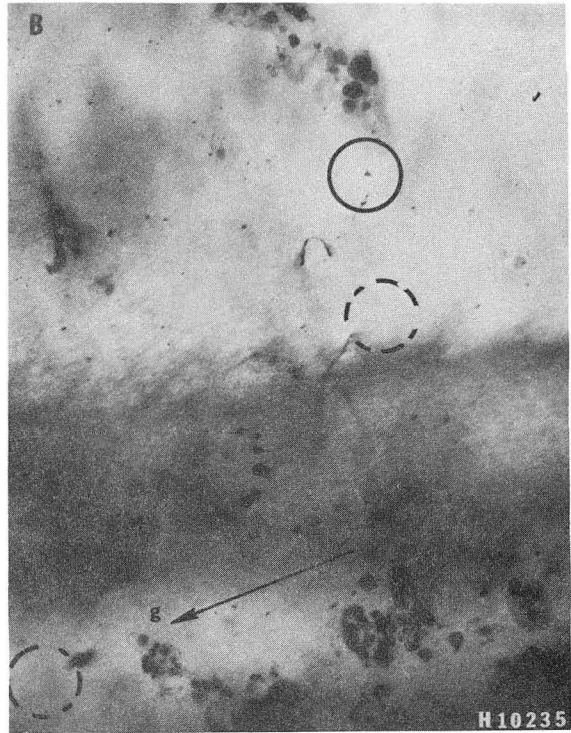
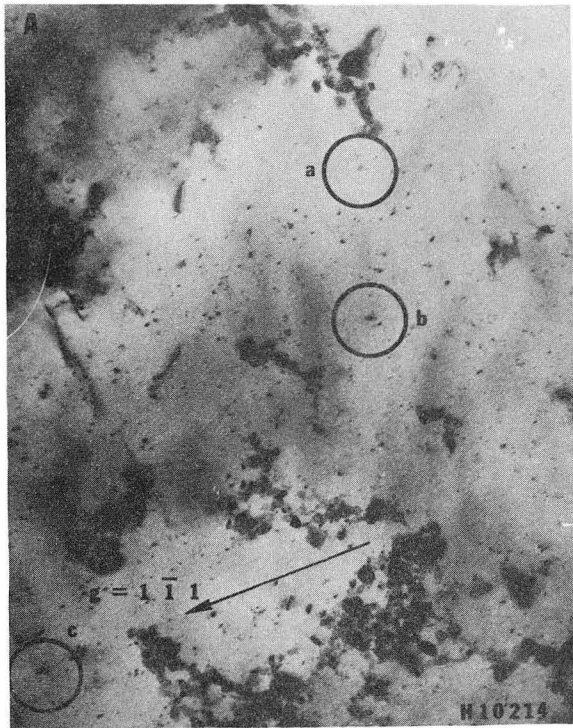
part of the micrograph taken after the anneal we can see that part of the foil has disappeared. Another annealing series is shown in Fig. IV-10. The defects at b and c annihilate after the first anneal at 610°C while the SFT at a disappears after the second anneal.

Figure IV-11 shows the collapse of a SFT, $L \approx 2000\text{\AA}$, and the following shrinkage of the loop, during several anneals. The collapse was observed directly to take place spontaneously during heating at about 300°C. After the collapse, the loop is on the plane normal to the foil surface (Fig. IV-12). After the last anneal, the loop appears to have been shrinking from one corner.

To observe any blunting of corners is difficult, although blunting seems to be the case for several of the observed defects (Fig. IV-13). Any shrinkage as that reported by Yokota (1968) in Au; shrinkage along one edge, has not been observed by us. A few irregularly shaped defects have been seen after anneals (Fig. IV-13 and Fig. IV-14), but generally the defects seem to keep their shape during annealing. In Fig. IV-15 is shown a FT, $L \approx 850\text{\AA}$, with dissociated dislocations along the edges.

The small defects seen on many of the micrographs are probably due to ion-damage. The defects appear during electron microscopy all over the foil, not only in the illuminated area. This suggests ion damage at the top surface of the foil, and might also be due to polishing conditions (Rühle et al., 1965, Thomas and Bell, 1967). The knock-on potential for Ag is too high to allow electron damage even at 650 kV.

Fig. IV-10. Disappearance of SFT in silver by annealing in the HVEM at 650 kV. (A) is before the anneal. (B) is after the first anneal at 610°C for 15 min. (C) is after the second anneal at 600°C for 1 hr. (D) is after the third anneal at 590°C for 35 min. The SFT are marked.



XBB 735-3108

Fig. IV-10.

Fig. IV-11. TE micrographs of the same area of a silver-foil taken during heating "in situ". (A) A quenched-in SFT, $L \approx 2000 \text{ \AA}$, before the start of the heating sequence. (B) During cooling from 400°C . The SFT has collapsed into a Fran loop seen edge on. (C) Cooled down. (D) Cooled down after reheating to 560°C for 45 min. (E) After 2. reheating to 560°C . (F) After 3. reheating. The same magnification on all micrographs.

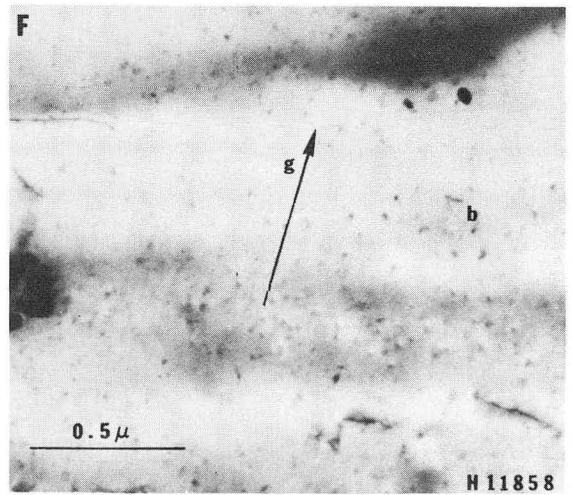
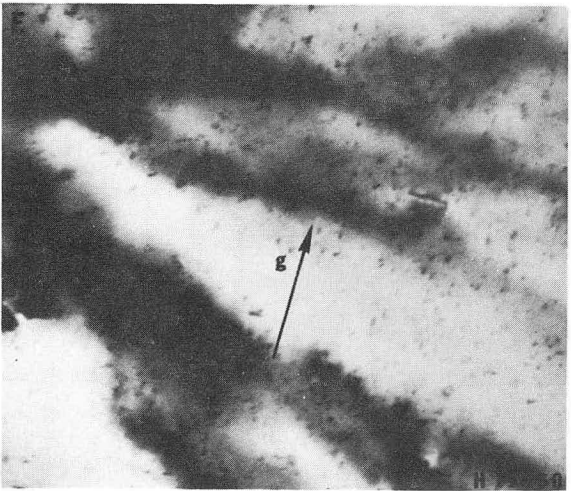
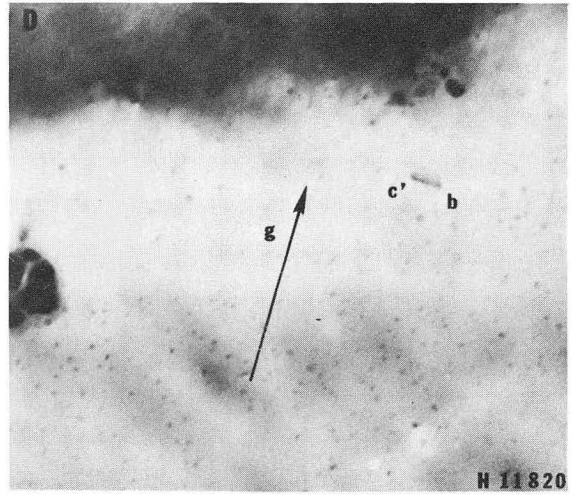
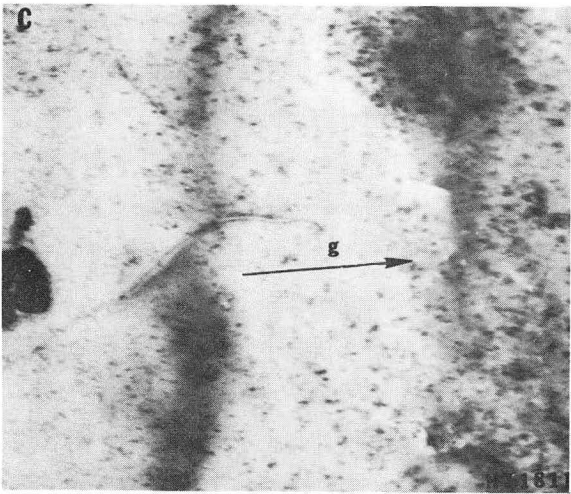
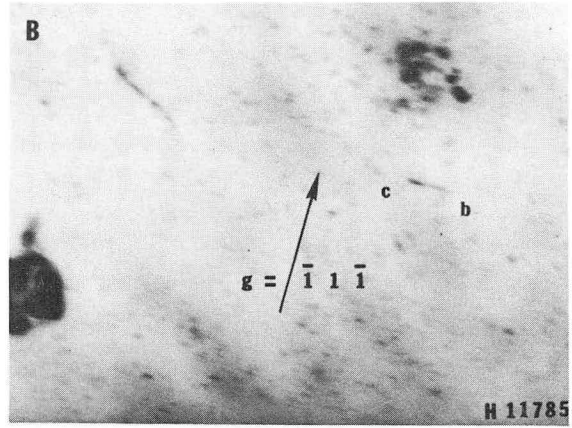
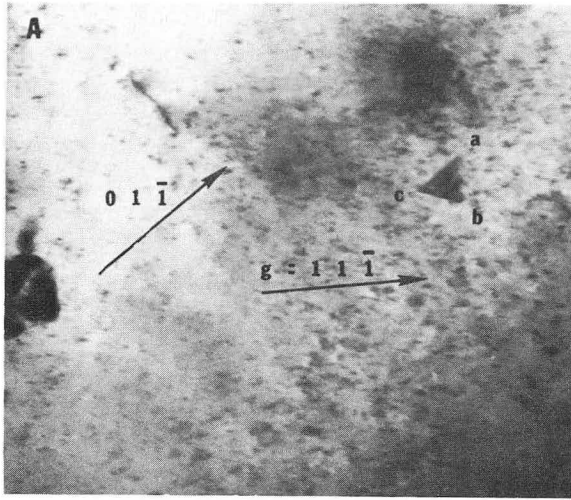
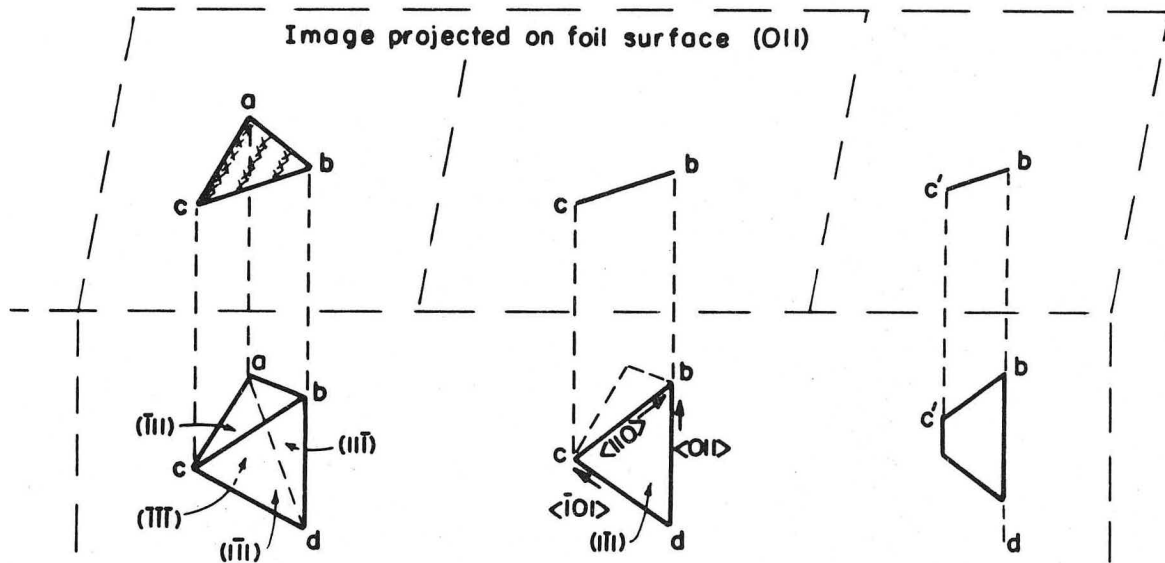


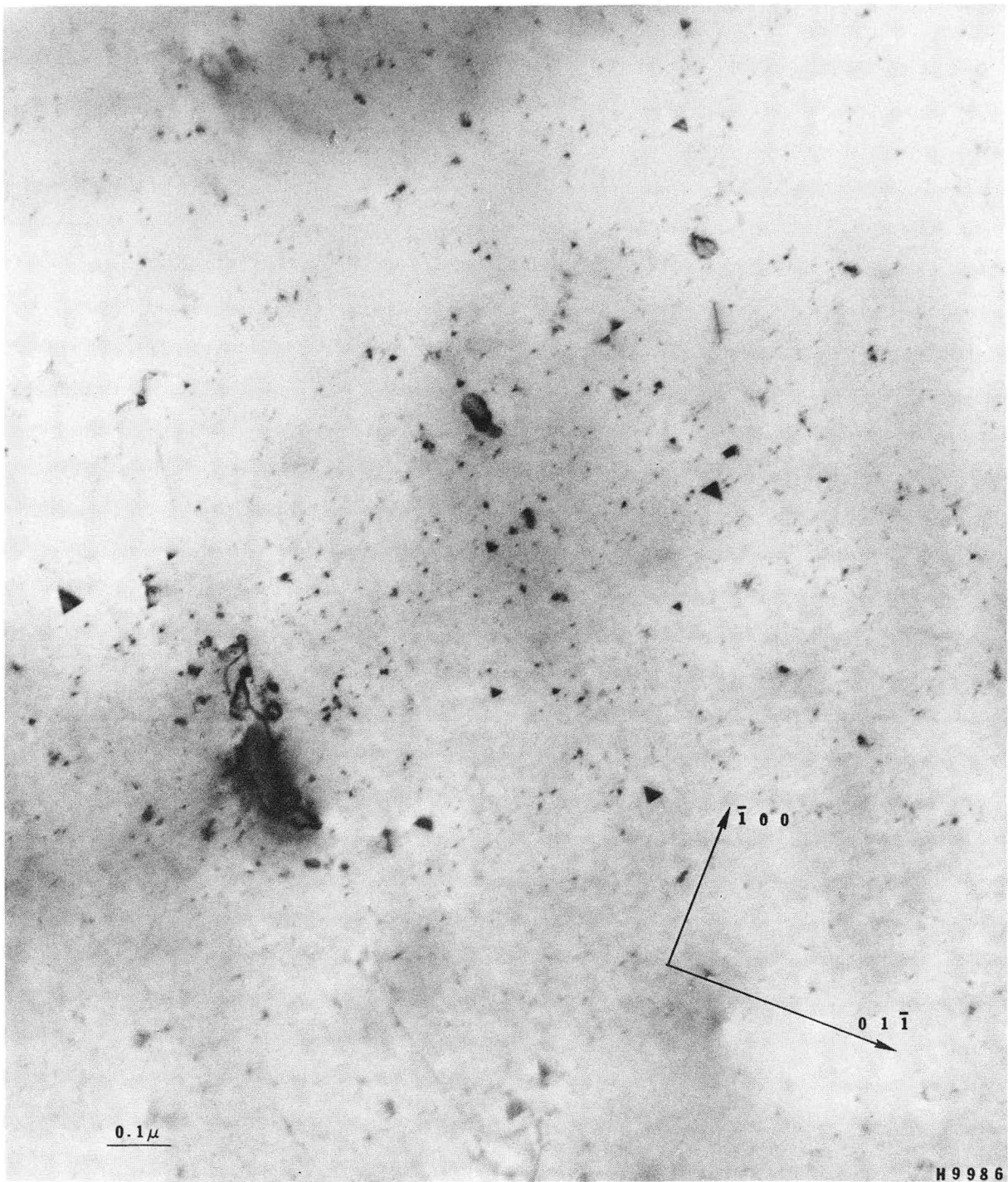
Fig. IV-11.

XBB 735-3106



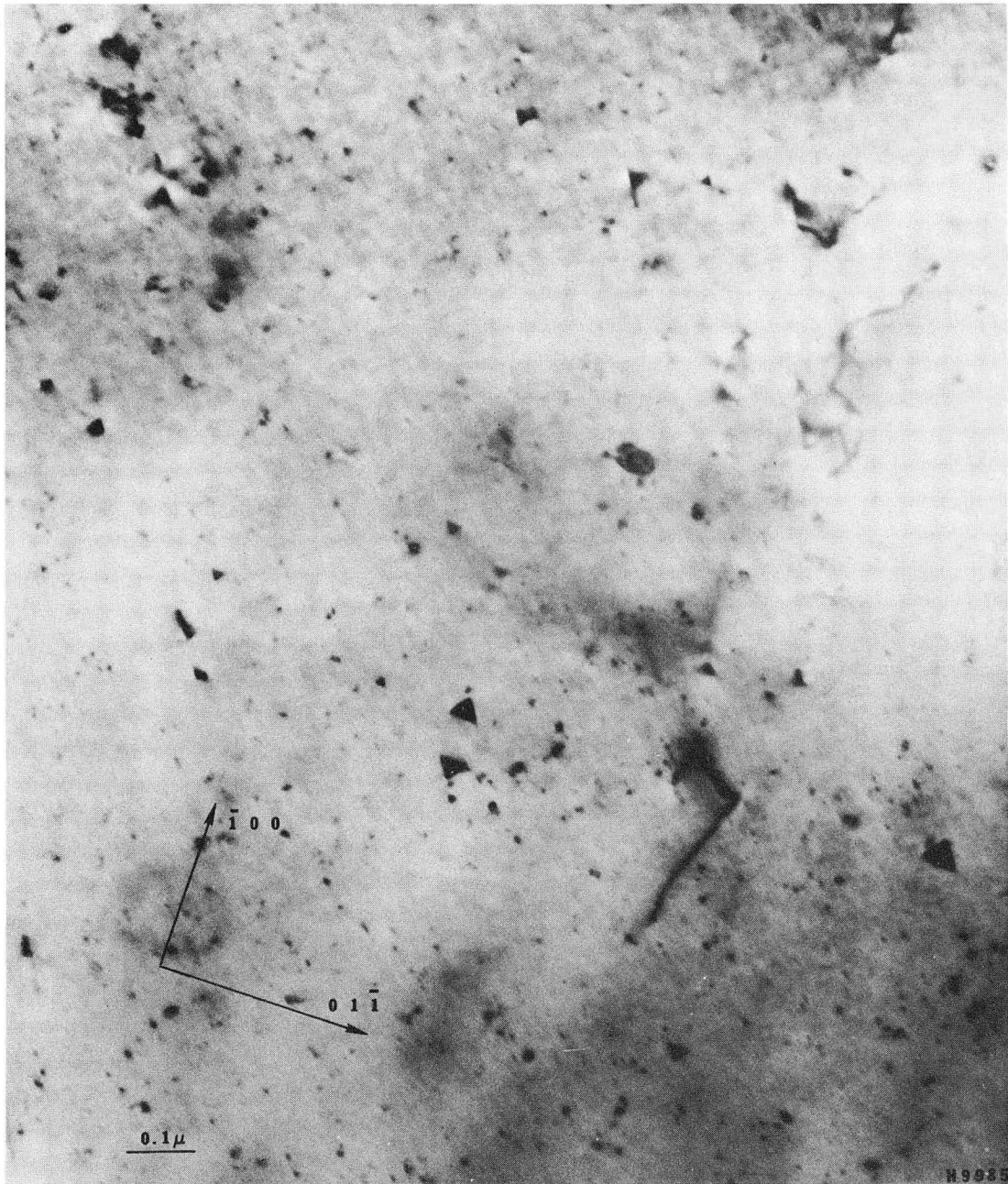
XBL 735-6110

Fig. IV-12. A schematical view of what is happening during the anneal shown in Fig. IV-11. During the first anneal, the SFT, $abcd$, is collapsing from the corner a , forming the Frank loop bcd , with the projection bc on the foil surface. After the last anneal, c seems to have moved to c' and this can be explained as the shrinkage shown in the last drawing.



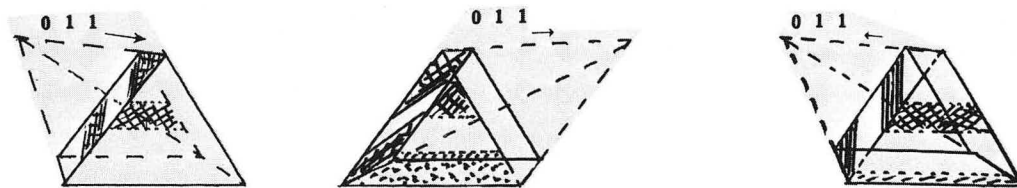
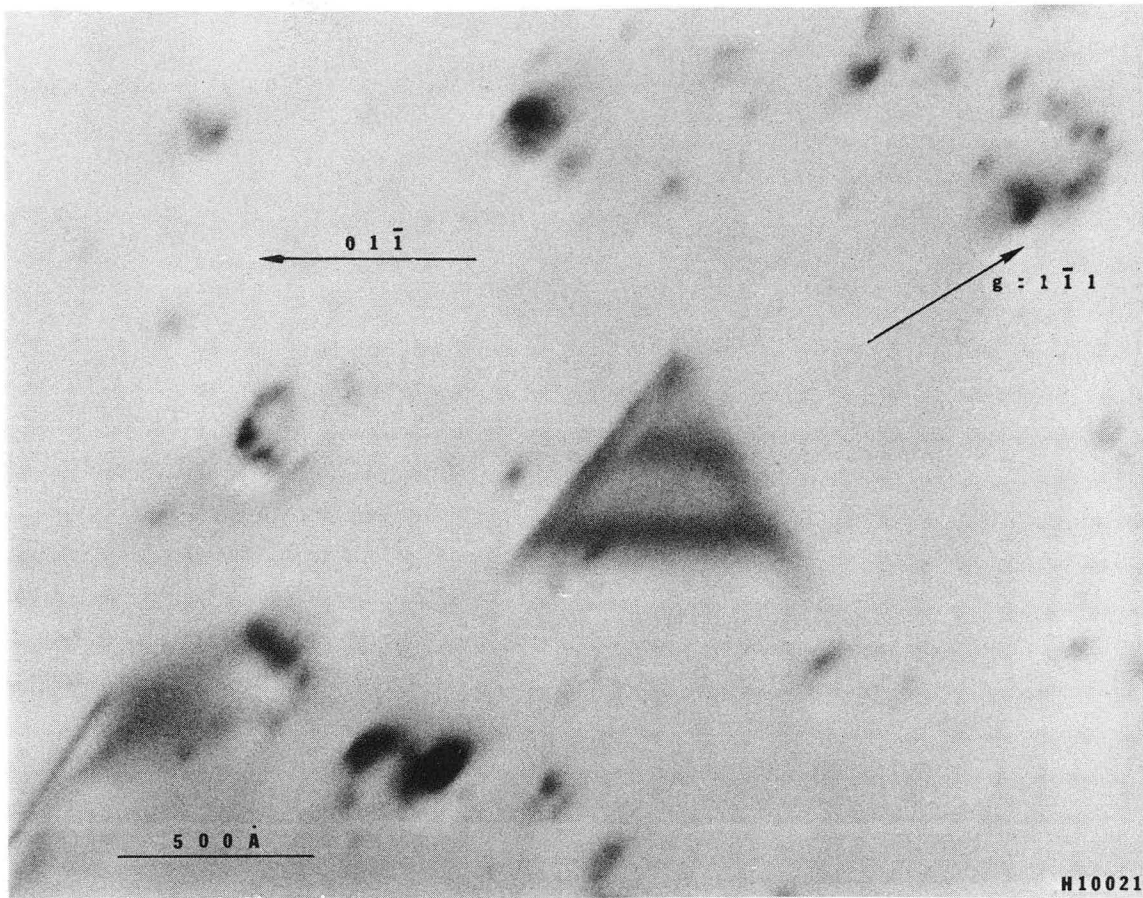
XBB 735-3114

Fig. IV-13. A silver foil after an anneal at 650°C for 5 min containing SFT. Annealed in situ in the HVEM at 650 kV. (011) orientation.



XBB 735-3113

Fig. IV-14. A silver foil after an anneal at 650°C for 5 min containing SFT. Annealed in situ in the HVEM at 650 kV. (011) orientation.



XBB 735-3141

Fig. IV-15. Frank triangle in a silver foil after an anneal in the HVEM at 650 kV at 650°C for 5 min. Same foil as in Figs. IV-13 and IV-14. (011) orientation. In the drawings are shown some possible configurations.

SUMMARY

By establishing a way of differentiating between the contrast from SFT and loops in the $\{110\}$ -orientation, we found quenched-in SFT with edge sizes up to 2000\AA , and triangular extended Frank loops with edge-sizes in the range 650\AA - 1350\AA , in agreement with the theoretically expected size-ranges.

We found that SFT with $L < 600\text{\AA}$ might shrink as SFT, and that they also might completely anneal out during anneals above 600°C . Collapse of a SFT, $L = 2000\text{\AA}$ was observed directly at 300°C , with further shrinkage taking place from one corner of the loop.

V. DISCUSSION

Faulted quenched-in defects are observed ranging in size from $L = 200\text{\AA}$ and upwards for clearly defined SFT, and from $L = 800\text{\AA}$ and larger for dissociated Frank triangles, L being the length of the edges of the defects. This is as should be expected looking at the total energy of the intermediate truncated stacking-fault tetrahedra. Experimentally, Loretto et al. (1965) found $\lambda_o = 750\text{\AA}$ as the maximum size of the SFT formed in silver by deformation. They also found the minimum size of FT to be $\lambda_F = 800\text{\AA}$.

There has been some arguments as to whether λ_o should be taken as L_c (Loretto et al., 1965, Jössang and Hirth, 1966) or as L_E (Humble et al., 1967), but $\lambda_o = L_c$ seems to be most likely (Jössang, 1968) due to the high stresses required $L > L_c$ to go from FT to SFT, even at $L = L_c + 5\%$. L_c being the min size for metastable FT, L_E being the size where the energies of the FT and the SFT are equal.

In the case of deformed gold, λ_o is found to be 200\AA and $\lambda_F = 230\text{\AA}$ (Loretto et al., 1965) which yield $\gamma_{Au} = 56 \text{ ergs/cm}^2$ with $L_c = \lambda_o$. Humble et al. (1967) uses the mean value of λ_o and λ_F as L_E and find $\gamma_{Au} = 45 \text{ ergs/cm}^2$, while Jössang and Hirth (1966) use $\lambda_o = L_c$ and find $\gamma_{Au} = 55 \text{ ergs/cm}^2$ and $L_E = 265\text{\AA}$. At $L = 200\text{\AA}$ the difference in the energies of the SFT and FT is 36.1 eV (Fig. II-4). For increasing L , ΔE decreases and becomes $\Delta E = 31 \text{ eV}$ at $L = 265 \text{ \AA}$, $\Delta E = 28 \text{ eV}$ at $L = 1500\text{\AA}$ and $\Delta E = 15 \text{ eV}$ at $L = 5800\text{\AA}$. ΔE represents the activation barrier for collapse of a SFT by glide from a corner. The barrier for going from FT to SFT increases very rapidly with increasing L from being zero at L_c to 1.6 eV at $L_c + 5\%$, 8.8 eV at $L_c + 15\%$ and 31 eV at $L = L_E$.

Escaig's (1970b) calculations, which he claims are in agreement with Jössang and Hirth (1966), give an energy barrier $\Delta E \approx 14.5$ eV for $L = 200\text{\AA}$ and a barrier of about 8.8 eV for going from FT to SFT. (The right-hand scale of Fig. 7 in Escaig's paper is used. The left-hand scale gives three times the values of the right-hand scale). The difference in energies of the FT and the SFT is 5.7 eV for $L = 200\text{\AA}$, while the formula of Jössang and Hirth (1966) gives 38.9 eV with $\gamma = 54$ ergs/cm².

Escaig's calculations using a variable ϕ lead to a reduction of Jössang and Hirth's values of the energy barrier of 15-20% (Escaig, 1970b) and the stability range should also be changed accordingly giving an increased L_c , but keeping L_E the same. For $L_t = 300$ b, Escaig finds $\Delta E = 9.6$ eV which is considerably lower than Jössang and Hirth's values.

For silver, Humble et al. (1967) calculate an E_{\min} being the energy of both the complete SFT and the dissociated (h) FT of edge size L_E . They find $E_{\min} \approx 20$ eV for $L_E = \ell = 750\text{\AA}$, $h = 65\text{\AA}$, and $\gamma = 17.5$ ergs/cm². The corresponding energy barrier ΔE is deduced to be 80-120 eV from their stresses of 415-690 kg/cm².

Using $L_c = 750\text{\AA}$, Jössang and Hirth (1966) find $\gamma = 17.5$ ergs/cm² and $L_E \approx 990\text{\AA}$. We have used Jössang and Hirth's formula (see Appendix 2) with $\gamma = 18$ ergs/cm² and find the stability range in silver to be $L_c \approx 690\text{\AA}$ and $L_E \approx 960\text{\AA}$. The energy barrier ΔE (for going from SFT to FT) is found to be 170 eV for $L = 700\text{\AA}$ decreasing to 134 eV for $L = 2000\text{\AA}$. The energy barrier for going from FT to SFT is found to be

1.25 eV for 700Å and 30 eV for 800Å, increasing rapidly with L. Escaig's (1970b) stability range shows $L_c \approx 600\text{Å}$ and $L_E \approx 800\text{Å}$ in silver.

For the different reported values of the energy barriers in gold and silver, we see that collapse of a SFT into a FT (extended) is virtually impossible, even at high temperatures, by the glide mechanism featuring glide of three Shockley partials from one corner. It is also highly unlikely for an extended FT with $L > L_c$ to become a SFT by the reverse glide rearrangement. The larger (than L_c) SFT have probably grown as SFT from smaller sized ones.

Yet observations show collapse of SFT during annealing in silver in the present work and in gold (Yokota, 1968) which points to the question of other probable collapse mechanisms, the magnitude of the stacking fault energy, the validity of the linear isotropic elasticity theory and the total energy of the system.

Escaig's (1970b) model with blunted 120° corners on the SFT leads to a non-conservative collapse mechanism that explains Yokota's (1968) observations in gold both qualitatively and quantitatively. His calculations for this model gives an energy barrier of about 0.25 eV for gold and subsequently the activation energy for reaching PQ^* equal to $U_D + 0.25 \text{ eV} = 2.05 \text{ eV}$, giving a reasonable probability of collapse at 300°C . This collapse mechanism results in blunted extended FT's as is observed. However, his calculations for the same mechanism in silver yield an energy barrier of about 23 eV, much too high to explain our observations of collapse.

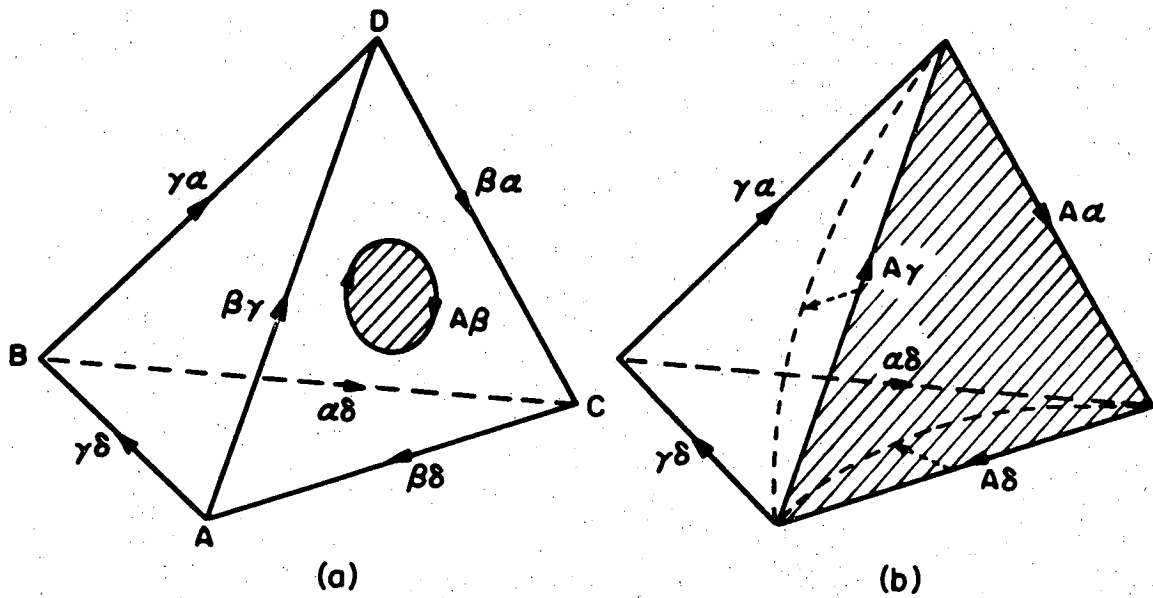
Finally, Escaig (1970a,b) proposes a modified nucleation theory to predict collapse of SFT by the blunted corner mechanism in silver. This

theory, however, is not believed to be valid (see Appendix 4).

Analyzing our annealing results, we find that large tetrahedra, i.e., $L > 800\text{\AA}$, collapse while the behavior of smaller SFT indicates shrinkage, which is expected according to the stability range.

As there seems to be quite impossible to get collapse from a corner by glide of three Shockley partials due to the prohibitive energy barrier, we have taken a closer look at the mechanism featuring collapse of the SFT by the nucleation of a Shockley dislocation loop on one of its faces. Calculations by Meshii and Kauffman (1960) yield an activation energy of 6.6 eV for nucleation of a Shockley loop on a SFT in gold, while finding 4.7 eV experimentally. However, they have not taken into account the interaction of the Shockley loop with the stair rod dislocations along the edges of the SFT. This interaction might be disregarded when the loop nucleates in the middle of the triangular SFT face on large tetrahedra, but it seems likely that this interaction term may be important when loops form near a corner.

The Shockley loop is a loop of a Shockley partial dislocation having a Burgers vector of the type $\vec{b} = \frac{a}{6} \langle 112 \rangle$ in the loop plane, i.e., glissile on an $\{111\}$ -plane. Shown in Fig. V-1 is a Shockley loop with $\vec{b} = \frac{a}{6} [1\bar{1}2] = A\beta$ on the $(\bar{1}11)$ face of a SFT. The Shockley loop will react with the stair rod dislocations along the edges of the $(\bar{1}11)$ face in the following way: $A\beta + \beta\gamma = A\gamma$, $A\beta + \beta\delta = A\delta$ (both glissile) and $A\beta + \beta\alpha = A\alpha$ (sessile). $A\gamma$ and $A\delta$ will glide on the $(\bar{1}\bar{1}\bar{1})$ and the $(11\bar{1})$ face respectively and react with the rest of the stairrods to make a Frank loop $A\alpha$ on $(1\bar{1}\bar{1})$, which will be an extended Frank triangle in the case with a low stacking fault energy.



XBL 735-6106

Fig. V-1. (a) A Shockley loop on the face of a SFT.
(b) The Shockley partials have reached with the edges AD, AC and CD. Shaded area is unfaulted.

The energy difference ΔW between the energy of the complete SFT, W_{SFT} , and the energy of the SFT with a Shockley loop on one face, $W_{\text{SFT/S}}$ is given $\Delta W = W_{\text{SFT}} - W_{\text{SFT/S}}$ by

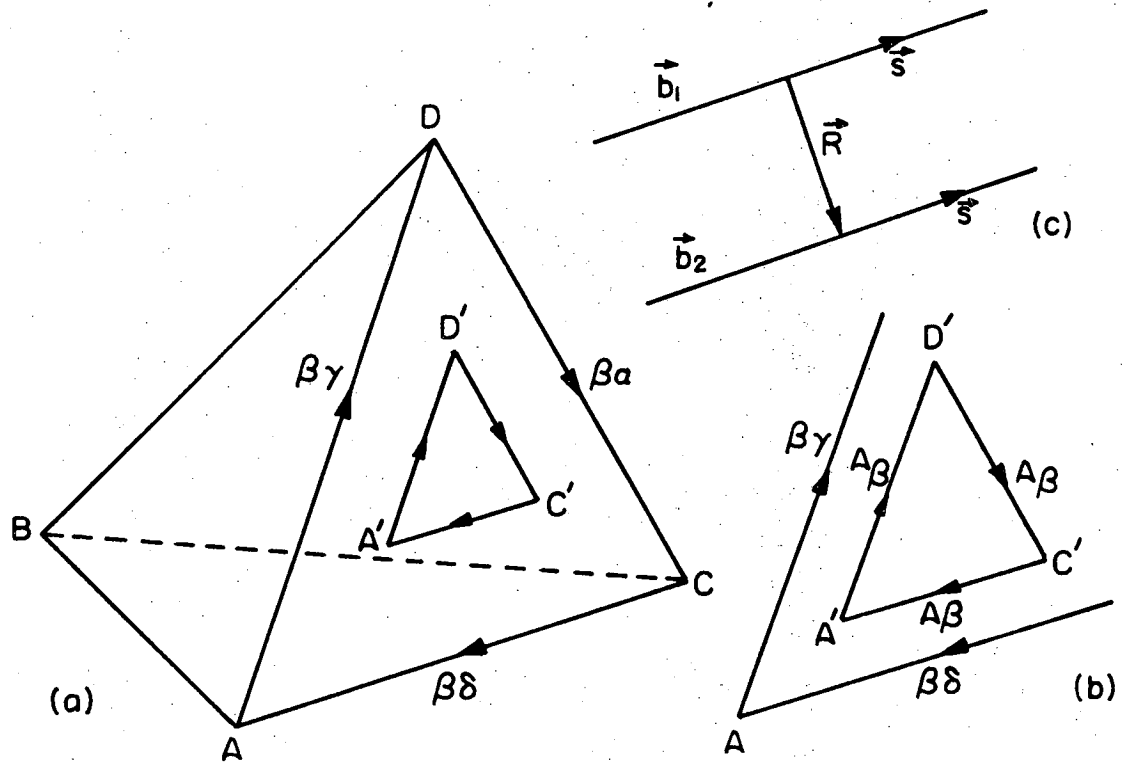
$$\Delta W = -\pi r^2 \cdot \gamma + 2\pi r \frac{2 - \nu}{2(1 - \nu)} \frac{\mu}{4\pi} \frac{a^2}{6} \left(\ln \frac{4r}{\rho} - 2 \right) + W_{\text{int}}(\alpha\beta; \beta\gamma, \beta\alpha, \beta\delta) \quad (\text{V-1})$$

The first term is due to the decrease in faulted area, the second term is the energy of the Shockley partial in the loop (Hirth and Lothe, 1968, p. 145) and the third term represents the energy due to the interactions between the Shockley loop and the stair rod dislocations. This interaction term would be somewhat complicated to calculate because it involves the interaction between curved dislocations and straight ones.

However, to get a feeling of the influence of the interaction term on ΔW , we will simplify the situation; approximating by using a triangular loop instead of the circular one (Fig. V-2). Here we look at the interaction between the straight segment of the stair rod and the neighboring straight segment of the Shockley in the loop. We only consider the coplanar, nearest-neighbor interactions.

The energy of interaction, per unit length, between two parallel coplanar dislocations with Burgers vectors \bar{b}_1 and \bar{b}_2 separated by \bar{R} , is given by Hirth and Lothe (1968, p. 110), (Fig. V-2c)

$$\frac{W_{12}}{L} = - \frac{\mu(\bar{b}_1 \cdot \bar{s})(\bar{b}_2 \cdot \bar{s})}{2\pi} \ln \frac{R}{R_a} - \frac{\mu}{2\pi(1 - \nu)} (\bar{b}_1 \times \bar{s}) \cdot (\bar{b}_2 \times \bar{s}) \ln \frac{R}{R_a} - \frac{\mu}{2\pi(1 - \nu) R^2} ((\bar{b}_1 \times \bar{s}) \cdot \bar{R})((\bar{b}_2 \times \bar{s}) \cdot \bar{R}) \quad (\text{V-2})$$



XBL 7 36- 6237

Fig. V-2. (a) A triangular Shockley dislocation loop on the face of a SFT. (b) Detail of the Shockley loop at one corner of the SFT. (c) Two parallel dislocations on the same plane separated by R . \vec{b}_1 and \vec{b}_2 are the Burgers vectors, and \vec{s} is the direction (sense). On the SFT the senses are indicated by arrows.

R_a is an integration constant larger than R , i.e., $\ln R/R_a < 0$. In the case shown on Fig. V-2b we look at the three interaction-terms; between the dislocations at AC and A'C', AD and A'D' and between CD and C'D'. We have $\bar{b}_2 = A\beta = \frac{a}{6}[1\bar{1}2]$, and \bar{b}_1 and \bar{s} in the three cases will be: $\bar{b}_1 = \beta\gamma = \frac{a}{6}[10\bar{1}]$ and $\bar{s} = \frac{1}{\sqrt{2}}[101]$, $\bar{b}_1 = \beta\delta = \frac{a}{6}[0\bar{1}\bar{1}]$ and $\bar{s} = \frac{1}{\sqrt{2}}[01\bar{1}]$, and $\bar{b}_1 = \beta\alpha = \frac{a}{6}[1\bar{1}0]$ and $\bar{s} = \frac{1}{\sqrt{2}}[\bar{1}\bar{1}0]$. Both the first and third term in Eq. (V-2) will disappear as $(\bar{b}_1 \cdot \bar{s}) = 0$ and $(\bar{b}_2 \times \bar{s}) \cdot \bar{R} = 0$, and we get

$$\frac{W_{12}}{L} = - \frac{\mu}{2\pi(1-\nu)} (\bar{b}_1 \times \bar{s}) \cdot (\bar{b}_2 \times \bar{s}) \ln \frac{R}{R_a} \quad (V-3)$$

of which the results of the vectorial terms are given in Table V-1 for the three cases. W_{12}/L is negative for the interactions between AD and

Table V-1. Values of the vectorial terms in Eq. (V-3) for the interaction between the stair rods of the SFT and the triangular Shockley loop shown in Fig. V-2.

	AD/A'D'	AC/A'C'	CD/C'D'
\bar{b}_1	$\frac{a}{6}[10\bar{1}]$	$\frac{a}{6}[0\bar{1}\bar{1}]$	$\frac{a}{6}[1\bar{1}0]$
\bar{s}	$\frac{1}{\sqrt{2}}[101]$	$\frac{1}{\sqrt{2}}[01\bar{1}]$	$\frac{1}{\sqrt{2}}[\bar{1}\bar{1}0]$
$(\bar{b}_1 \times \bar{s}) \cdot (\bar{b}_2 \times \bar{s})$	$-a^2/36$	$-a^2/36$	$2a^2/36$

A'D' and for the interactions between AC and A'C', representing attractive forces. For the interaction between CD and C'D' we get W_{12}/L positive, and a repulsive force.

Taking L as the length of the sides of the triangular Shockley loop, R_1 as the distance between the loop side and the SFT-edge normal to the direction of the Burgers vector \bar{b}_2 , and R_2 as the other two distances, we get an approximate expression for $W_{int}(\alpha\beta; \beta\gamma, \beta\alpha, \beta\delta)$:

$$W_{int} = \frac{\mu}{\pi(1-\nu)} \frac{a^2}{36} L \ln \frac{R_2}{R_1} \quad (V-4)$$

If the Shockley triangle nucleates in the middle of the face, $R_1 = R_2$ and the interaction term in ΔW can be disregarded. However, when the triangle nucleates near the corner A; $R_2 < R_1$ and $W_{int} < 0$ which results in a lowering of ΔW , Eq. (V-1) using a triangular loop instead of the circular one. An approximate expression for ΔW is now

$$\Delta W = \frac{a^2 \mu}{4\pi(1-\nu)} L \left\{ \frac{2-\nu}{4} \left(\ln \frac{L}{\rho} - 2.1 \right) + \frac{1}{9} \ln \frac{R_2}{R_1} \right\} - \frac{\sqrt{3}}{4} L^2 \gamma \quad (V-5)$$

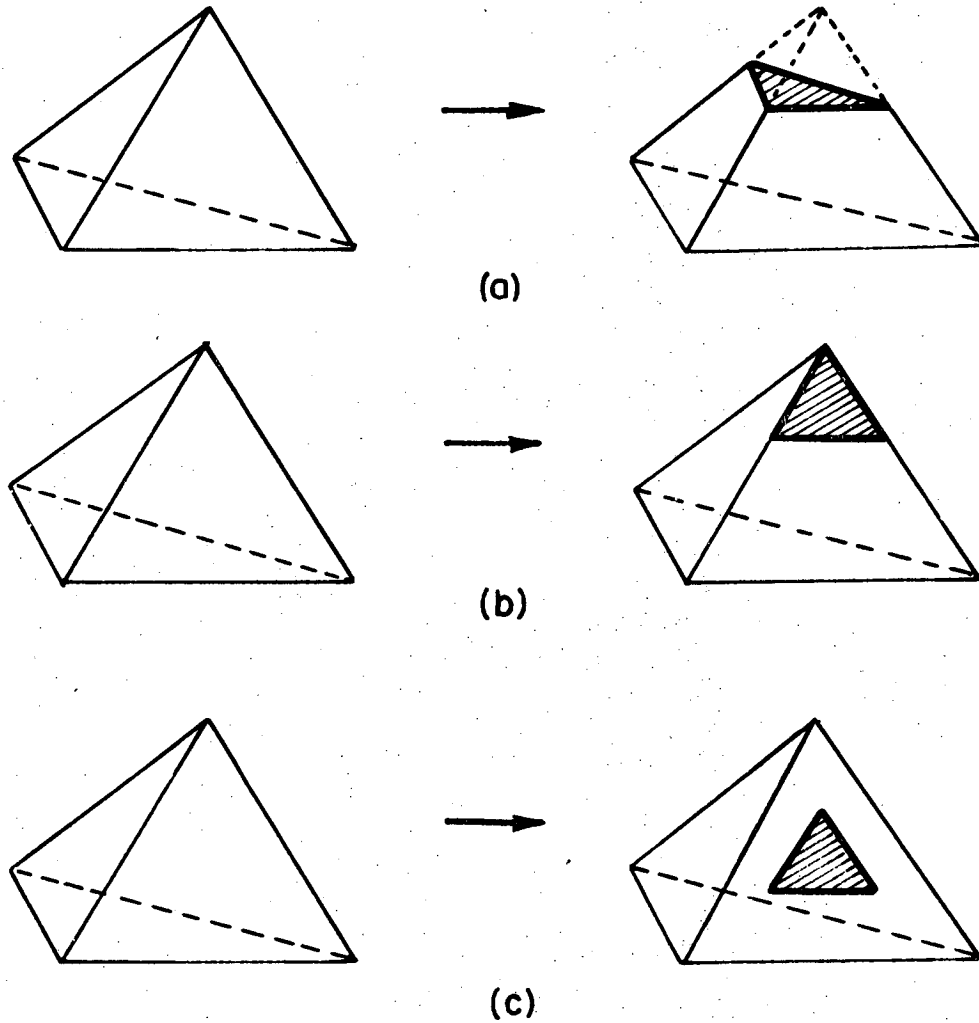
The $\ln(R_1/R_2)$ term can represent a considerable lowering of the critical ΔW needed for nucleation of this loop, and would thus easily explain conservative collapse of SFT in gold by the nucleation of a Shockley-loop near one corner, as the theoretical value given by Meshii and Kauffman (1960) is 6.6 eV for the nucleation of a Shockley-loop in the middle of the SFT-face.

At this point it would be useful to recollect some of the more important factors in the energy calculations; the cut-off parameters α and L , the elasticity constants, and the equations being based on isotropic continuum elasticity theory. Taking this into consideration, we have tried to assess the values of the energies and energy-barriers involved in the different collapse mechanisms such as: (I) collapse

of one corner of the SFT into a Shockley triangle (Fig. V-3a), (II) unfauling of one of the faces of the SFT from the corner (Fig. V-3b) and (III) unfauling one of the faces of the SFT by the nucleation of a Shockley-loop on the face (Fig. V-3c). All representing different initial stages of the conservative collapse of the SFT. The equations involved are given in Appendix 5.

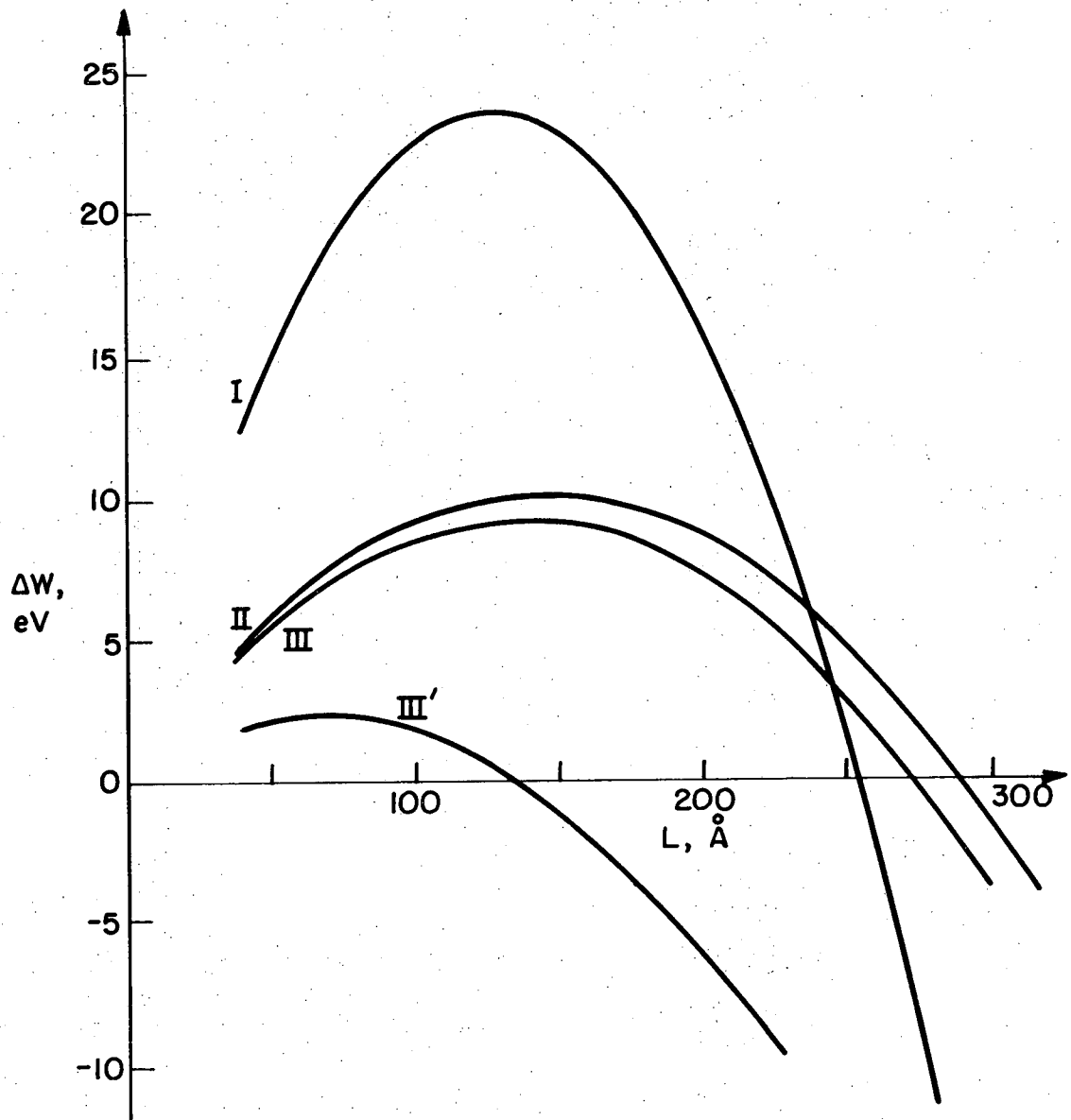
By using $\alpha = \frac{1}{2}$ (Hirth and Lothe, 1968, p. 212), we find energy-barriers too high to allow any of the mechanisms to be activated thermally, both in silver and in gold. The self-energies of the dislocations are proportional to $L \cdot \ln L_K$, the cut-off parameter L_K being equal to the size L of the defects in these cases. In an otherwise perfect crystal, L_K should be the distance to the surface, however, L_K is reduced due to interactions with other dislocations and defects, and due to end-defects. It can further be argued for a reduction in L_K to compensate for not using anisotropic elasticity theory because anisotropy should tend to minimize the energy in the actual directions.

We thus calculated the energies and energy-barriers for mechanisms I and II with a $L_K = 100\text{\AA}$. The results are shown graphically in Fig. V-4. As we can see, the activation energies are still too high, but the critical values are reduced from $L^* \approx 200\text{\AA}$ and $\Delta W^* \approx 36$ eV to $L^* \approx 150\text{\AA}$ and $\Delta W^* \approx 25$ eV for mechanism I, and from $L^* \approx 500\text{\AA}$ and $\Delta W^* \approx 52$ eV to $L^* \approx 130\text{\AA}$ and $\Delta W^* \approx 10$ eV for mechanism II. (It might be mentioned that a similar reduction could be obtained by using $L_K = L/2$, or $\alpha = 1/4$ which represents a change in the cut-off parameter with respect to the core-energy.)



XBL 739-1905

Fig. V-3. Initial mechanisms for the conservative collapse of a SFT. (a) Mechanism I, collapse starting at a corner, proceeding by Shockley's moving along the three faces. (b) Mechanism II, unfaulting of one face starting from a corner. (c) Mechanism III, formation of a Shockley loop on the face.



XBL 739-1904

Fig. V-4. Energies ΔW for collapse of a SFT-corner (I), for the unfauling of one face of the SFT from a corner (II), for the formation of an unfauled Shockley triangle (III) and for the formation of an unfauled Shockley triangle near one corner of the SFT, (III'), as functions of the size L .

The most important point, however, is the reduction of the activation-energy for the nucleation of the Shockley loop, which we have equaled to a triangle for the sake of simplicity. As this loop is inside other configurations, we have used $L_K = 50\text{\AA}$ as a likely cut-off parameter. The energy curve for this loop is shown in Fig. V-4. The energy-barrier is about 9 eV for $L^* \approx 140\text{\AA}$ in silver (about 3 eV in gold). The last curve in Fig. V-4 takes into account the interaction between a Shockley triangle near one corner and the three stair rod dislocations by using a correction term equal to $L \cdot A \cdot 12 \cdot \ln 1/4$ in the energy (Eq. V-5 and Eq. A5-12). $A = 4.018 \cdot 10^{-3}$ eV/ \AA for silver. $R_2/R_1 = 1/4$. This reduction term is a reasonable one taking into account its dependence on total size and the position of possible nucleation centra.

In this picture we will get collapse into a truncated SFT at about $L \approx 300\text{\AA}$, where no extra energy is needed for collapse into a unfaulted corner (II) which spontaneously will collapse into the truncated SFT-corner and further on to the dissociated Frank loop. Regarding the right hand side of Fig. V-4, the energy curves should drop off slower due to interactions with other parts of the SFT which should be incorporated for larger L's.

The main point is that the nucleation of a Shockley loop near one corner is much more likely than in the middle of the face of the SFT, explaining conservative collapse thermally activated in both silver and in gold. Quantitatively we have shown this by choosing reasonable cut-off parameters for the energy calculations.

We would not expect the conservative collapse mechanism to work with small SFT; i.e., $L < L_E$, as the total energy of the defect would

increase in going from a SFT to an extended FT. The higher stability of the SFT would be due to stronger interactions between all edges which also would influence the energetics of the Shockley loop.

As we have observed, smaller SFT seem to anneal out by shrinkage as SFT. (The energy of the SFT decrease with a decrease in size.) We must therefore discuss probable shrinkage mechanisms.

Kuhlmann-Wilsdorf (1965) did some calculations for gold and suggested that the ledge-mechanisms, migrating steps of atomic height, i.e., jog-lines traversing the tetrahedron face, can cause growth of SFT as well as shrinkage. Her relatively low value for the energy of the ledges with $U_{L*}^V \cdot b \sim 0.05$ eV for a V-ledge (and $U_{L*}^I \sim 2.5 U_{L*}^V$ for an I-ledge) agrees with the activation energy for the climb process leading to tetrahedron growth in gold found by Jaim and Siegel (1972) to be ~ 0.07 eV (± 0.02 eV). In this case the V-ledge is made up by two stair rods $\delta\alpha$ - $\alpha\delta$ (Fig. A1-16) and the I-ledge is made up by the stair rod pair of the type $\frac{a}{3}\langle 100 \rangle$, (which is a unfauling of the $\alpha\delta$ - $\delta\alpha$ ledge (Fig. A1-15)).

The activation energy for nucleating a V-ledge along an edge of the SFT is given by Kuhlmann-Wilsdorf (1965) to be

$$E^* \approx \left\{ U_{L*}^V - \sqrt{3} b \gamma - \frac{1/3 kT}{b} \right\} \ell - \frac{3\sqrt{3}}{2} b^2 \gamma + E_D \quad (V-6)$$

The terms $\frac{1}{2}\sqrt{3} b \cdot \ell$ and $\frac{3}{2}\sqrt{3} b^2$ take care of the change in faulted area due to the formation of the ledge. (The "fault" of the ledge is included in U_{L*}^V). The term $\frac{1}{3} kT$ is due to the entropy of vibration and E_D is the energy of self-diffusion taking into account that the emission

of one vacancy is needed to make the ledge. (One vacancy is emitted every time the ledge moves one atomic distance.) For gold Kuhlmann-Wilsdorf (1965) gives $U_{L^*}^V \cdot b = 0.047$ eV by using a stress of $\mu/30$ between the two partials. With $\gamma_{Au} = 54$ ergs/cm², $b_{Au} = 2.88$ Å, and $E_{DAu} = 1.8$ eV, we get an activation energy of $E^* \approx 2.5$ eV for $T = 600^\circ\text{K}$ and $L = 288\text{Å}$.

Similarly, using Kuhlmann-Wilsdorf's arguments on silver, with $b = 2.89\text{Å}$, $\gamma_{Ag} = 18$ ergs/cm² and $E_{DAg} = 1.9$ eV, we find $U_{L^*}^V \cdot b = 0.057$ eV with $\mu_V = 3.38 \cdot 10^{11}$ dyn/cm² (Voigt average), and $U_{L^*}^V \cdot b = 0.043$ eV with $\mu_R = 2.56 \cdot 10^{11}$ dyn/cm² (Reuss average) (Table V-2). In this table, the corresponding activation energies E^* as found from Eq. (V-6) are given for $T = 900^\circ\text{K}$ and two L values.

Table V-2. The activation energies for V-ledges.

μ $\cdot 10^{11}$ dyn/cm ²	$U_{L^*}^V \cdot b$ eV	$E_{L=289\text{Å}}^*$ eV	$E_{L=578\text{Å}}^*$ eV
3.38	0.057	4.2	6.5
2.56	0.043	2.8	3.7

Here we can see the importance the choice of μ , and we have to realize that anisotropy will influence the value of μ .

Furthermore, quantitative calculations involving configurations of core dimensions are questionable. This is especially so in this case with a dislocation dipole with anti-parallel Burger's vectors one atomic distance apart. Anyway, one will expect this configuration to have a low

energy. Our estimates of the activation energy are in a range suggesting that this ledge mechanism should not be ruled out at all. It might be operative even for medium sized SFT.

The nucleation of obtuse ledges from a corner can not be ruled out either. Even if the energy of the I-ledge is 2.5 times the energy of the V-ledge (per atomic plane), it would be quite probable to believe that the critical nucleation energy would be reached for a L^* less than the total edge length L . One argument for this is the net attractive forces between this ledge and the edge (Cotterill and Doyama, 1964). Also, calculating U_L^I the same way as U_L^V gives $U_L^I = \sqrt{2} U_L^V$.

A third ledge mechanism might be the configuration shown in Fig. II-9, with acute ledges. This again can represent a critical nucleus with a size less than the whole edge length L . Once more, due to the configuration being of core dimensions, no attempt to assess this possibility quantitatively has been done (Hirth and Lothe, 1968).

Finally, it might also be mentioned that the ledge mechanism is thought to be operative in cases of precipitation and dissolution of such (Aaronson et al., 1970).

Extended Frank loops must disappear by shrinkage; by climb of the dislocations bounding the faulted area. In order for this climb to proceed it is commonly believed that jogs must form at the corners, and that the 60° corner is a stable configuration representing an activation barrier for "unzipping", i.e., splitting up the stair rod dislocation common to the extended dislocations. Yokota (1968) shows that the active corners for climb should be 120° corners rather than 60° corners, as the extended dislocations are constricted at the 120° corners.

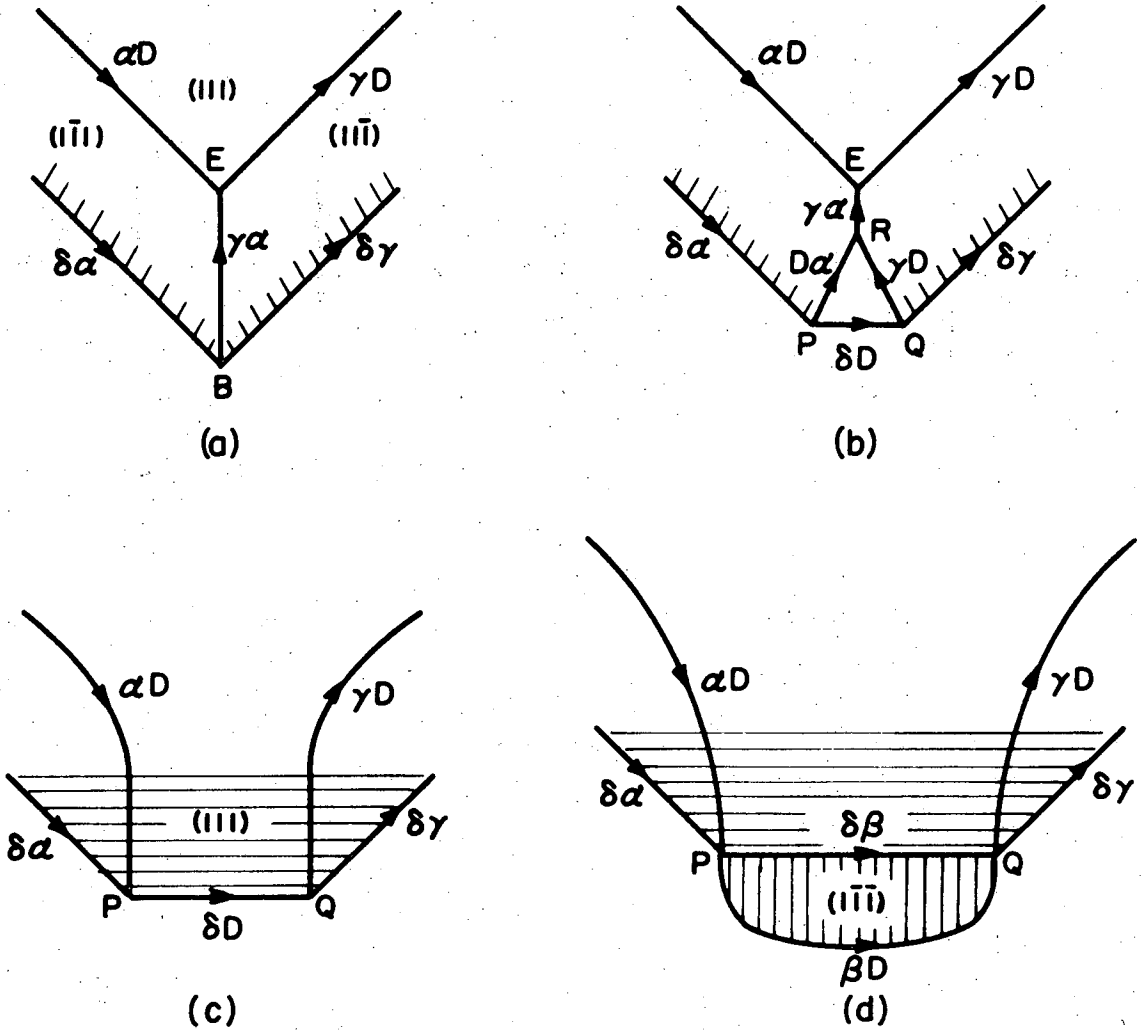
The different configurations that the 60° and the 120° corners can have are shown in Fig. V-5.

Escaig (1970b) calculated an energy minimum for a corner blunted by emission of three vacancies (Fig. V-5b). For gold we would rather get the situation similar to Fig. V-5c due to less dissociation. In silver further "unzipping" is necessary and Escaig calculated an energy barrier of about 3-4 eV to nucleate a critical length PQ^* which together with U_D gives an activation energy of about 5-6 eV which is too high to explain the shrinkage of loops in silver (Smallman et al., 1968) at about 600°C , which also is observed by us.

As the whole configuration is of core dimensions it is difficult to calculate the energy. It might be considerably less than calculated by Escaig (1970b) especially considering the rather low values estimated for the energy of ledges.

As soon as the corner is "unzipped" further climb should take place provided that jogs can nucleate and that the vacancy can migrate. As long as the Frank dislocation PQ is undissociated, jogs would preferably nucleate here. PQ would probably stay undissociated if several jogs inhabit PQ . This can explain the shrinkage we have seen.

So far, all calculations have assumed a constant stacking fault energy γ . However, it is quite natural to believe that γ is a function of the temperature. Most of the energy barriers calculated for collapse of SFT would be lowered with increasing temperature if γ increases with T (Jössang, 1968). Unfortunately very little is available concerning the behavior of γ with T . Ericson (1966) has observed the temperature



XBL 735-6107

Fig. V-5. Details of a corner of a extended Frank loop on (111). PQR is unfaulted.

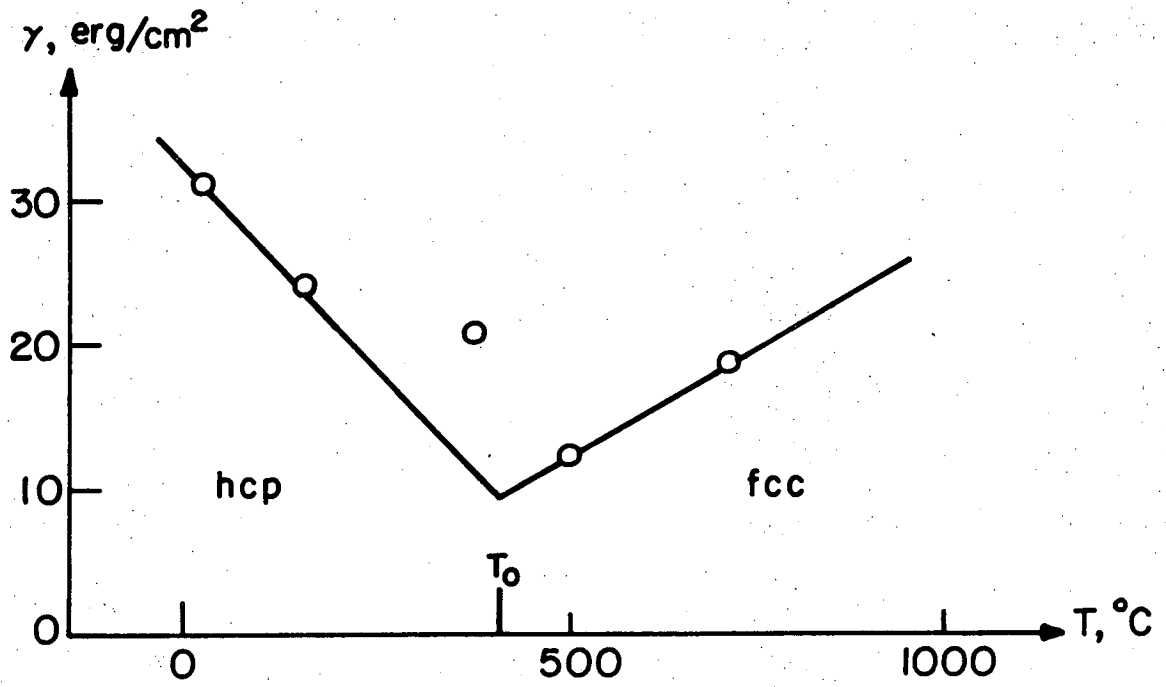
dependence of γ in Co, and finds an increase in γ with T in the temperature range 420°C to 700°C (Fig. V-6).

However, Co has a phase transformation from hcp to fcc at about $T_G = 420^\circ\text{C}$ with fcc as the high temperature phase up to $T_m = 1495^\circ\text{C}$. In the hcp phase, γ decreases with increasing temperature, 20°C to 420°C.

On the other hand, comparison with surface tension suggests a decrease in γ with increasing T , and it might be that γ in Co decreases in the high temperature region of the fcc phase, $T > 1000^\circ\text{C}$. To calculate γ involves a knowledge of the interaction potential to better than 1% uncertainty, which we do not have.

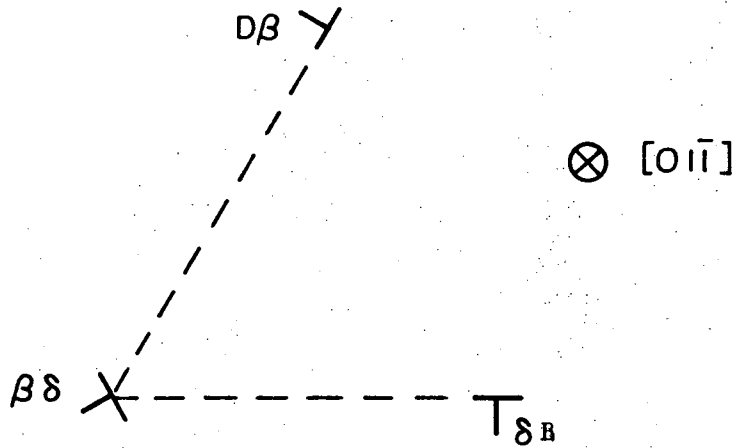
The present investigation of γ as a function of temperature did only give an indication, if any, that γ decreases with increasing temperature.

In calculations of γ or the energies of various defects it must be realized that the isotropic elasticity theory used is only an approximation as most metals are anisotropic (Hirth and Lothe, 1968; Jössang et al., 1965). Using anisotropic theory, Jössang et al. (1965) report a 1.22 times larger dissociation width d than the isotropic value, in the case of the barrier shown in Fig. V-7. In silver this would be $d_a = 26\text{\AA}$ anisotropic with $d_i = 21\text{\AA}$, isotropic. In the case of the dissociated screw-dislocation $d_a = 0.62 d_i$ with $d_i(\text{Ag}) = 30\text{\AA}$, and in the case of the dissociated edge dislocation, $d_a = 0.83 d_i$ with $d_i(\text{Ag}) = 76\text{\AA}$. Thus, in measuring the dissociation width experimentally, anisotropic elasticity theory must be used in determining γ . The differences in energies might be as large as a factor of 4. However, as the anisotropy



XBL 735-6103

Fig. V-6. The stacking fault energy γ in Co as a function of T .



XBL 736-6250

Fig. V-7. A dislocation barrier consisting of a $\beta\delta$ stair rod dislocation and two Shockley dislocations $D\beta$ and $\beta\delta$.

effect on the stacking fault energy γ varies with the directions at the dislocations, giving both higher or lower γ than the isotropic γ , it is not expected that the energy of the SFT should be much affected by the anisotropy effect (Jössang, 1972).

Finally, in calculating the energy barriers and activation energies one should consider the whole system, or at least not one single defect as a closed system. Even if the energy of the defect goes through a high maximum one might consider a lowering of the energy of the surrounding system, which is very difficult to calculate. Knowing, for example, the chemical potentials of the vacancies would be important, but in the present case we do not have this knowledge.

SUMMARY

The size ranges of faulted defects in gold and silver has been discussed, along with the different energy barriers involved in the collapse and/or shrinkage of these defects. It seems to be fairly well established that the annealing out of the faulted defects in gold does not pose any problem. For silver, however, the case is a little more complicated.

It is proposed that the ledge mechanisms are probable mechanisms for shrinkage of SFT, and in the case of collapse, nucleation of a Shockley loop near the corner instead of in the middle of the face might be energetically feasible. Escaig's modified nucleation theory can not be operative, but his suggestions regarding shrinkage of loops from one corner seems to be within reasonable ranges energetically.

It is emphasized that the calculations involving dislocation configurations of core dimensions can only be roughly approximative. This together with complications with regard to anisotropy and the value of the stacking fault energy, makes attempts to assess the possibilities quantitatively very questionable.

"So we can say then that the sum of the relationships of all our experiences is always tetrahedral . . ."

R. Buckminster Fuller
Utopia or Oblivion

VI. CONCLUSION

A study of the annealing of quenched-in stacking fault tetrahedra (SFT) and extended faulted Frank loops (FT) in thin foils of silver by hot stage high voltage transmission electron microscopy has shown:

- Quenched-in defects are SFT with edge sizes up to 2000\AA and FT (triangles) with edge sizes in the range 650\AA to 1350\AA .
- SFT in the size range $L < 600\text{\AA}$ shrink as SFT during anneals above 600°C .
- SFT may completely anneal out above 600°C .
- Collapse of a large SFT, $L \sim 2000\text{\AA}$ has been observed directly at 300°C .
- Loops might shrink from one corner during anneal.

As the experimental evidence shows collapse and/or shrinkage of SFT and FT in silver, Escaig's predictions are verified. However, the following theoretical points must be considered:

- Escaig's modified nucleation theory must be disregarded as it is not in accordance with thermodynamic laws.
- Calculations of energy-barriers might be questionable in several cases, considering that corner configurations often are of core dimensions, that the stacking fault energy might be a function of the temperature, that anisotropic elasticity theory should be applied in most cases and that the energy of the whole system should be considered.

Based on the preceding, the following conclusions are drawn for the annealing behavior of SFT and FT's:

- The sizes of the quenched-in defects are in the expected range following the theoretical calculations.
- Collapse by glide of three Shockley's from one corner must most likely be ruled out both in Ag and in Au.
- Collapse by climb and glide from one 120° corner is possible for SFT in Au, but unlikely in Ag.
- Collapse of SFT in Ag might occur by nucleation of a Shockley glide loop near one corner.
- Shrinkage is probable for relatively small SFT in Ag and in Au by the ledge mechanisms.
- Shrinkage of FT's can take place from a 120° corner in silver as well as in gold.

Further work should include:

- Quantitative observations of the collapse and shrinkage in order to measure the activation energy.
- Observations of eventual climb of the loops by jogs.
- Determination of the variation of the stacking fault energy with temperature by node measurements and by using the weak beam technique (Cockayne et al., 1969).

ACKNOWLEDGEMENTS

I wish to express my sincere gratitude to Professor Jack Washburn for his guidance, penetrating questions and patience during this investigation. I would also like to thank Professor Gareth Thomas for his interest and helpful suggestions.

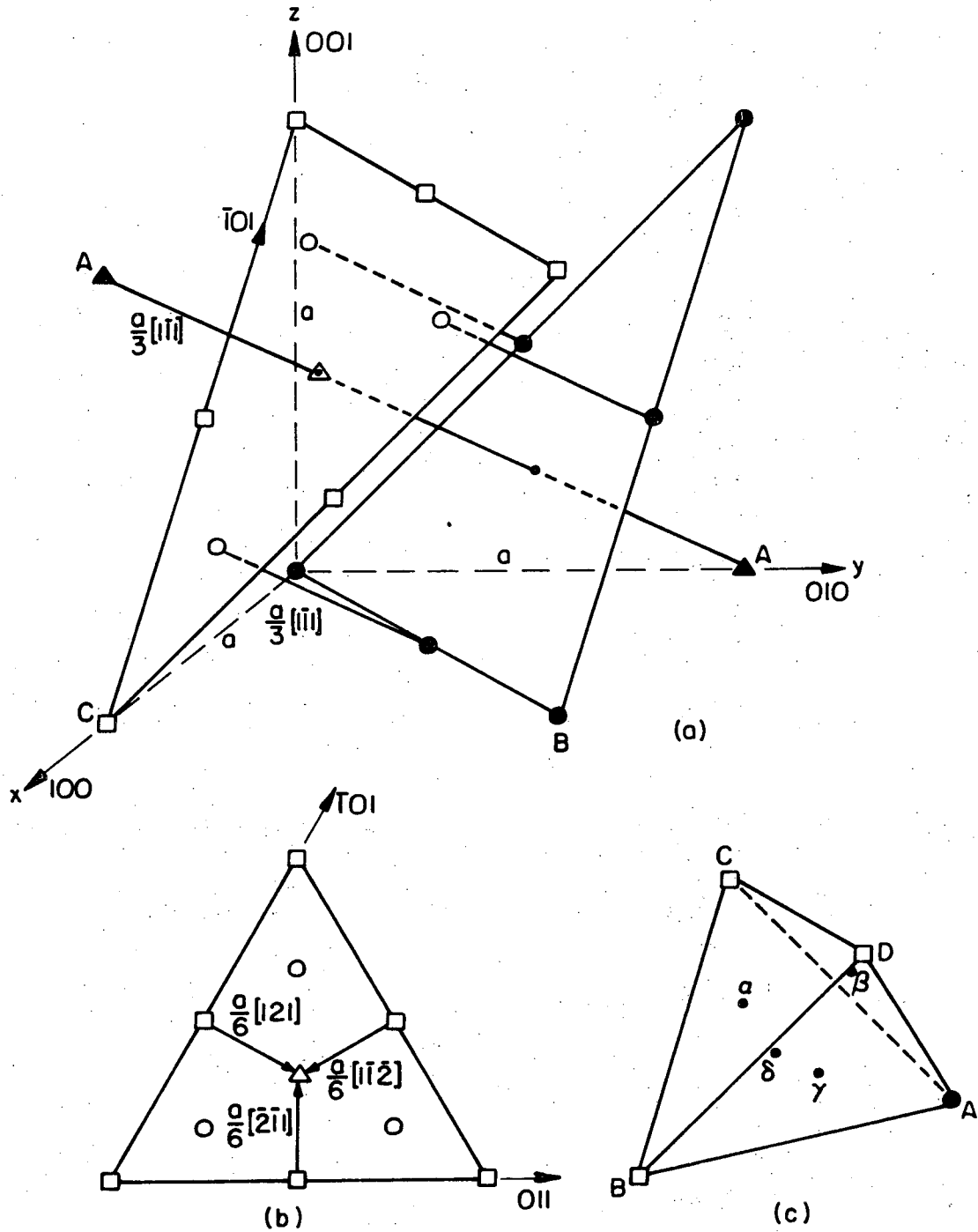
Special thanks for stimulating discussions are also due to Drs. J. Lothe, T. Jössang, J. Feder, L. DeJonghe and Mr. K. Seshan. Without the help of the support staff at the EM lab and at IMRD, this work would not have been possible. However, timewise the conclusion must be drawn: Never tell anybody that you are not in an extreme hurry, otherwise all others will be in more of a hurry than you, . . . The encouragement of Gail Fredell during difficult moments contributed to, amongst other results, the saving of a certain EM from violent demolition.

Partial financial support from the Norwegian Research Council for Science and the Humanities are deeply appreciated. Finally, the financial support of the U. S. Atomic Energy Commission through the Inorganic Materials Research Division of the Lawrence Berkeley Laboratory is acknowledged.

APPENDIX 1. EXTENDED DISLOCATIONS AND JOGS

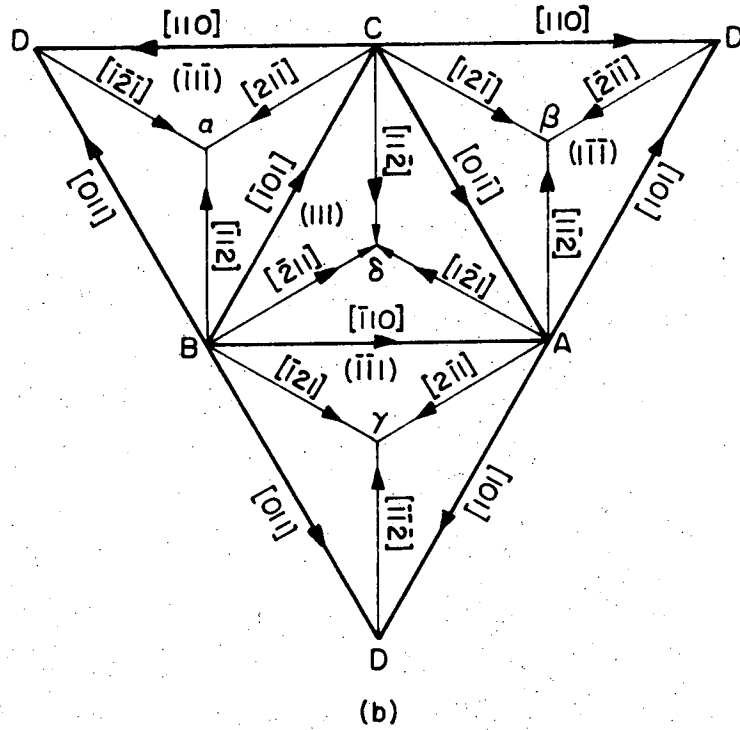
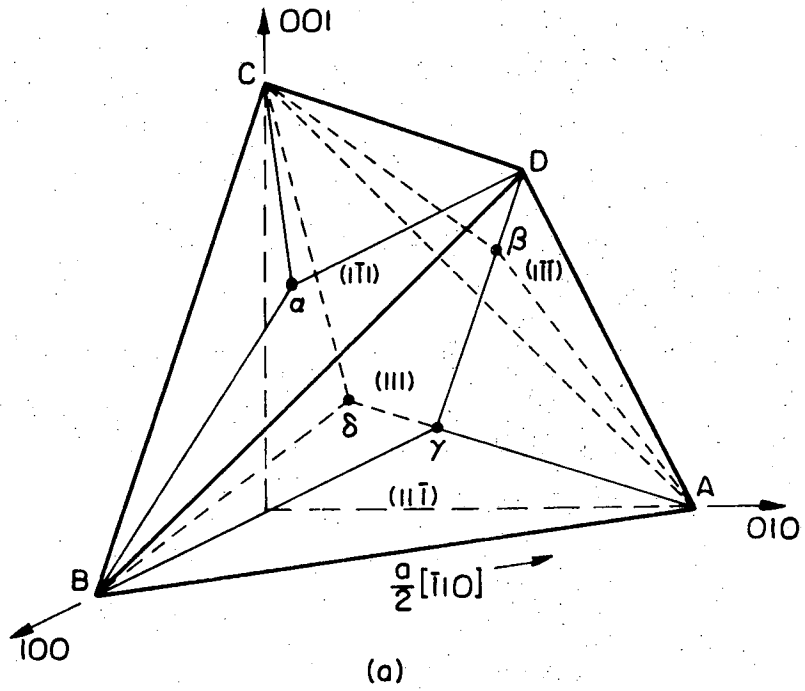
The stacking sequence of the close-packed {111}-planes in the fcc structure can be described by ABCABCABC. Here A, B and C refer to the three possible layer positions in a projection normal to the close-packed layers (Fig. A1-1). (If one layer of atoms, e.g., a B-layer, is removed from the normal sequence, an intrinsic stacking-fault is created and the stacking sequence becomes ABCACABC. Here we see that across the fault the C positions are above each other with only one layer between and the same is the case with the two A layers across the fault. Looking at the (111̄)-planes in Fig. A1-1, the displacement is $\pm \frac{a}{3}[111]$, +-ve when the -(111̄)-side of the fault is displaced relative to the +(111̄)-side and vice versa, --ve when the +(111̄)-side is displaced relative to the -(111̄)-side. This is equivalent to shearing or displacing the crystal on the +-ve side of the fault by $\frac{a}{6}[\bar{2}11]$, $\frac{a}{6}[1\bar{1}\bar{2}]$ or $\frac{a}{6}[121]$. (αC , αB or αD in the Thompson notation, Fig. A1-2) (or αA). All displacements outside the Thompson tetrahedron faces having a vector starting with a greek letter with magnitudes within the tetrahedra, will give an intrinsic fault.

If the crystal on the outside of this Thompson tetrahedron is displaced by the opposite vectors, i.e., vectors starting with a capital



XBL736-6225

Fig. A1-1. (a) The sequence of close packed $(1\bar{1}1)$ -planes in fcc. ABCAB... in the $[1\bar{1}1]$ -direction. (b) The A and B positions are projected on the C-plane. (c) The Thompson tetrahedron.



XBL736-6226

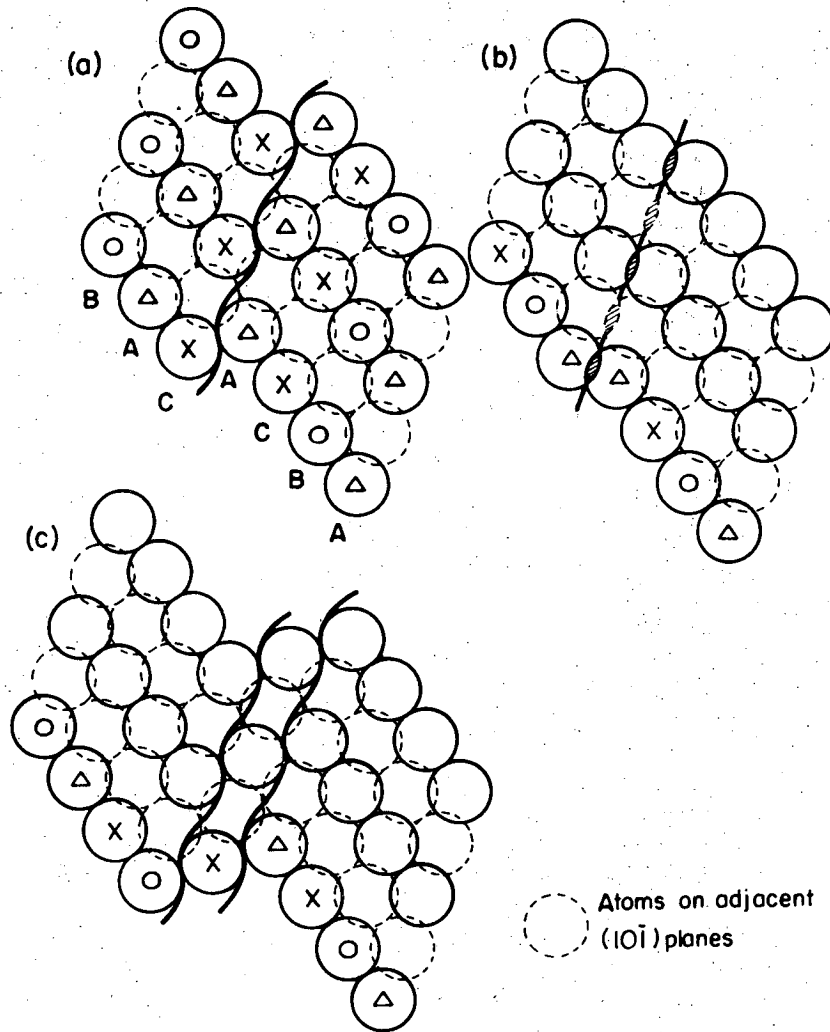
Fig. A1-2. (a) The Thompson tetrahedron with notations. α is the projection of A on the plane opposite A, β is the projection of B on the plane opposite B, and so one. (b) The tetrahedron opened up at D. All the planes are seen from the inside.

letter, a high energy fault is created. E.g., the displacement $C\alpha$, $B\alpha$, $D\alpha$ or $A\alpha$ of the crystal on the +ve side of the $(\bar{1}\bar{1}1)$ fault creates a stacking sequence $ABCA\downarrow ABC$ in violation of close packing on the fault plane. The displacement $A\alpha$ is due to inserting an extra plane A. The same fault can be created by removing two planes, B and C, and the displacement would be $2\alpha A$.

If the extra layer A is changed to a C layer, we get the sequence $ABC\downarrow ACBC\dots$ which is classified as an extrinsic stacking fault with the displacement $A\alpha$ of the crystal on the +ve side of the fault. By displacements on the $(\bar{1}\bar{1}1)$ -planes two shearing operations are needed. E.g., αB of all the planes above the fault and a new operation αB (or αC or αD) of all the planes above the fault from the next nearest plane and on. The three different types of faults are shown in Fig. A1-3.

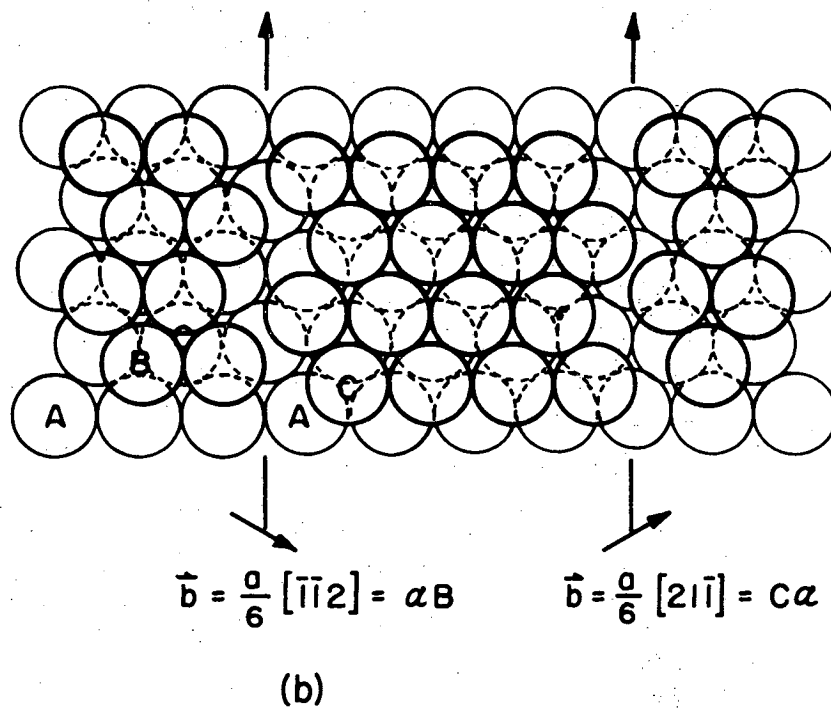
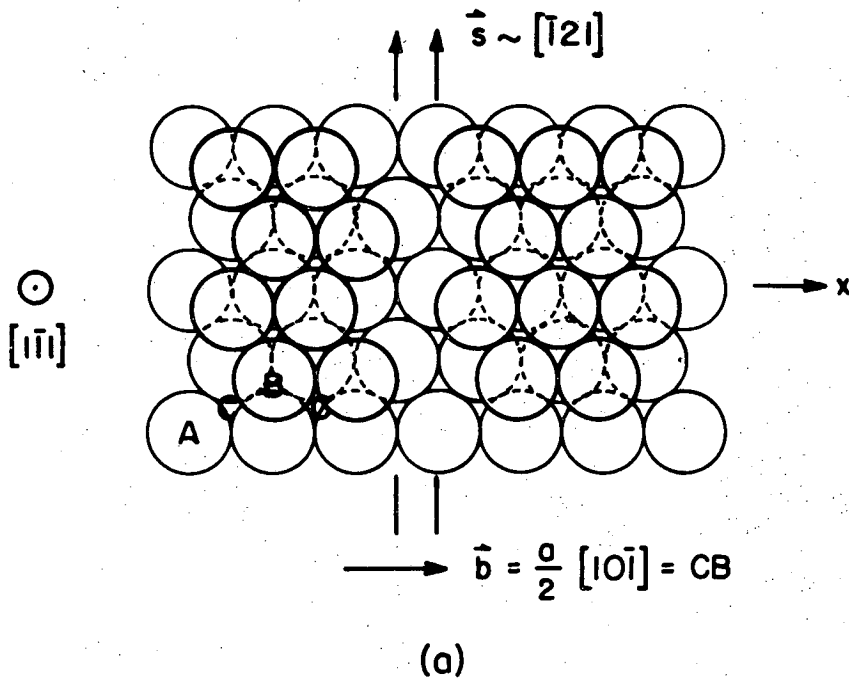
The shear causing the displacement of the type $\frac{a}{6}\langle 112 \rangle$ can be produced by a partial dislocation. Partial dislocations of this type, $\frac{a}{6}\langle 112 \rangle$ are called Shockley partials and are glissile on the $\{111\}$ -planes.

In a fcc metal with low stacking fault energy γ , a perfect dislocation $\bar{b} = \frac{a}{2}\langle 110 \rangle$ (AB and so on in Thompson's notations) will dissociate into two Shockley partials enclosing a stacking fault. This is shown in Fig. A1-4. A perfect $\frac{a}{2}\langle 110 \rangle$ -dislocation in fcc is actually made up by parts of two extra $\{110\}$ -planes, which occurs in a ABABAB... sequence. These two extra planes can move independently and movement of one gives the displacement $\frac{a}{6}\langle 112 \rangle$. The sequence of the partial dislocations is important as it determines the nature of the fault (intrinsic or extrinsic).



XBL736-6227

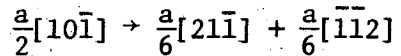
Fig. A1-3. A cut along the $(10\bar{1})$ -plane showing the stacking sequence across; (a) An intrinsic fault. (b) A high-energy fault. (c) An extrinsic fault. A, B and C the $(1\bar{1}1)$ -layers.



XBL 735-6109

Fig. A1-4. The dissociation of the edge-dislocation CB into Shockley partial dislocations enclosing an intrinsic fault. The extra (101)-planes are under the paper plane.

The situation in Fig. Al-4 shows an intrinsic fault made by the dissociation of the perfect edge dislocation $\vec{b} = \frac{a}{2}[10\bar{1}] = CB$ into the two Shockley partials $C\alpha$ and αB after the following reaction:



or



The vectorial product of the sense \vec{s} of the dislocation and of the direction \vec{x} it is moving; $\vec{s} \times \vec{x}$, points into the side of the fault where the crystal is displaced by the Burgers vector \vec{b} . With the directions given in Fig. Al-4, the crystal on the lower $[\bar{1}\bar{1}\bar{1}]$ -side of the fault is displaced by \vec{b} relative to the upper part.

Climb

The dissociated or extended dislocation can climb by vacancy absorption or emission by the creation and motion of jog lines (extended jogs). Figure Al-5 shows a pair of jog lines, ABCD and EFGH, created by emission of one row of vacancies along BG or AH. All the enclosed faults are intrinsic in this figure.

The partial dislocations $\delta\alpha$ and $\alpha\delta/CB$ are sessile stair-rod dislocations given by the reactions

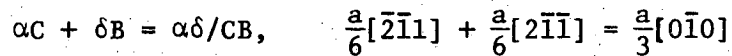
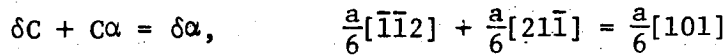
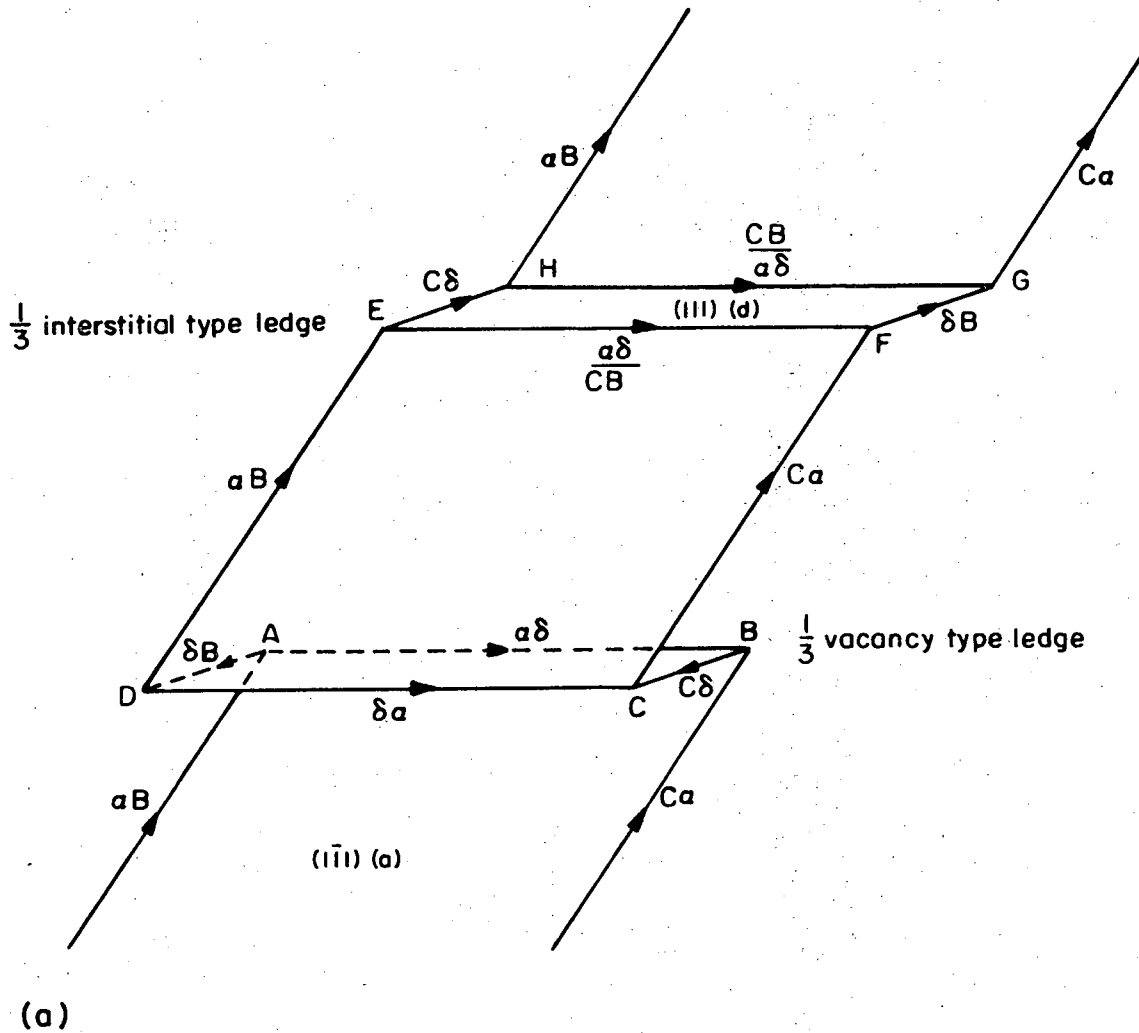


Figure Al-6 schematically shows a cut along the $(10\bar{1})$ -plane with the width of the joglines larger than 1 atomic distance in order to make the Burgers circuits clear. The ledge made by the $\alpha\delta$ - $\delta\alpha$ pair is acute and of the $\frac{1}{3}$ -vacancy type (Fig. Al-7a), while the ledge enclosed by the



XBL736-6228

Fig. A1-5. Climb of an extended dislocation; $(\alpha B + C\alpha)$, by giving off one row of vacancies along BG or AH , creating a pair of joglines $ABCD$ and $EFGH$. The senses of the dislocations are given by the arrows, and the Burgers vectors are in Thompson notations.

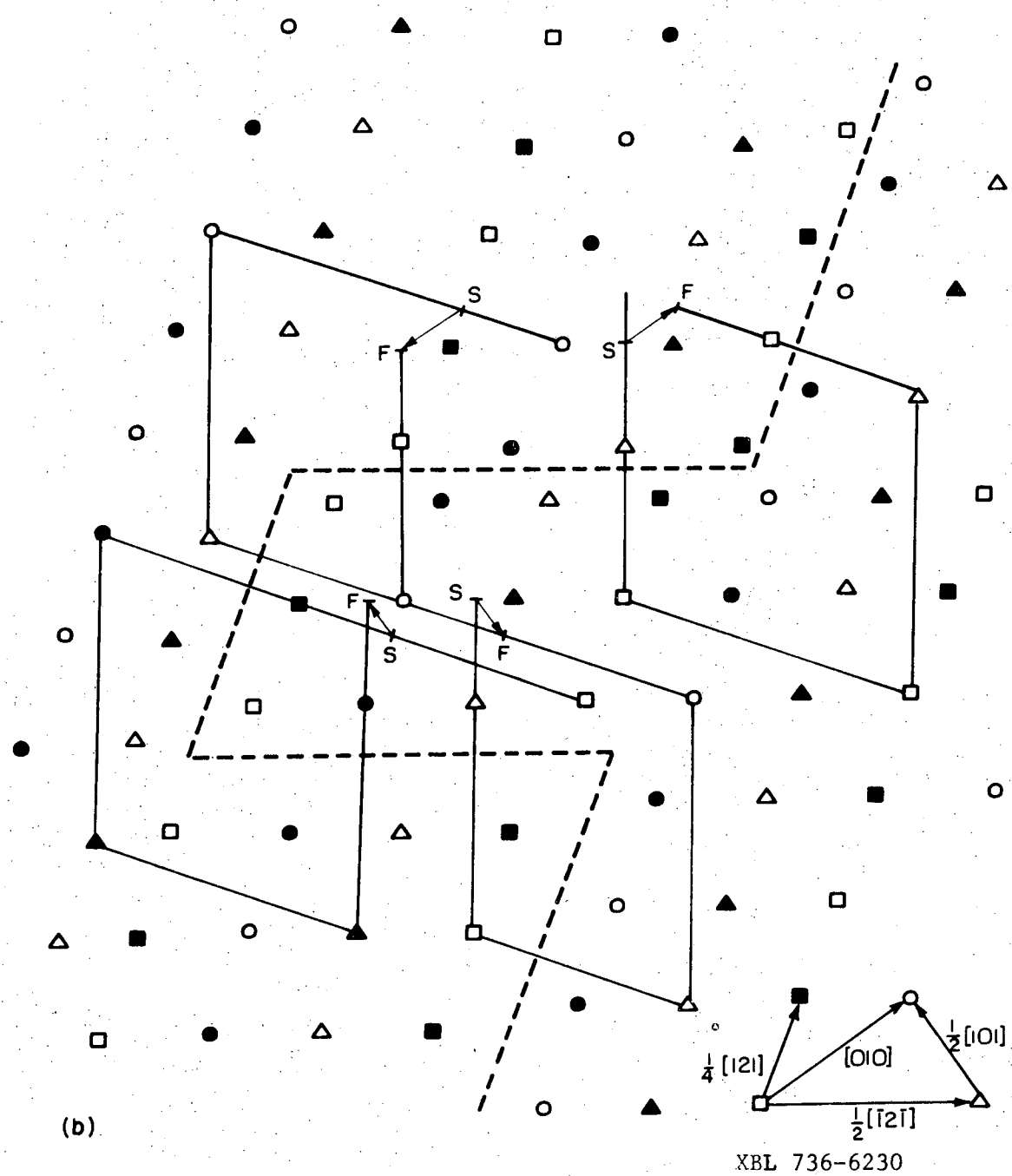
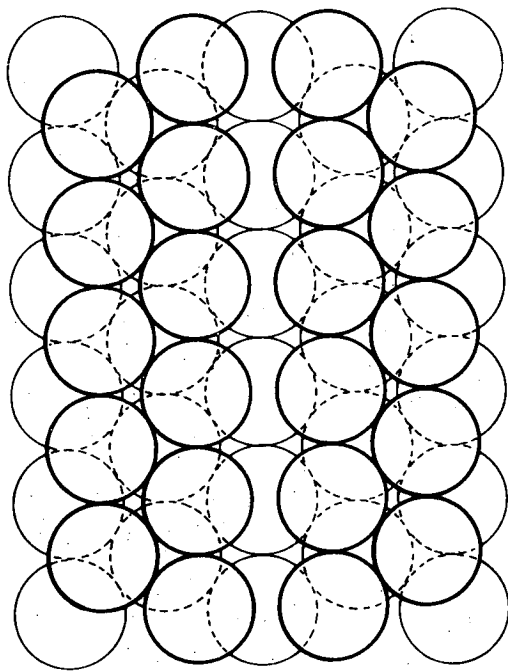
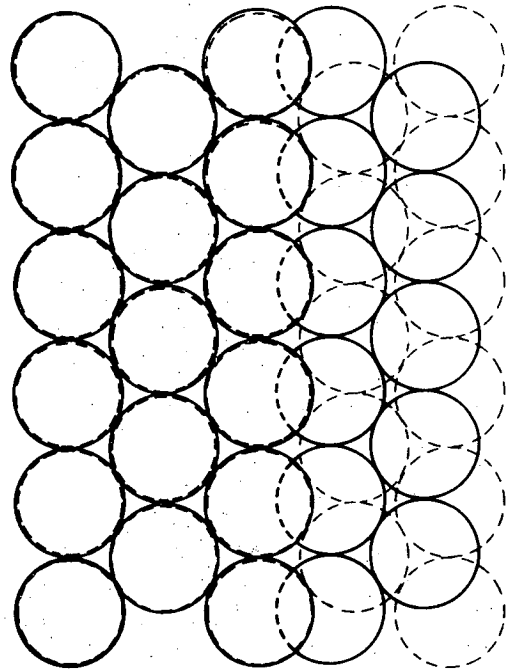


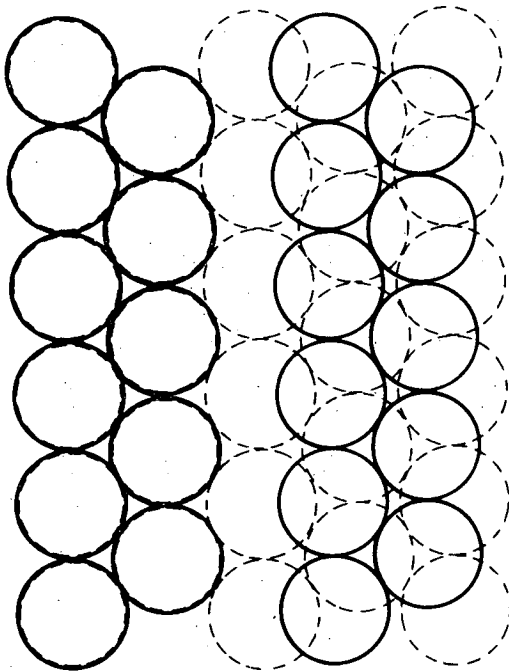
Figure A1-6. Schematic cut on the $(10\bar{1})$ -plane along the faulted area of Fig. A1-5. The dotted line is the cut through the fault plane. Also shown are the Burgers circuits around the dislocations in the $(10\bar{1})$ -direction. All faults are intrinsic. The filled marks represents sites above and below the paper plane. The directions are in the $(10\bar{1})$ plane.



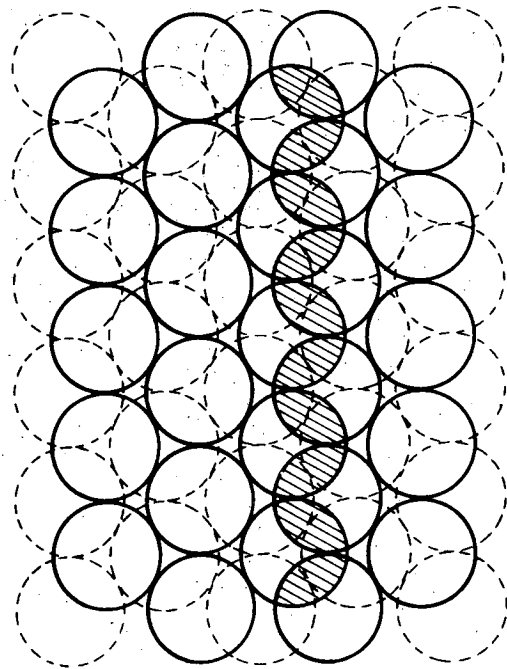
a



b



c



d

ABL 755-0094

Fig. A1-7. (a) A row of $1/3$ vacancies in the layer of outlined atoms. (b) A row of $1/3$ interstitials. (c) A row of $2/3$ vacancies. (d) A row of $2/3$ interstitials. Drawn are two (111)-layers above each other.

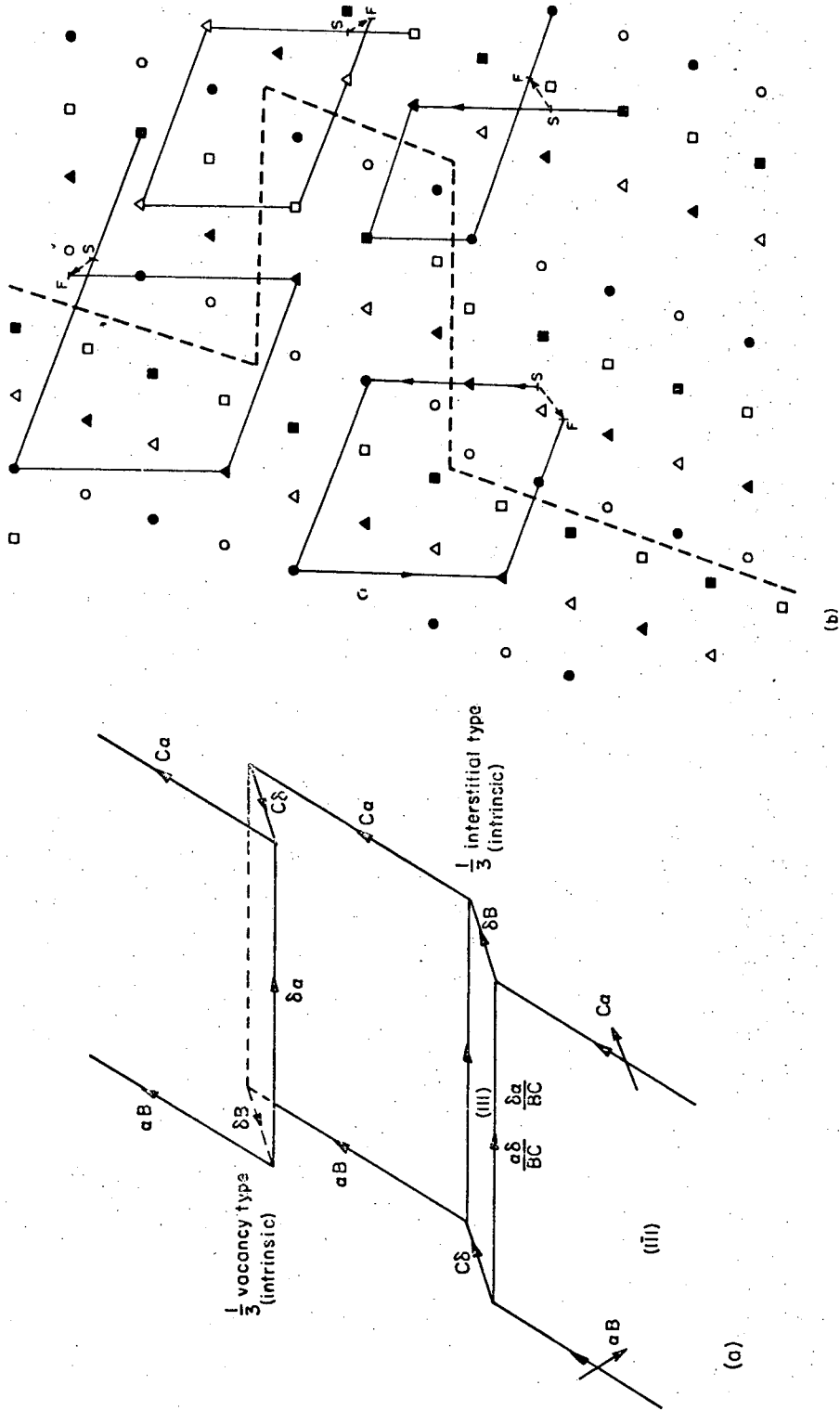
$\alpha\delta/\text{CB}-\text{CB}/\alpha\delta$ pair is obtuse and of the $\frac{1}{3}$ -interstitial type (Fig. A1-7b).

Pairs of jog lines created by vacancy absorption are shown in Figs. A1-8 and A1-9. In Fig. A1-8 the extended jogs are intrinsic faults while the ledges in Fig. A1-9 are high energy faults. In all these three cases, the acute ledges are of the $\frac{1}{3}$ -vacancy type and the obtuse ledges are of the $\frac{1}{3}$ -interstitial type.

Loops and SFT

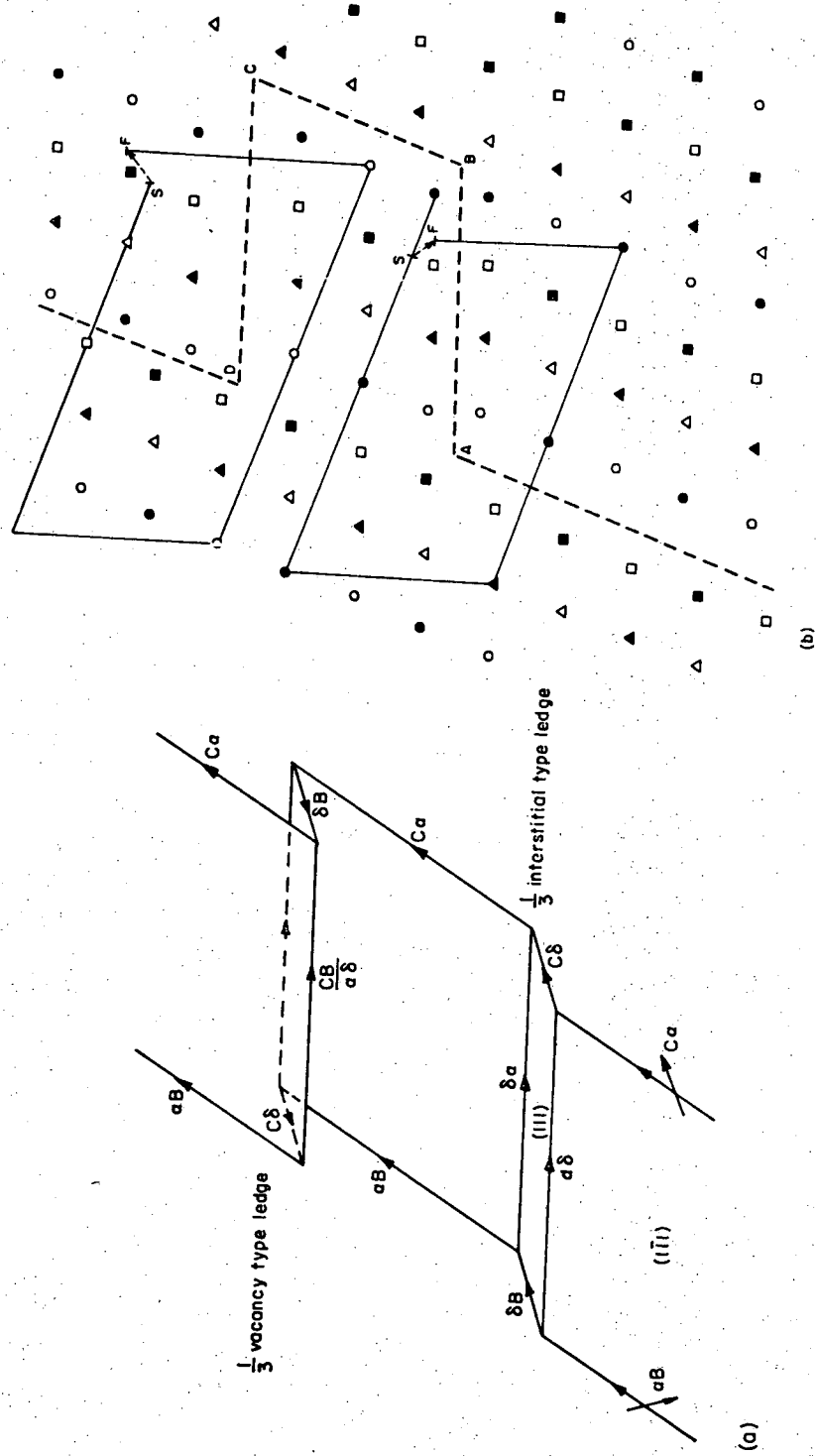
A missing part of a $\{111\}$ -plane created for example by a vacancy disc, would result in a stacking fault (intrinsic) enclosed by a $\frac{a}{3}\langle 111 \rangle$ -type Frank partial dislocation. The loop shown in Fig. A1-10a,b is a sessile Frank loop created by a collapse of a vacancy disc on the (111) -plane. The Burgers vector is $\vec{b} = \frac{a}{3}[111] = \delta D$ (Fig. A1-12a). The nucleation and motion of a Shockley loop, e.g., $B\delta$ in Fig. A1-10c, would unfault the faulted loop and create a perfect dislocation loop $\vec{b} = BD = \frac{a}{2}[011]$, $\delta D + B\delta = BD$. In Fig. A1-11a,b is shown a interstitial Frank loop $D\delta$, Fig. A1-12b. It is necessary to nucleate and move two Shockley loops on adjacent planes below the fault to unfault this loop, Fig. A1-11c. The reaction is $D\delta + C\delta + A\delta = DB = \frac{a}{2}[0\bar{1}\bar{1}]$. The resultant of the two Shockley loops, $C\delta + A\delta = \delta B$, makes an operation that is not allowed in one step.

The Frank partial can dissociate into a stair rod and a Shockley partial with the reaction $\delta D = \delta\alpha + \alpha D$, $\frac{a}{3}[111] = \frac{a}{6}[\bar{1}01] + \frac{a}{6}[121]$ (Fig. A1-13). This is the reaction creating a dissociated Frank loop and finally a stacking fault tetrahedron (Fig. A1-14).



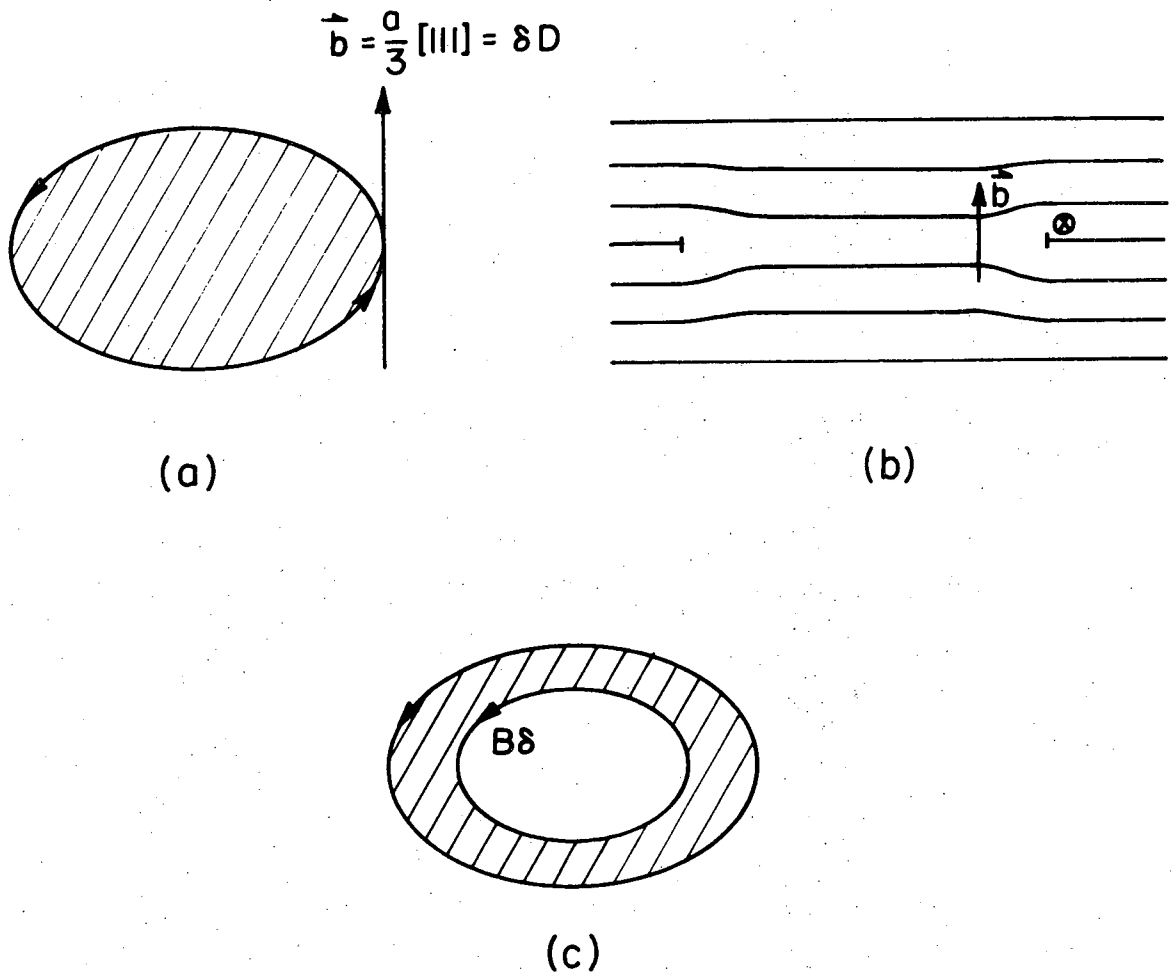
XBL736-6232

Fig. A1-8. (a) Climb of an extended dislocation, $(\alpha B + C\delta)$, by the absorption of a row of vacancies, creating a pair of joglines. The acute ledge is of the $\frac{1}{3}$ vacancy type, while the obtuse ledge is of the $\frac{1}{3}$ interstitial type. All the faults are intrinsic. (b) A cut on the (101) -plane across the fault. For clarity the ledges are several atomic distances deep.



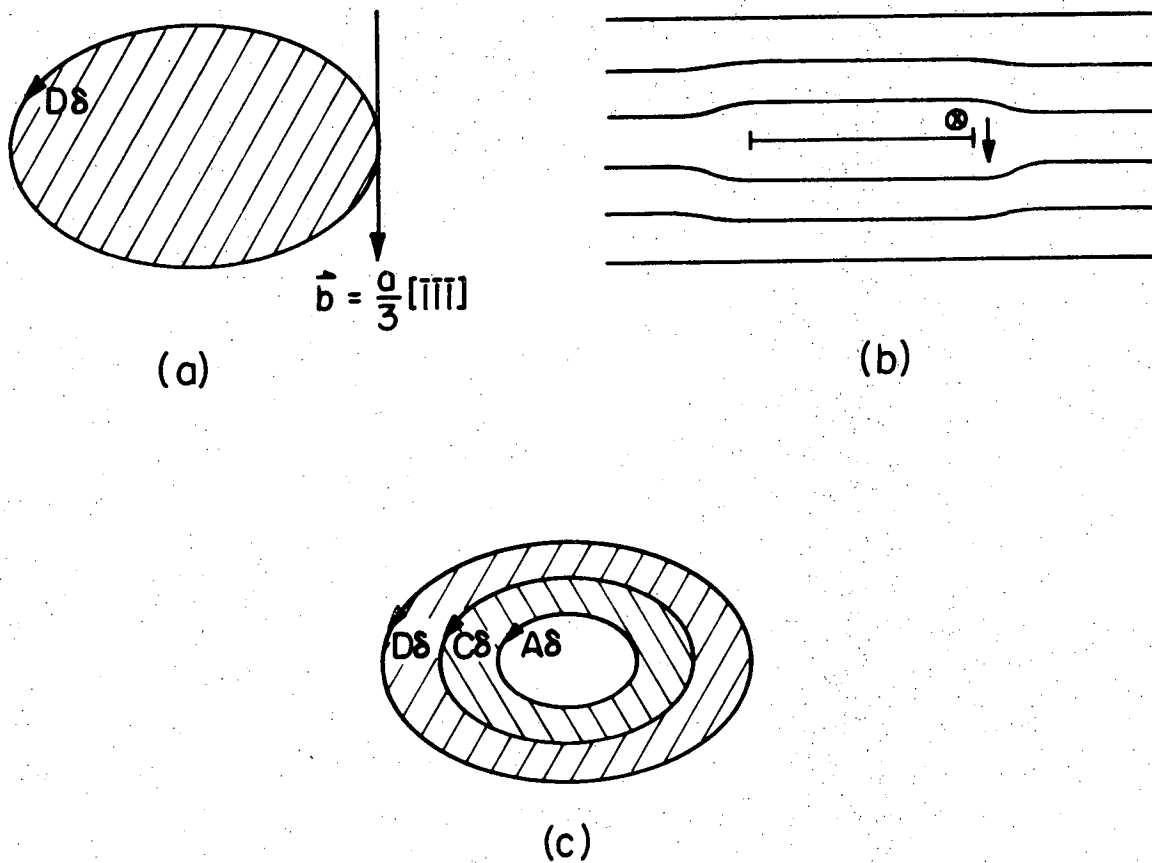
XBL736-6233

Fig. A1-9. (a) Climb of an extended dislocation, $(\alpha B + C\alpha)$, by the absorption of a row of vacancies, creating a pair of joglines. The ledges in this case are high-energy faults. (b) A cut on the (101) -plane across the fault. The displacements over the cuts AB and CD of the ledges represents high-energy faults.



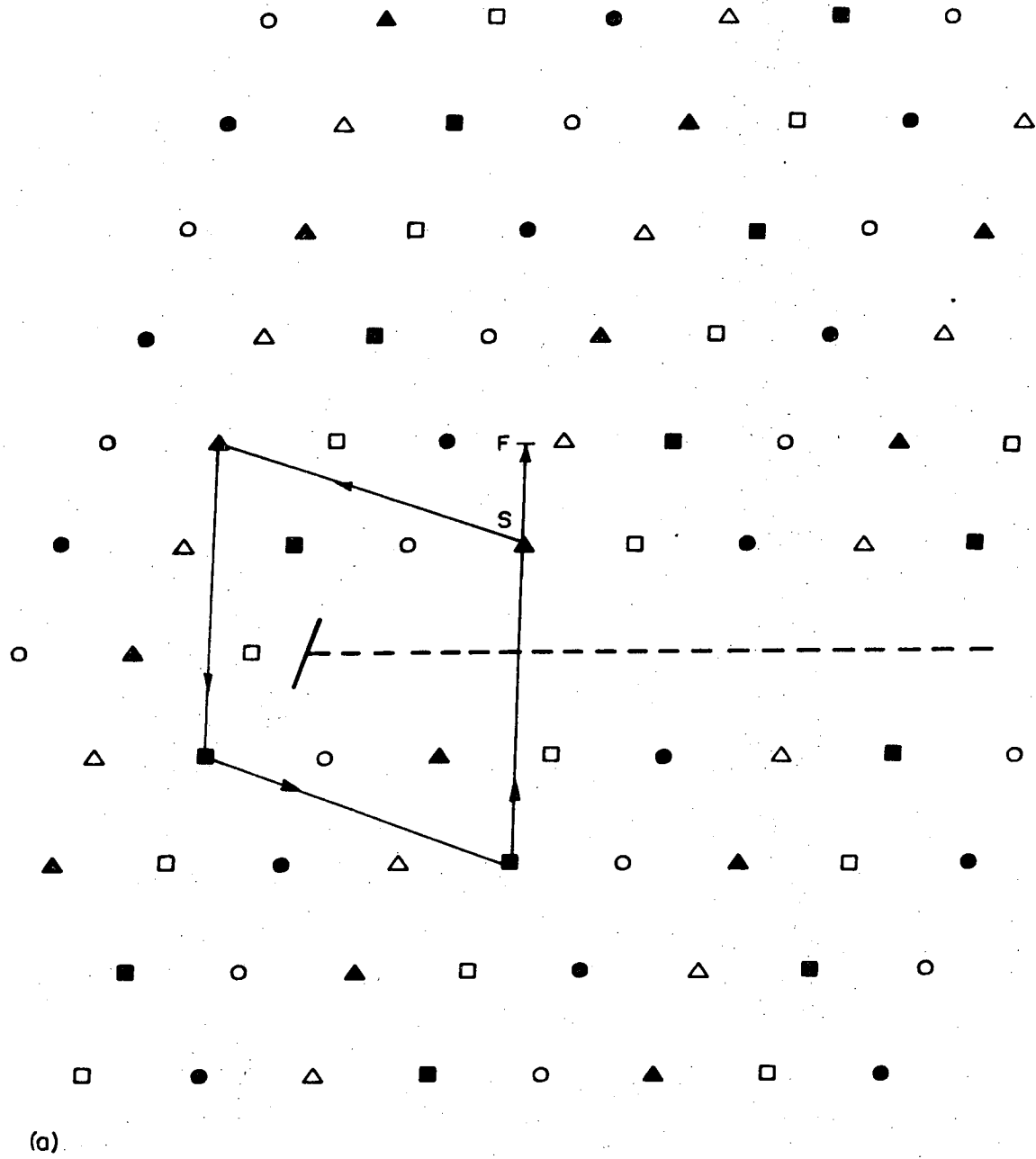
XBL 735-6095

Fig. A1-10. (a) A vacancy type Frank loop on the (111)-plane. (b) A cut through the loop. (c) The loop being unfaulted by a Shockley loop. The sense \vec{s} is marked by arrows along the dislocations.



XBL 735-6096

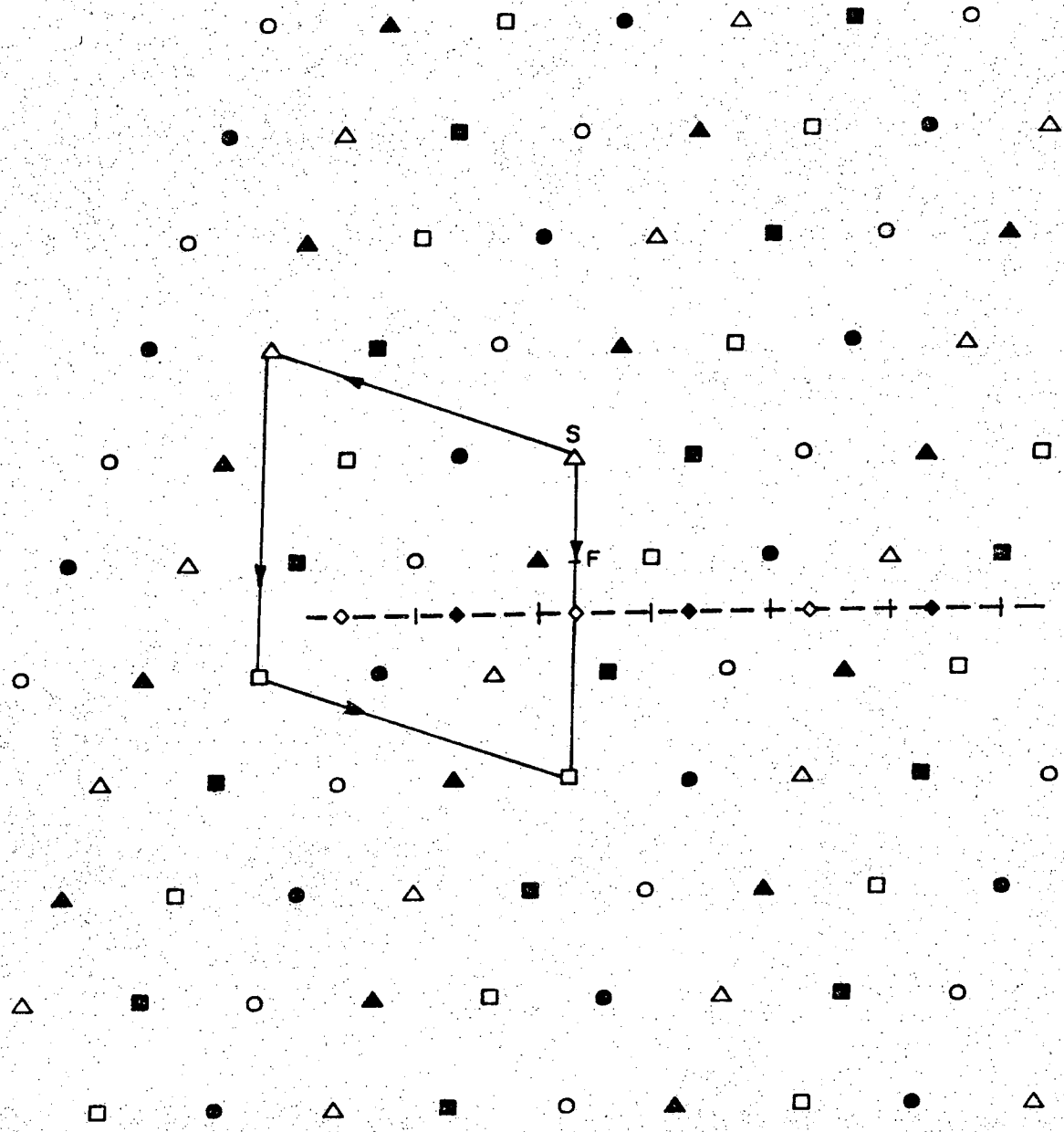
Fig. A1-11. (a) An interstitial type Frank loop on the (111)-plane. (b) A cut through the loop. (c) The loop being unfaulted by two Shockley loops. The sense \vec{s} is marked by arrows along the dislocations.



(a)

XBL 736-6270

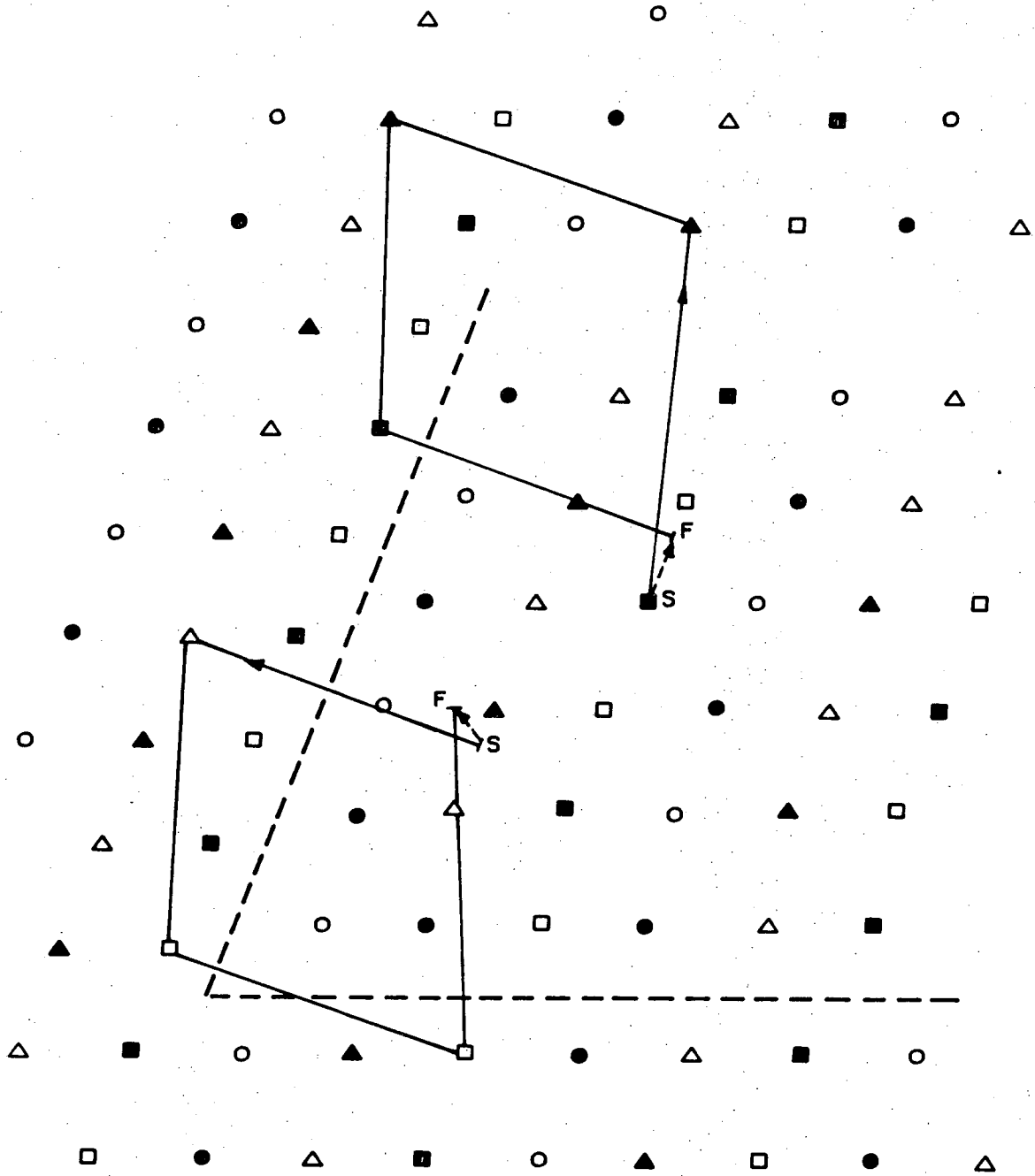
Fig. A1-12. (a) A cut on the $(10\bar{1})$ -plane through the edge of the Frank loop in Fig. A1-10. An intrinsic SF.



(b)

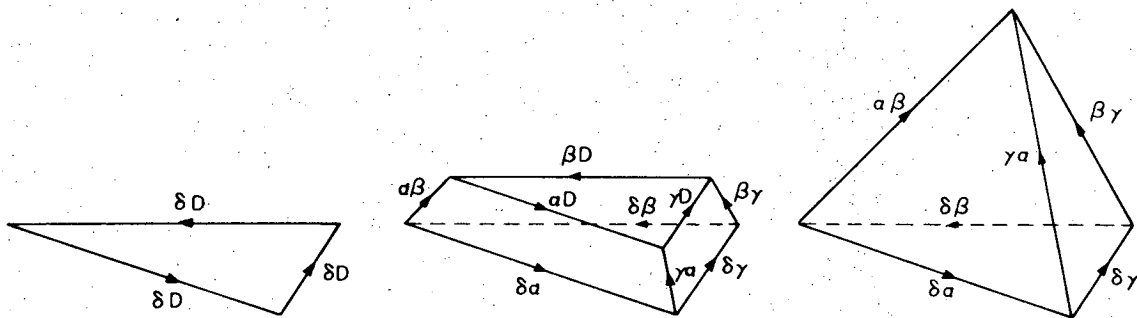
XBL 736-6234

Fig. A1-12. (b) A cut on the $(10\bar{1})$ -plane through the edge of the Frank loop in Fig. A1-11. An extrinsic SF.



XBL736-6235

Fig. A1-13. A cut on the $(10\bar{1})$ -plane through the edge of a dissociated Frank loop.

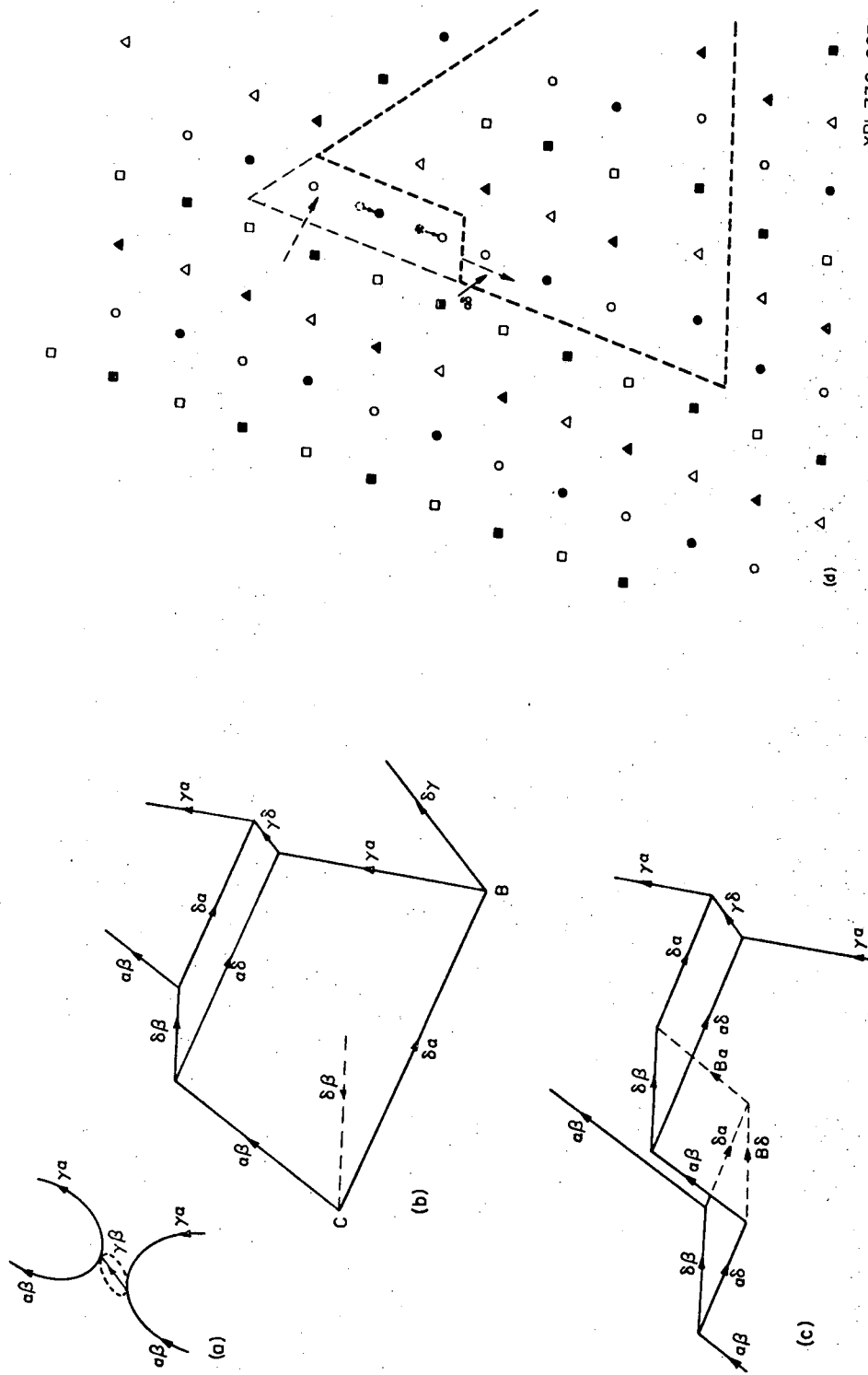


XBL736-6236

Fig. A1-14. The formation of a SFT from a Frank loop by dissociation of the Frank partials δD , creating the dissociated loop (b) and finally the complete SFT (c).

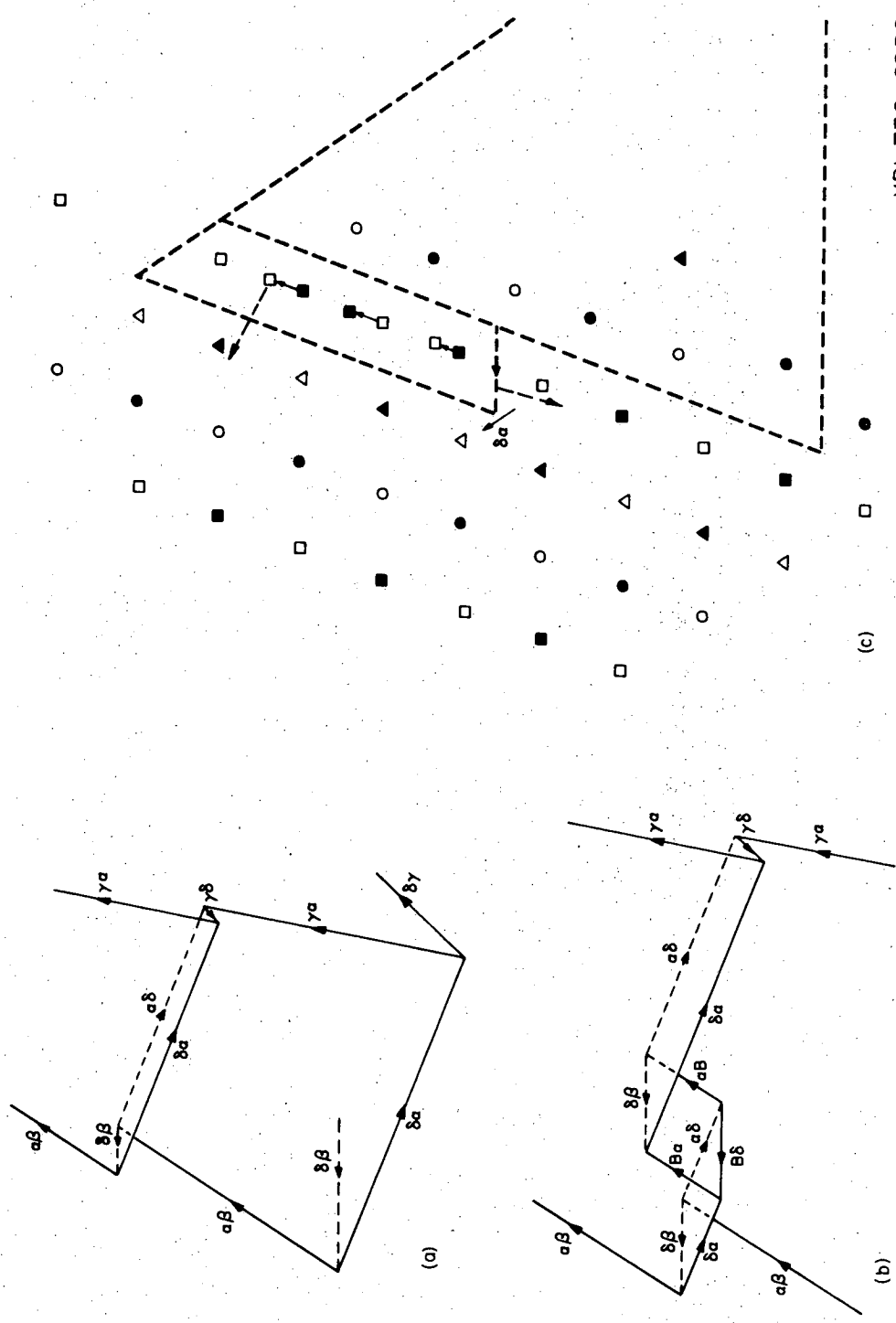
Once formed, the complete SFT can grow or shrink by the formation of joglines (or ledges) on the $\{111\}$ -surface. The most probable situations are sketched in Fig. A1-15. The ledge in Fig. A1-15 is an obtuse ledge, $\frac{1}{3}$ -interstitial type, high energy fault, involving the absorption or emission of one vacancy for each $\frac{a}{4}[121]$ step the whole ledge moves. The same motion dynamics are the case for the ledge in Fig. A1-16, which is acute and of the $\frac{1}{3}$ -vacancy type and intrinsic.

The ledges in Fig. A1-17 and A1-18 are actually glissile and involve the absorption of one row of vacancies along the tetrahedron edge to form Fig. A1-17, or the emission of one row of vacancies to form Fig. A1-18. The first one is obtuse and of the $\frac{2}{3}$ -vacancy type, while the second one is acute and of the $\frac{2}{3}$ -interstitial type and extrinsic.



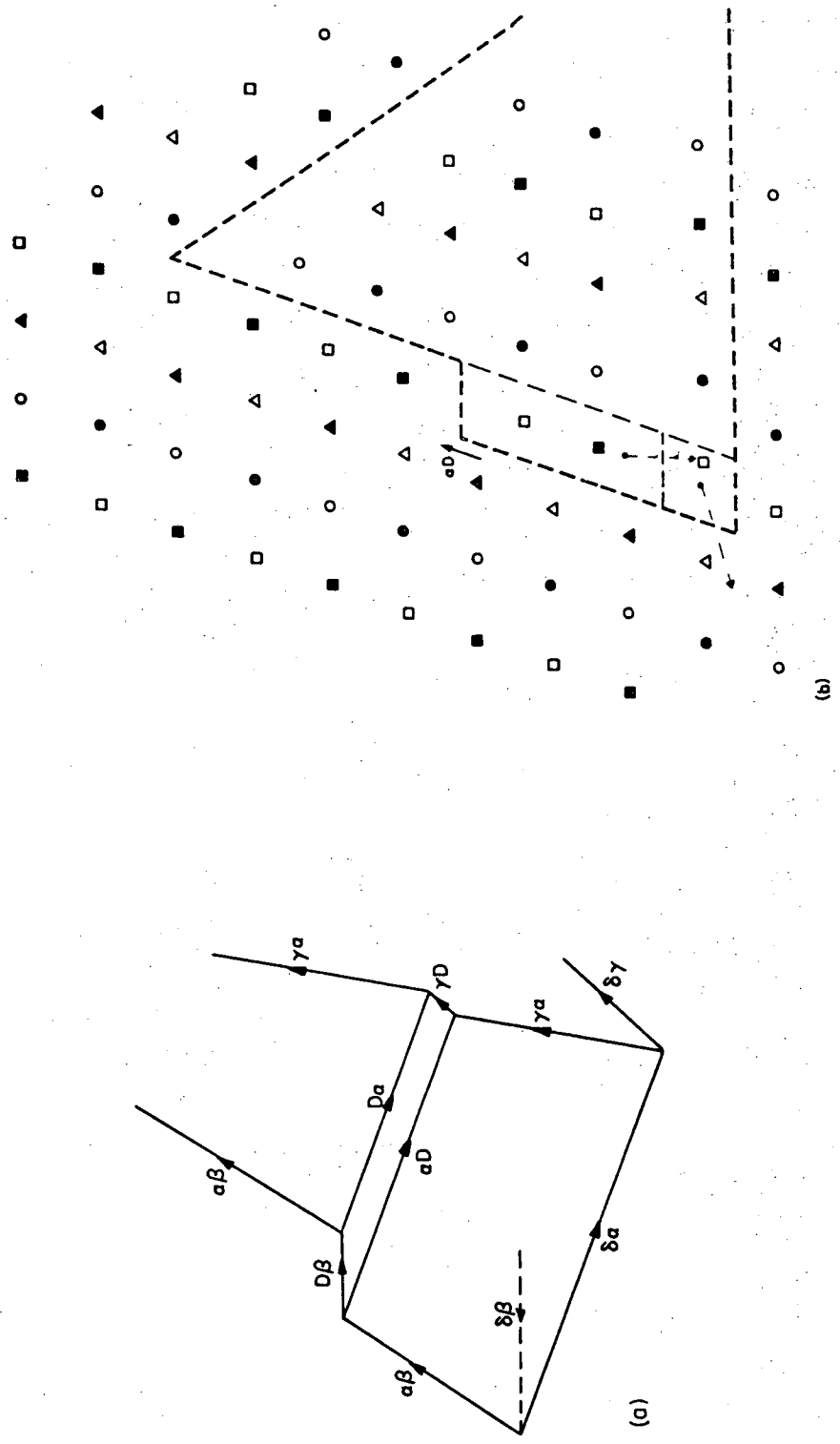
XBL 736-6231

Fig. A1-15. An obtuse, $1/3$ interstitial type ledge on the (111) -surface of the SFT. (a) The splitting of a jog into a pair of joggles. (b) The result being this ledge. (c) The detail of the climb mechanism. (d) A cut on the $(10\bar{1})$ -plane showing the atomic displacements schematically.



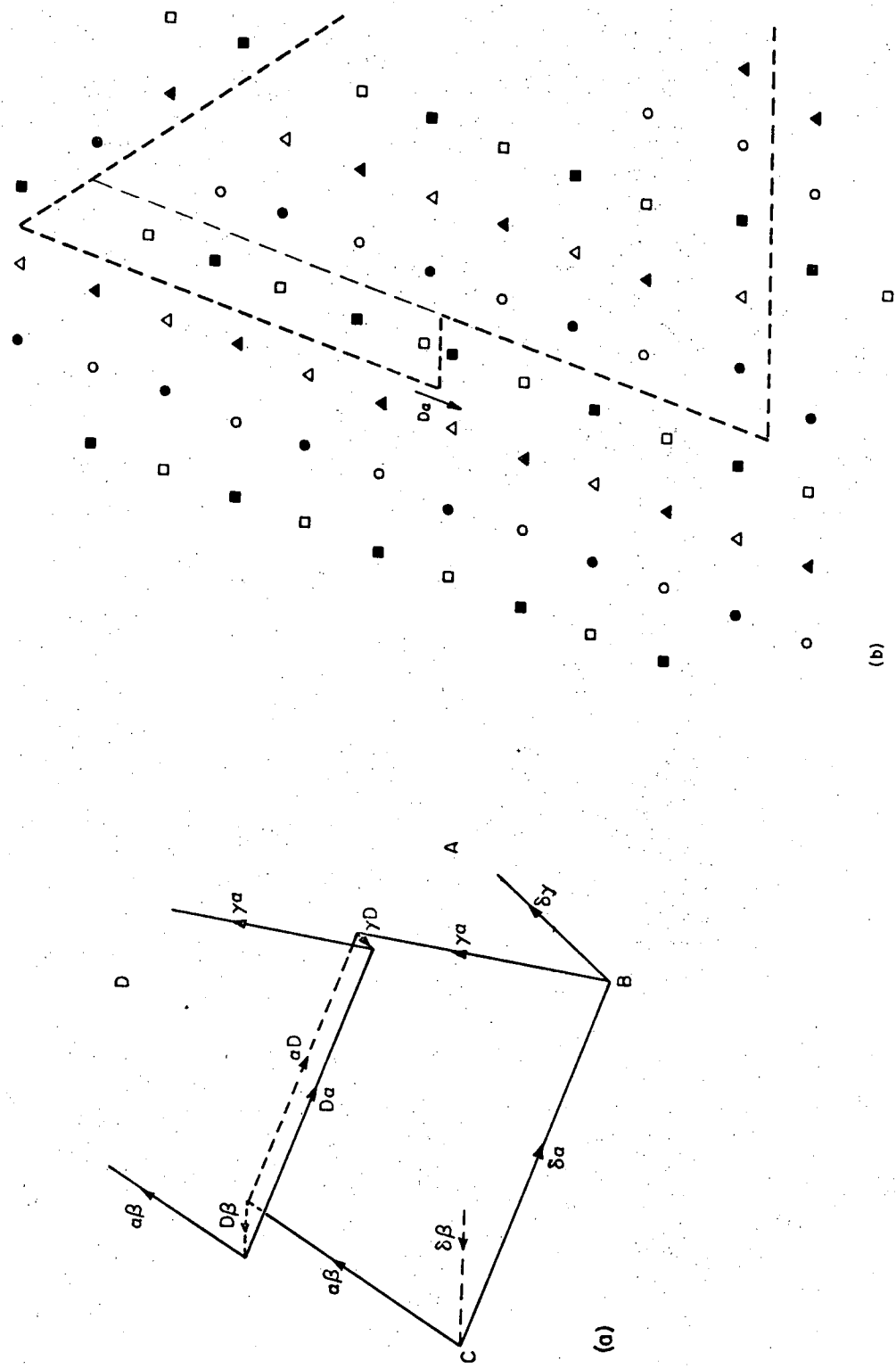
XBL 736-6252

Fig. Al-16. An acute, 1/3 vacancy type ledge on the (111)-surface of the SFT. (a) The arrangement of partials around the ledge. (b) Detail of the ledge after the condensation of one vacancy. (c) A cut through the ledge on the (101)-plane showing the atomic displacements schematically.



XBL 736-6253

Fig. Al-17. An obtuse, 2/3 vacancy type ledge on the (111)-surface of the SFT. (a) The arrangement of the partials around the ledge. (b) A cut through the ledge on the (101)-plane showing the atomic displacements schematically.



XBL736-6229

Fig. Al-18. An acute, 2/3 interstitial type ledge on the (111)-surface of the SPT. (a) The arrangement of partials around the ledge. (b) A cut on the (101)-plane through the ledge showing the atomic displacements schematically.

APPENDIX 2. ENERGIES OF FAULTED DEFECTS IN Ag

The partial dislocations in an extended dislocation (see Appendix 1) will at equilibrium be separated by d_e given by (Hirth and Lothe 1968)

$$d_e = \frac{\mu}{2\pi\gamma} \left[(\bar{b}_2 \cdot \bar{s}_2)(\bar{b}_3 \cdot \bar{s}_3) + \frac{(\bar{b}_2 \times \bar{s}_2)(\bar{b}_3 \times \bar{s}_3)}{1-\nu} \right] \quad (\text{A2-1})$$

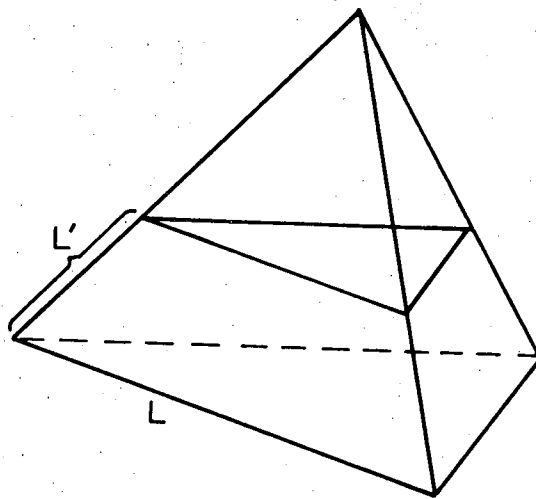
where \bar{b}_2 and \bar{b}_3 are the Burgers vectors of the two parallel partials, and \bar{s}_2 and \bar{s}_3 are their respective senses. μ is the shear modulus, ν is Poisson's ratio and γ is the stacking fault energy.

Given in Table A2-1 are values calculated after Eq. (A2-1) for d_e in the case of a perfect dislocation; $\bar{b}_1 = \frac{a}{2}\langle 110 \rangle$, AB type, in the edge-orientation (Fig. A1-4) and in the screw-orientation, dissociated into two parallel Shockley partials \bar{b}_2 and \bar{b}_3 of the type $\frac{a}{6}\langle 112 \rangle$ (δB). d_e is also given for the case of a Frank partial; $b = \frac{a}{3}\langle 111 \rangle$, (δD), in the edge orientation, splitting into a stairrod; $\bar{b}_2 = \frac{a}{6}\langle 110 \rangle$, ($\alpha\beta$), and a Shockley partial; $\bar{b}_3 = \frac{a}{6}\langle 112 \rangle$ (Fig. A1-13), both parallel and edge-dislocations. In this last case, Eq. (A2-1) reduces to $d_e = \mu a^2 / [36\pi\gamma(1-\nu)]$. The constants for silver is used, $\mu = 3.38 \cdot 10^{11}$ dynes/cm², $\nu = 0.354$, $\gamma = 18$ ergs/cm² (Hirth and Lothe 1968, Escaig 1970b). a is the lattice constant; $a = 4.0857\text{\AA}$.

Table A2-1. The dissociation width d_e for dislocations with Burgers vector \vec{b}_1 and directions (senses) \vec{s}_1 dissociated into two dislocations with b_2 and b_3 .

\vec{b}_1	$\frac{a}{2}\langle 110 \rangle$	$\frac{a}{2}\langle 110 \rangle$	$\frac{a}{3}\langle 111 \rangle$
\vec{s}_1	normal to \vec{b}_1 (edge-dislocation)	parallel with \vec{b}_1 (screw-dislocation)	normal to \vec{b}_1 (edge-dislocation)
d_e	76Å	30Å	43Å

To find the energies of intermediate truncated stacking fault tetrahedra in silver, the formula given by Jössang and Hirth (1966)



XBL 736 - 6238

Fig. A2-1. The intermediate truncated STF, with L' as a variable going from $L' = 0$ for an undissociated triangle to $L' = L$ for a complete SFT.

is used

$$W_{\text{trunc}} = \frac{\mu a^2}{24\pi(1-\nu)} L \left\{ 2 \left(2 - \frac{L'}{L} \right) \ln \frac{4L}{b} + F\left(\frac{L'}{L}\right) + \nu G\left(\frac{L'}{L}\right) \right\} + \sqrt{3} L^2 \left\{ 1 - \frac{3}{4} \left(1 - \frac{L'}{L} \right)^2 \right\} \gamma \quad (\text{A2-2})$$

The values of $F(L'/L)$ and $G(L'/L)$ are tabulated by Jössang and Hirth (1966). $L'/L = x$ is the degree of truncation with L being the length of the edge of the undissociated loop, $L' = 0$, or the length of the edges of the complete SFT, $L' = L$, $0 < x < 1$ for all the intermediate stages (Fig. A2-1). The energy of the undissociated Frank triangle, $x = 0$, is given by

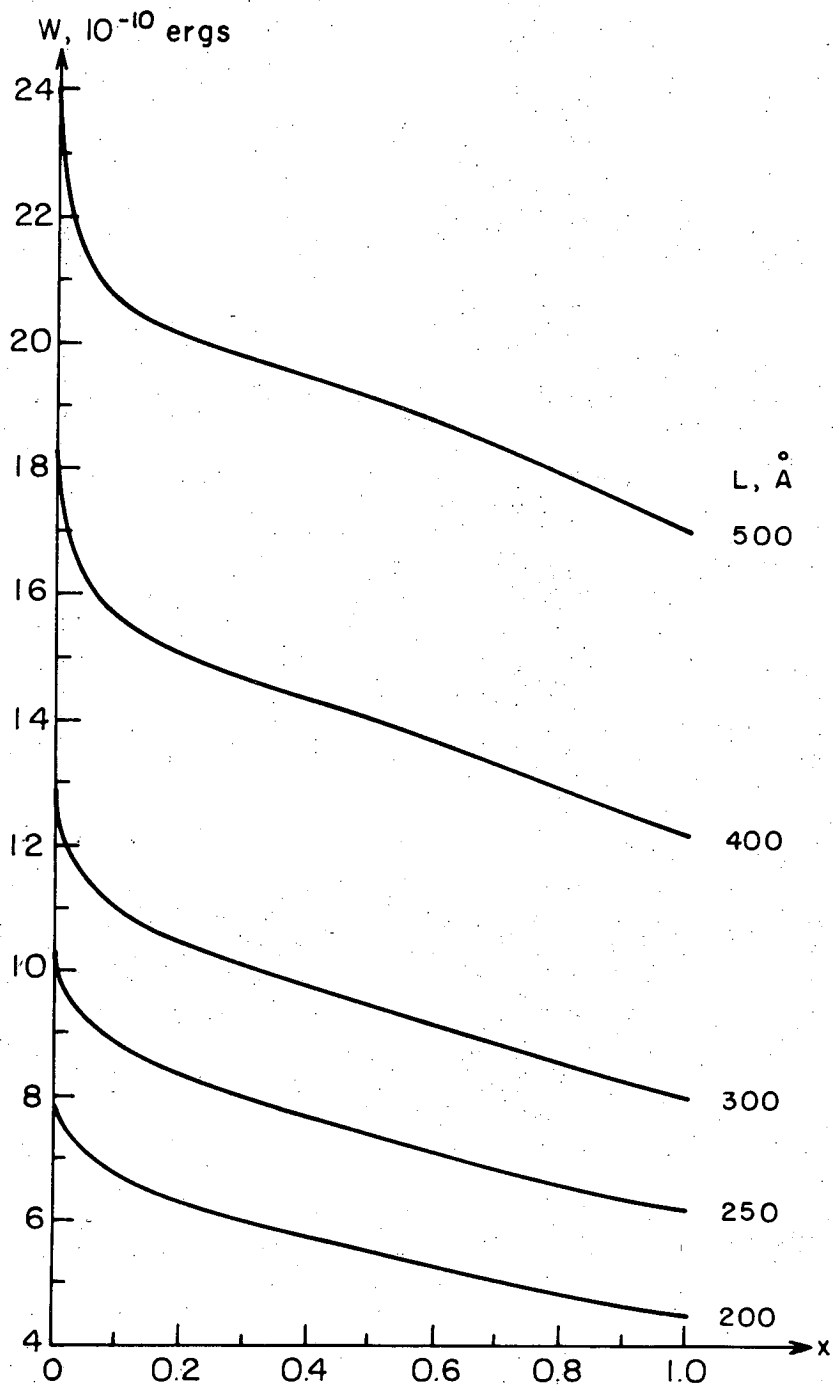
$$W = \frac{\mu a^2}{4\pi(1-\nu)} L \left[\ln \frac{4L}{b} - 0.20 \right] + \frac{\sqrt{3}}{4} L^2 \gamma \quad (\text{A2-3})$$

For the perfect (complete) SFT, $x = 1$, Eq. (A2-2) reduces to

$$W_{\text{SFT}} = \frac{\mu a^2}{12\pi(1-\nu)} L \left[\ln \frac{4L}{b} + 1.03 + 0.96 \nu \right] + \sqrt{3} L^2 \gamma \quad (\text{A2-4})$$

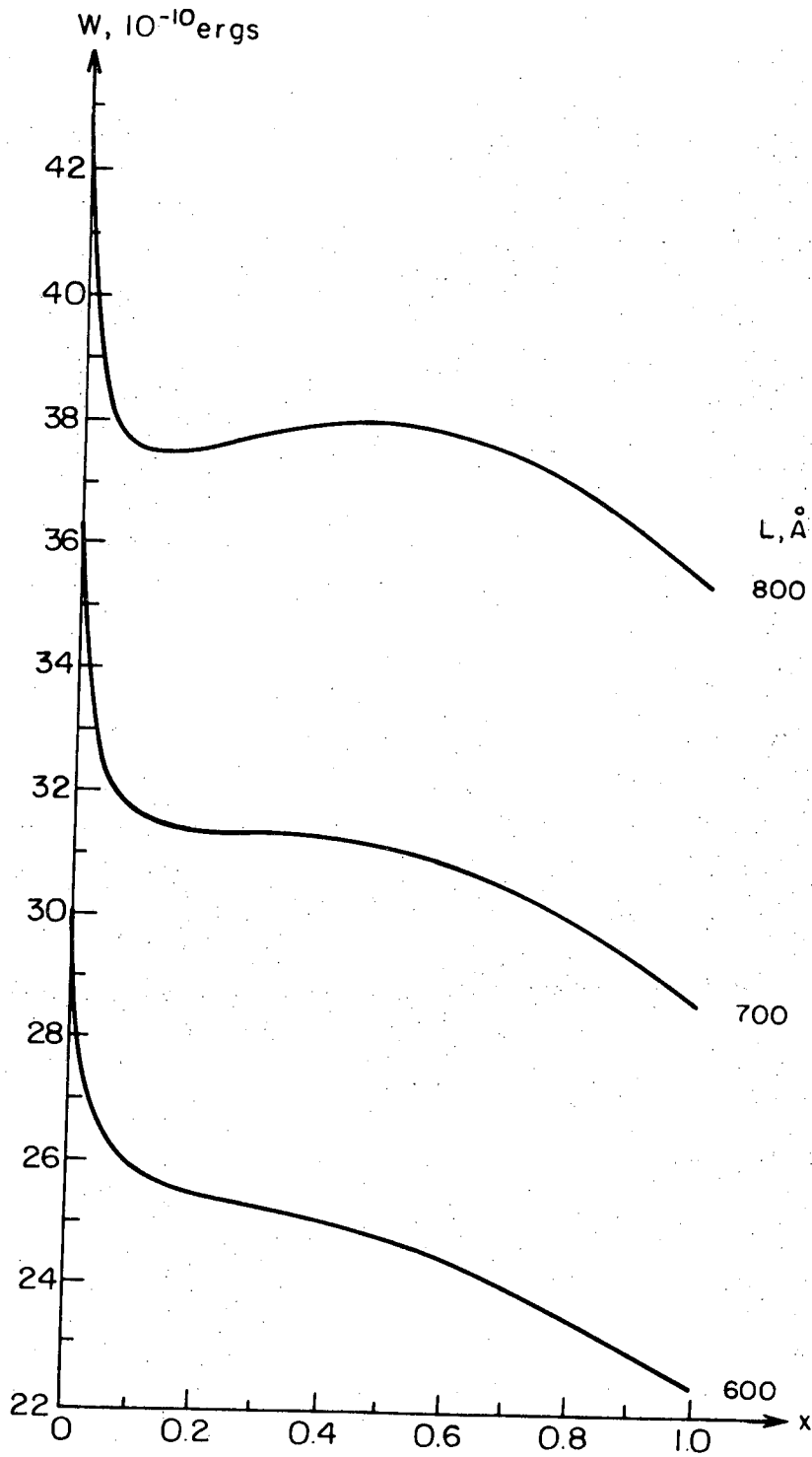
The energies have been calculated for the case of silver for different values of L and the results are shown in Figs. A2-2 to A2-6. Figure A2-7 shows the energies of the complete SFT together with the minimum and maximum energies of the intermediate truncated SFT as a function of L .

From these figures we find $L_c \approx 690\text{\AA}$ and $L_E \approx 960\text{\AA}$ which gives the stability ranges for the dissociated Frank triangle and the SFT (Hirth and Lothe 1968) in silver. The SFT is the only stable configuration for $L < L_c$, the most stable configuration for $L_c < L < L_E$, while metastable for $L > L_E$. For $L > L_E$, the dissociated Frank triangle is the most stable configuration while it is metastable for $L_c < L < L_E$.



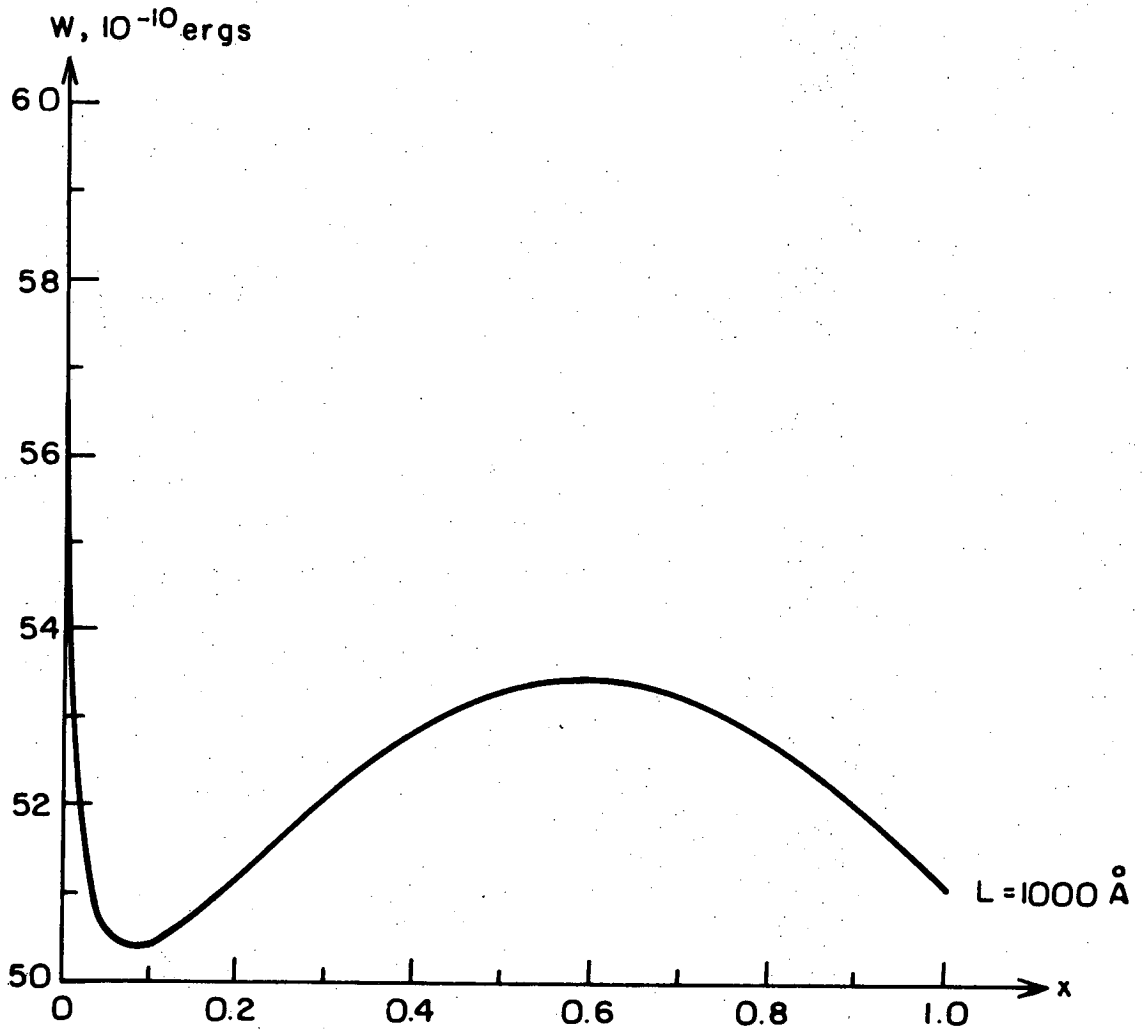
XBL 736-6239

Fig. A2-2. Variation of the energy of the truncated SFT with the degree of truncation, x , for $L = 200\text{\AA}$, 250\AA , 300\AA , 400\AA , and 500\AA . $x = 0$ represents the undissociated Frank triangle and $x = 1$ the complete SFT.



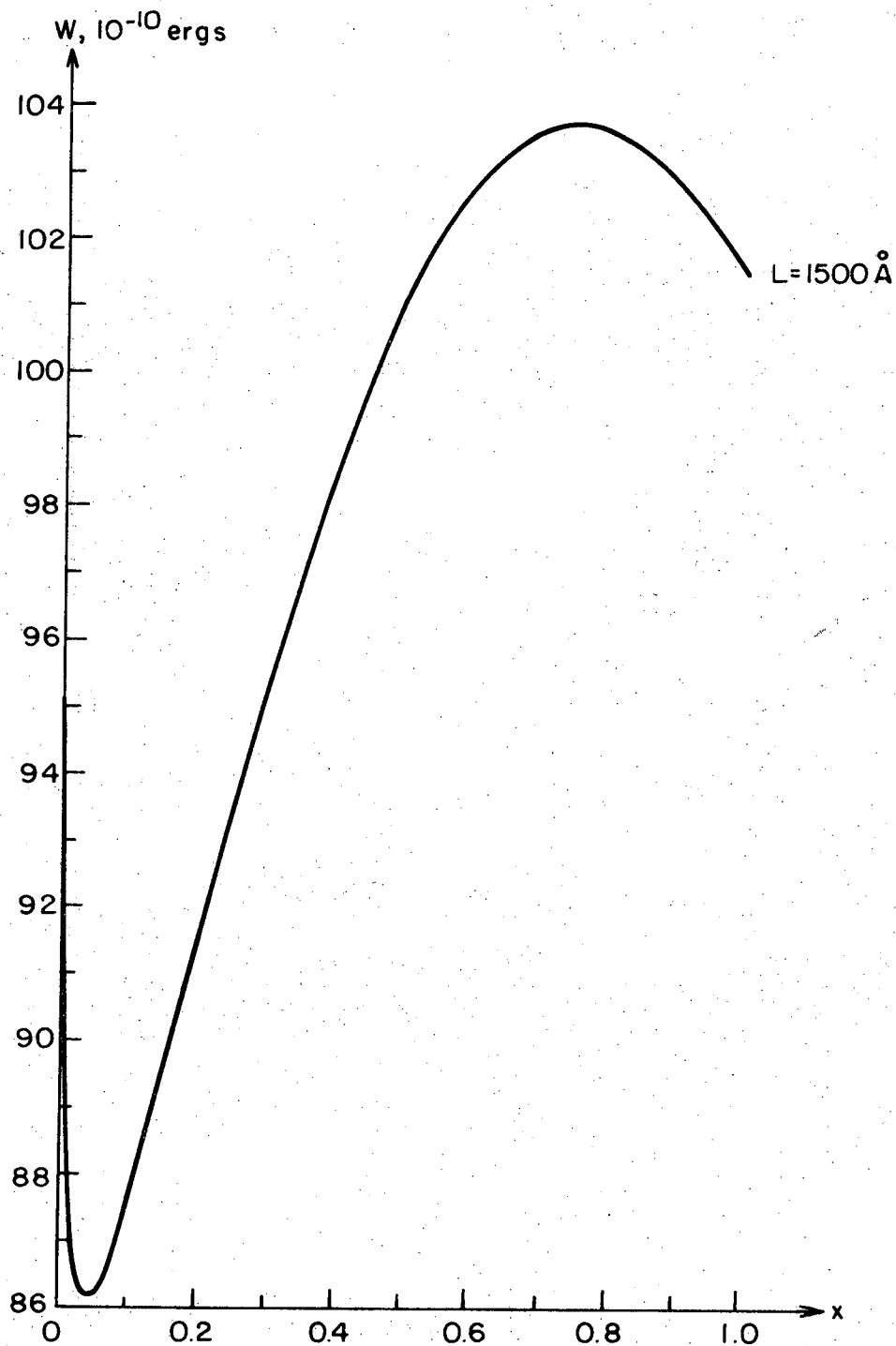
XBL 736- 6240

Fig. A2-3. As Fig. A2-2, but with $L = 600\text{\AA}$, 700\AA and 800\AA .



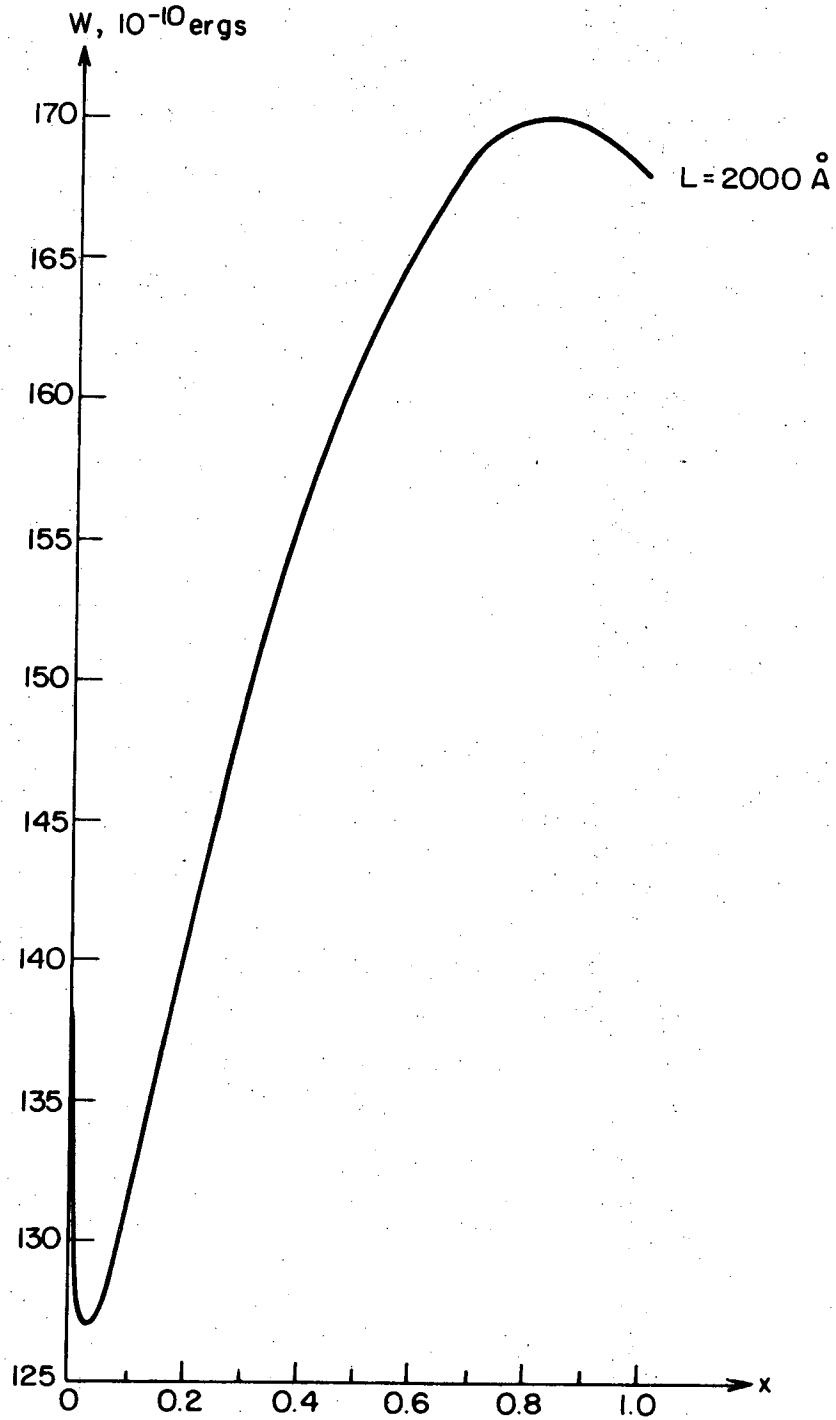
XBL 736-6241

Fig. A2-4. As Fig. A2-2, but with $L = 1000\text{\AA}$.



XBL736-6242

Fig. A2-5. As Fig. A2-2, but with $L = 1500 \text{ \AA}$.



XBL 736-6243

Fig. A2-6. As Fig. A2-2, but with $L = 2000\text{\AA}$.

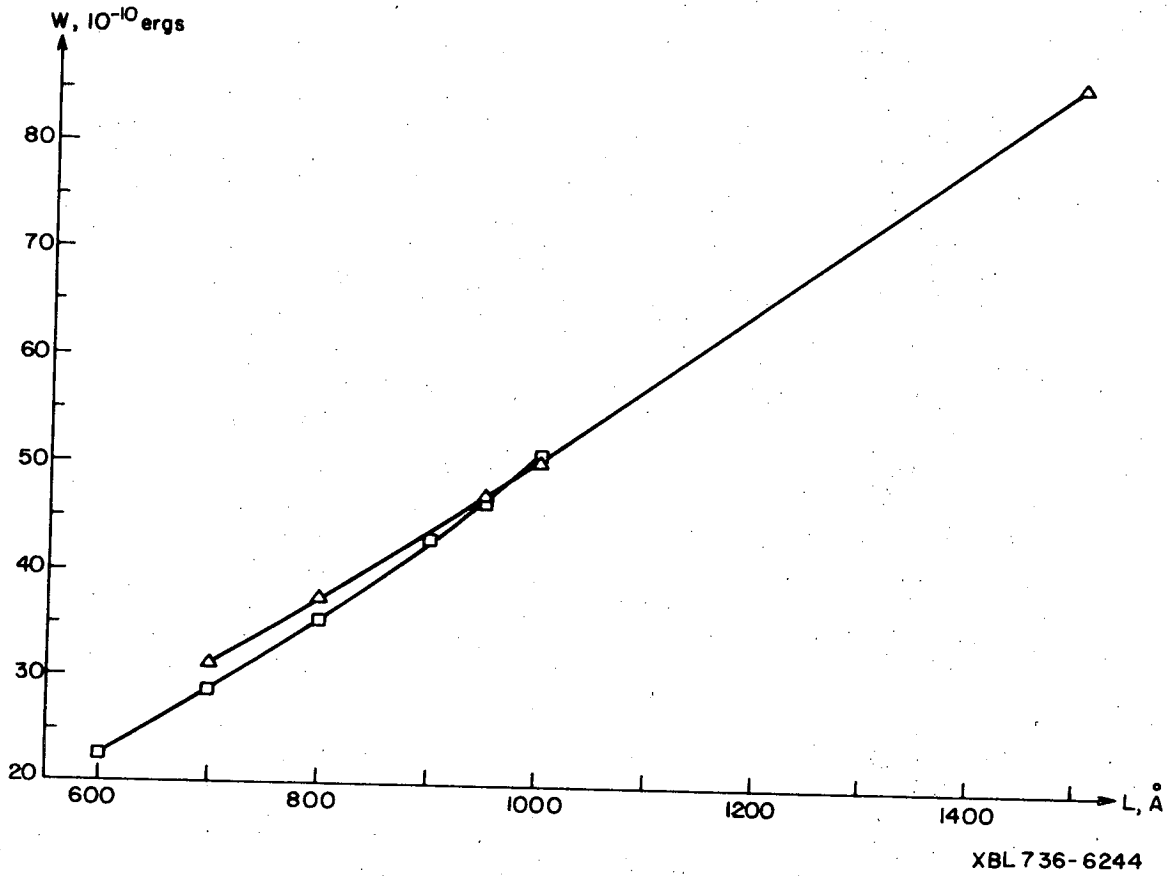


Fig. A2-7. A plot of the energies; W_{SFT} and W_{DFT} as a function of L taken from Table A2-2. W_{SFT} ; \square . W_{DFT} ; \triangle .

Table A2-2. Energies W_{Δ} of the undissociated Frank triangle, W_{DFT} of the dissociated Frank triangle and W_{SFT} of the complete SFT calculated for different edgesizes L . ΔW are energy barriers.

L Å	W_{Δ} 10^{-10} erg	ΔW 10^{-10} erg	W_{DFT} 10^{-10} erg	ΔW 10^{-10} erg	W_{max} 10^{-10} erg	ΔW 10^{-10} erg	W_{SFT} 10^{-10} erg
200	7.85						4.49
250	10.29						6.13
300	12.86						7.95
400	18.27						12.11
500	23.99						16.96
600	29.99						22.48
700	36.31	4.96	31.35	0.02 (1.25eV)	31.37	2.72 (170eV)	28.65
800	42.85		37.52	0.48 (30eV)	38.00	2.53 (158eV)	35.47
900							42.96
950			47.06				46.94
1000	56.66		50.36	3.11 (195eV)	53.47	2.39 (149eV)	51.08
1500	95.15		86.18	17.54 (1000eV)	103.72	2.25 (140eV)	101.47
2000	138.68		127.04	42.96 (2700eV)	170.00	2.14 (134eV)	167.86

In Table A2-2, the extremal values are given together with the different energy barriers between the configurations; undissociated Frank triangle Δ , dissociated Frank triangle DFT and the complete SFT.

Table A2-3. Values of $x = L'/L$ for W_{DFT} , the energy minimum for the dissociated Frank triangle, x_e , and for the energy maximum W_{max} , x_b . L is the complete edgelenh, L' is the length of the trunkated edges and h_e is equal to the dissociation width.

L Å	x_e	L'_e Å	h_e Å	x_b	L'_b Å	$L-L'_b$ Å
700	0.23	161	139	0.27	189	511
800	0.14	112	97	0.46	368	432
950	0.10	95	82			
1000	0.08	80	69	0.60	600	400
1500	0.045	68	59	0.75	1125	375
2000	0.03	60	52	0.81	1620	380
∞		43				

From $x = L'/L$ for W_{DFT} , the energy minimum for the dissociated Frank triangle, we find the dissociation width $d_e = h_e$ for the different L , Table A2-3. For $L \rightarrow \infty$, i.e., for the splitting of a Frank partial into a parallel stairrod and a Shockley partial we have used the value from Table A2-1. The table (Table A2-3) also gives the value of L' , L'_b for the energy maximum W_{max} .

APPENDIX 3. CONTRAST FROM FAULTED DEFECTS

An imperfection in a crystal introduces an additional phase factor $e^{-i\alpha}$ in the amplitude of the scattered electron wave (diffracted beam) (Hirsch et al. 1965) where

$$\alpha = \frac{2\pi}{a} \vec{g} \cdot \vec{R} \quad (\text{A3-1})$$

\vec{g} is the operating reflection and \vec{R} is the displacement vector at a depth z in the crystal.

In the case of a general dislocation (Howie and Whelan 1962), the displacement vector \vec{R} is given by

$$\vec{R} = \frac{1}{2\pi} \left\{ \vec{b} \Phi + \vec{b}_e \frac{\sin 2\Phi}{4(1-\nu)} + \vec{b} \times \vec{s} \left(\frac{1-2\nu}{2(1-\nu)} \cdot \ln |r| + \frac{\cos 2\Phi}{4(1-\nu)} \right) \right\} \quad (\text{A3-2})$$

b_e is the edge component and r and Φ are coordinates in the crystal.

The three terms in \vec{R} are given as

$$\vec{R} = \vec{R}_1 + \vec{R}_2 + \vec{R}_3$$

Even if $\vec{g} \cdot \vec{R}_1 = 0$ and $\vec{g} \cdot \vec{R}_2 = 0$ and thus cause no contrast, the term

$\vec{g} \cdot \vec{R}_3$ might be nonzero and giving rise to the so-called residual contrast

$$\vec{R}_3 = \frac{\vec{b} \times \vec{s}}{8} \frac{1}{2\pi} (\ln(r^2) + 3 \cos 2\Phi) \quad (\text{A3-3})$$

Intensity profiles calculated on the dynamical theory suggests that the image will be effectively invisible if the parameter m (Howie and Whelan 1962) is

$$m = \frac{1}{8a} \vec{g} \cdot (\vec{b} \times \vec{s}) \lesssim 0.08 \quad (\text{A3-4a})$$

or

$$\frac{1}{a} \vec{g} \cdot (\vec{b} \times \vec{s}) \lesssim 0.64 \quad (\text{A3-4b})$$

The dislocation is not visible when $\frac{1}{a} \vec{g} \cdot \vec{b} = 0$ or $\pm \frac{1}{3}$ with $m \lesssim 0.08$, and it may not be visible when $\frac{1}{a} \vec{g} \cdot \vec{b} = -\frac{2}{3}$ (Silcox and Tunstall 1964).

In the case of stacking faults, the crystal below the fault plane \vec{N} is displaced by \vec{R} with respect to the upper part (Fig. A3-1).

In fcc crystals, the stacking faults are on $\{111\}$ -planes and have $\vec{R} = \frac{a}{3} \langle 111 \rangle$ which gives from Eq. (A3-7)

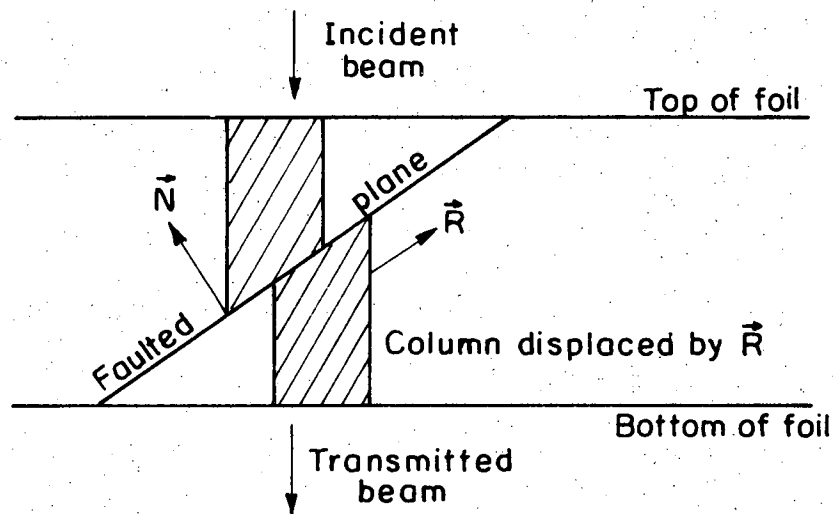
$$\alpha = 0, \pm \frac{2\pi}{3}, \pm \frac{4\pi}{3}, \pm 2\pi, \dots \frac{2\pi}{3} n, \quad (\text{A3-5})$$

with $n = 0, \pm 1, \pm 2, \dots = h + k + \ell$

$$\vec{g} = [h, k, \ell]$$

Fringe contrast from the fault is obtained when $\alpha = \frac{2\pi}{3} \pm 2\pi p$ and $\alpha = \frac{4\pi}{3} \pm 2\pi p$. The last case gives reversal of the fringe contrast in the first case. No contrast is obtained when $\alpha = 2\pi p$, $p = 0, 1, 2, \dots$

If we have an intrinsic SF on the (111) plane with $\vec{N} = [111]$ pointing towards the top of the foil, the displacement will be $\vec{R} = \frac{a}{3}[111]$ and as we have seen in Appendix 1, this displacement is equivalent to the displacements $\frac{a}{6}[2\bar{1}\bar{1}]$, $\frac{a}{6}[\bar{1}2\bar{1}]$ and $\frac{a}{6}[\bar{1}\bar{1}2]$, all vectors starting at δ in the Thompson tetrahedron. All these displacements give the same phase factor, $\alpha = \alpha' \pm 2\pi$.





















XBL736-6245

Fig. A3-1. Schematic cut through a crystal foil containing a faulted plane. The part of the foil below the fault is displaced by \vec{R} relative to the upper part. \vec{N} is the normal to the faultplane.

For the extrinsic fault, $\vec{R} = -\frac{a}{3}[111]$, giving $-\alpha$ as the phase factor. However, contrary to what is stated in Hirsch et al. (1966, p. 166) this fault can not be represented by the single displacements $A\delta$, $B\delta$ or $C\delta$ except in the case of the high energy fault. Instead it must be regarded as two overlapping intrinsic faults with the displacements δC and δA , δC and δB , or δA and δB . The resultant displacement being $B\delta$, $A\delta$ or $C\delta$. Anyway the phase factor is $-\alpha$ for the last case and $2\alpha \rightarrow -\alpha$ for the first case.

The result of this contrast considerations is given in Table A3-1.

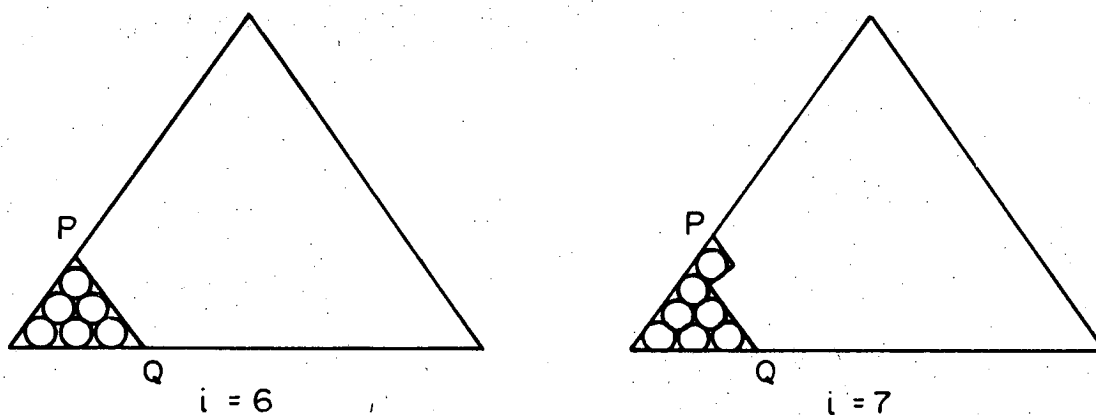
Table A3-1. Expected contrast, schematically drawn, from dislocations and stackingfaults in the cases of a dissociated and a undissociated Frank triangle and from a SFT, with $[011]$ being the foil normal, for different operating reflections \vec{g} . The "wavy" contrast are from the faults.

\vec{g}	FRANK TRIANGLES	DISS. FRANK TRIANGLES	SFT
$\bar{2}00$ ↓			
$\bar{1}\bar{1}\bar{1}$ ↙			
$\bar{1}\bar{1}1$ ↘			
$22\bar{2}$ ↗			
$02\bar{2}$ ←			
$\bar{3}\bar{1}1$ ↘			

APPENDIX 4. DISPROOF OF ESCAIG'S MODIFIED NUCLEATION THEORY

The general nucleation theory gives a nucleation rate expressed through an Arrhenius law; $J^* \sim \exp(-G^*/kT)$, where G^* is the maximum energy of the barrier. Escaig (1970) proposed a modified nucleation theory showing that the rate controlling energy of an activated process not always should be identified with the maximum energy of the barrier.

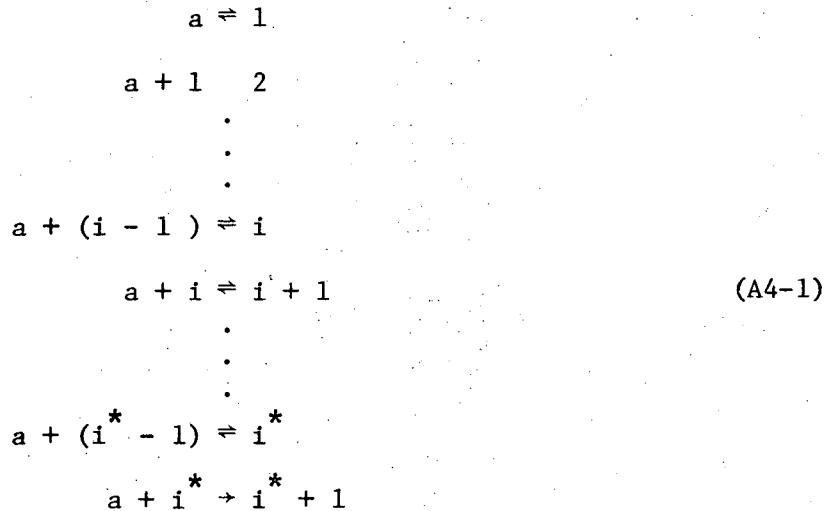
Taking the example of building up a critical 120° corner of length



XBL 736-6246

Fig. A4-1. A Frank stacking-fault triangle with one corner unfaulted by filling in i atoms to make the triangle shaped cluster of size i . At $i = 6$ PQ is complete, while at $i = 7$ a jog is formed on PQ.

PQ^* on the Frank triangle, Fig. A4-1, this would be expressed through a series of bimolecular equilibrium reactions;



where a is an atom of the metal and i is the triangle shaped cluster of i atoms which fills in the loop corner (Fig. A4-1).

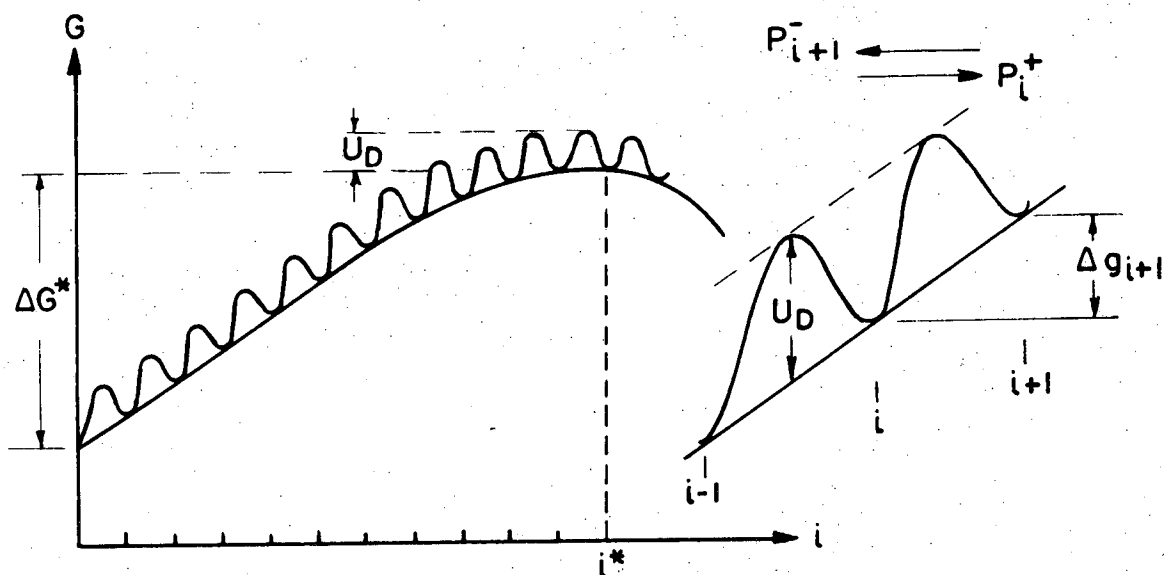
The nucleation rate is given by the last step in this equilibrium reaction (Hirth and Pound 1963);

$$J^{e*} = c_{i^*}^e \cdot A \cdot \nu \cdot \exp - U_D/kT \qquad (A4-2)$$

where $c_{i^*}^e$ is the equilibrium concentration of critical sized clusters i^* , A is a preexponential factor, ν is the atomic frequency and U_D is the activation energy of selfdiffusion as the process is nonconservative involving the emittance of vacancies. The energy curve is schematically shown in Fig. A4-2. The probability of going from i to $i + 1$; p_i^+ , and the probability of going from $i + 1$ to i ; p_{i+1}^- , is given by:

$$p_i^+ = A \cdot \nu \cdot \exp - (U_D + \Delta_{i+1})/kT \qquad (A4-3a)$$

$$p_{i+1}^- = A \cdot \nu \cdot \exp - (U_D + \Delta_{i+1} - (G_{i+1} - G_i))/kT \qquad (A4-3b)$$



XBL 736-6247

Fig. A4-2. The free energy G of the triangle shaped cluster (corner) as a function of the size i with the energy of selfdiffusion super-imposed, shown schematically. ΔG^* is the nucleation energy or the difference in energy between the critical corner i^* and the 60° corner ($i = 0$). The insert is a detail of the curve between $i - 1$ and $i + 1$. $\Delta g_{i+1} = G_{i+1} - G_i$, p_i^+ and p_{i+1}^- are the jump-frequencies, and $\Delta_{i+1} \approx 1/2 \Delta g_{i+1}$.

with G_i being the free energy of the i -sized corner and $\Delta_{i+1} \approx 1/2(G_{i+1} - G_i)$.

Then the respective fluxes are given by:

$$J_i^{e+} = c_i^e \cdot p_i^+ \quad (\text{A4-4a})$$

$$J_{i+1}^{e-} = c_{i+1}^e \cdot p_{i+1}^- \quad (\text{A4-4b})$$

and at equilibrium (e); $J_i^{e+} = J_{i+1}^{e-}$ due to the principle of detailed balance, yielding:

$$\begin{aligned} c_{i+1}^e &= c_i^e \cdot p_i^+ / p_{i+1}^- \\ &= c_i^e \cdot \exp - \Delta g_{i+1} / kT \end{aligned} \quad (\text{A4-5})$$

with

$$g_{i+1} = G_{i+1} - G_i$$

This gives us the equilibrium concentration of $i + 1$ sized corners;

$$c_{i+1}^e = c^e \cdot \exp - \Delta G_{i+1} / kT \quad (A4-6)$$

where c^e is the equilibrium concentration of perfect, 60° , corners and $\Delta G_{i+1} = G_{i+1} - G_0$ ($G_0 = G_{i=0}$). Thus we can put up the nucleation rate, Eq. (A4-2) adding for Δ_{i+1} ;

$$J^{e*} = c^e \cdot A \cdot v \cdot \exp - (\Delta G_{i*}^* + U_D - \Delta_{i+1}^*) / kT \quad (A4-7)$$

In the steady state treatment there is an actual flux through the system of i 's and we can put up a difference-differential equation (Feder 1964 and Feder et al. 1966);

$$\frac{\partial c}{\partial t} = J_{i-1}^+ + J_{i+1}^- - J_i^+ - J_i^- \quad (A4-8)$$

This equation might be solved yielding $\frac{\partial c}{\partial t} = \frac{\partial}{\partial i} \left\{ p_i^+ \cdot c_i^e \cdot \frac{\partial}{\partial i} (c_i / c_i^e) \right\}$ from which we get the "current" $J(i) = J_i^+ - J_{i+1}^-$ as the net number of corners growing from i to $i+1$ per unit time and volume;

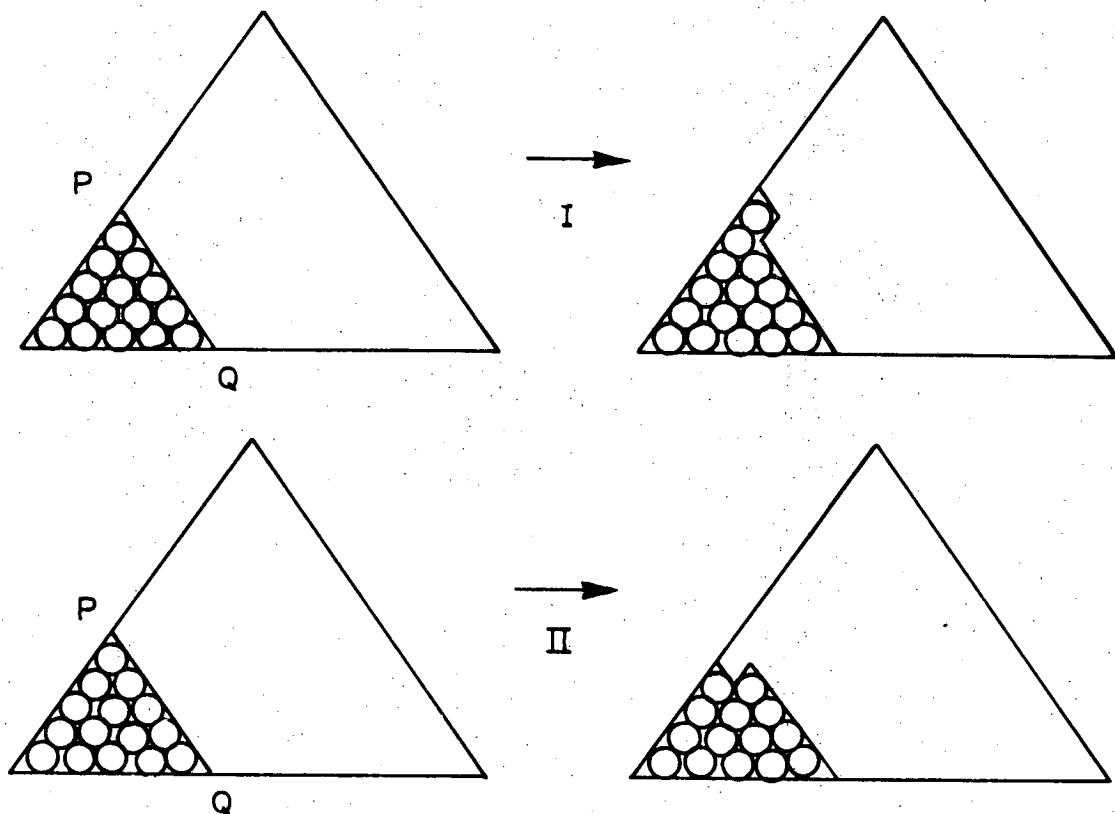
$$J(i) = -p_i^+ \cdot c_i^e \cdot \frac{\partial}{\partial i} (c_i / c_i^e) \quad (A4-9)$$

In the steady state, $\partial J / \partial i = 0$ and $J = J^S$ thus independent of cluster size, and $\partial c / \partial t = 0$. J^S is nothing but the steady state nucleation rate, and using the values for the critical-sized corner i^* ;

$$\begin{aligned} J^S &= Z \cdot p_{i^*}^+ \cdot c_{i^*}^e \\ &= c^e \cdot Z \cdot A \cdot v \cdot \exp - (\Delta G_{i^*}^* + U_D - \Delta_{i^*+1}^*) / kT \end{aligned} \quad (A4-10)$$

Z is the Zeldovich factor; $Z = -\frac{\partial}{\partial i} (c_i^s/c_i^e)$, a nonequilibrium factor representing the ratio of the actual flow through size i^* to the flux from an equilibrium population of i^* , c_i^s being the steady state distribution. Both for J^{e*} and J^s the rate determining factors are similar in that both are functions of $c_i^{e*}(\Delta G^*)$ and of U_D .

Escaig determines a nucleation rate based on a chain-reaction. Looking at Fig. A4-1 and A4-3, we can see that at certain steps in the reaction, the backwards reaction II is more difficult than the forward reaction I. These reactions start from a completed row PQ (Fig. A4-3). Once a completed

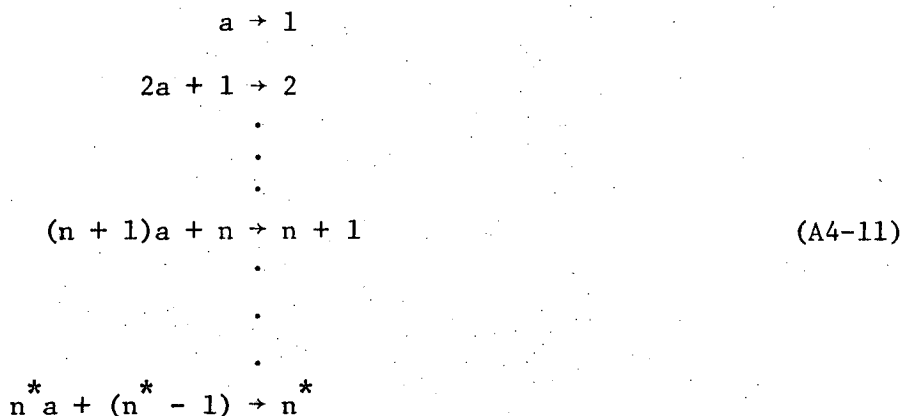


XBL 736-6249

Fig. A4-3. The two possible reactions involving the adding (I) or removal (II) of one atom from a Frank stacking-fault triangle with a unfaulted corner having a completed row PQ.

row PQ is formed it is easier to emit one vacancy (I) from, than to condense one vacancy (II) on the dislocation segment PQ. The length of a complete segment; $PQ = (n + 0.5)b$ with n equal to the number of atoms along PQ. The size of the corresponding corner is given by $i = 0.5n(n+1)$.

A simple calculation of the energy difference ΔU between the reactions I and II gives $\Delta U \approx 0.25$ eV (Escaig 1970a&b) which leads to a probability of going forward (I) a 100 times higher than going backwards (II) at about 400°C. By then completely neglecting the backwards reactions, Escaig puts up a set of chain-reactions;



each step involving the reactions (I) from a complete row PQ with n atoms along it and $i = 1/2n(n + 1)$ atoms in the corner, building a new complete row with $n + 1$ atoms along PQ and $i = 1/2n(n + 1) + n + 1 = 1/2(n + 1)(n + 2)$ atoms in the corner. The left side of Eq. (A4-11) indicates the new row of atoms added to the existing row giving the number of atoms along the new PQ (and the stepnumber on the right side). For all the intermediate steps i between n and $n + 1$ equilibrium are assumed. The energy situation is schematically shown in Fig. A4-4 and Fig. A4-5a,b. The

chain-reaction in Eq. (A4-11) is represented by the dotted curve in Fig. A4-4. The critical-sized corner is now denoted by n^* . The fully drawn curve takes into account that the stable corners of the defect are not 60° corners, but blunted by $i = 3$ atoms. This curve will also have the same oscillating character as the dotted one because of ΔU . This is shown in Fig. A4-5a,b in more detail where the free energy of the defect is given as a function of both i and n .

By neglecting the probability of the backwards reaction, p_n^- , this chain reaction gives the nucleation rate; $J^* = J_n^+ = c_n \cdot p_n^+ = J_{n \rightarrow n+1}$ as;

$$J^* = c_n \cdot A \cdot v \cdot \exp - (\Delta g_{n+1} + 1/2 \Delta U + U_D - \Delta) / kT \quad (A4-12)$$

with $\Delta g_{n+1} = G_{n+1} - G_n$ and $\Delta \approx 1/4 \Delta U$ (see Fig. A4-5a,b). c_n is the concentration of corners with n atoms along PQ. Taking the basic step as $n = 2 \rightarrow n = 5$ (Escaig 1970a,b) with $\Delta G_5 = G_{n=5} - G_{n=2}$ (Fig. A4-5a) we get the nucleation rate:

$$J^* = c_{n=2} \cdot A \cdot v \cdot \exp - (\Delta G_5 + 1/2 \Delta U + U_D - \Delta) / kT \quad (A4-13)$$

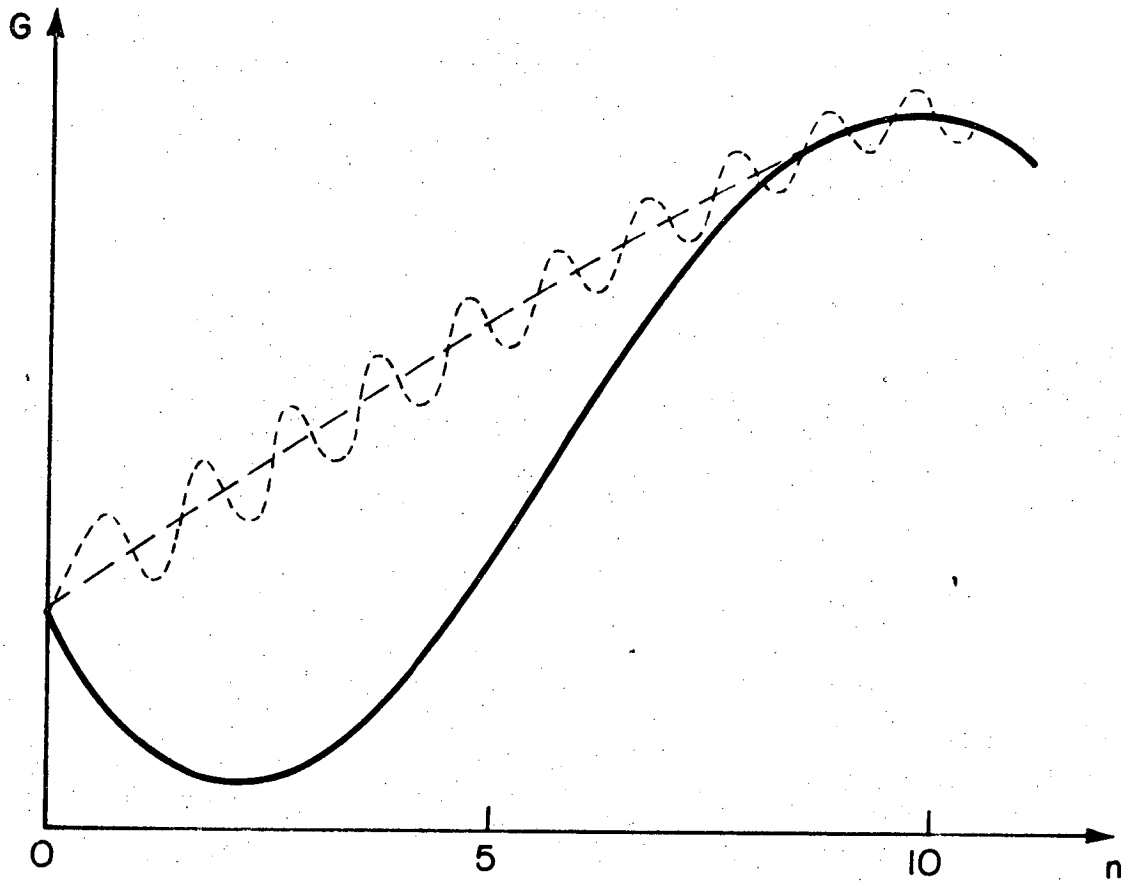
which gives an activation energy $\Delta G_5 \ll \Delta G_n^* = G_n^* - G_{n=2}$. However, in this calculation the backwards step is represented by the probability:

$$p_n^- = A \cdot v \cdot \exp - (U_D + \Delta) / kT (= p_{i=1/2n(n+1)}^-) \quad (A4-14)$$

which can not at all be neglected relative to p_n^+ given in Eq. (A4-12) as

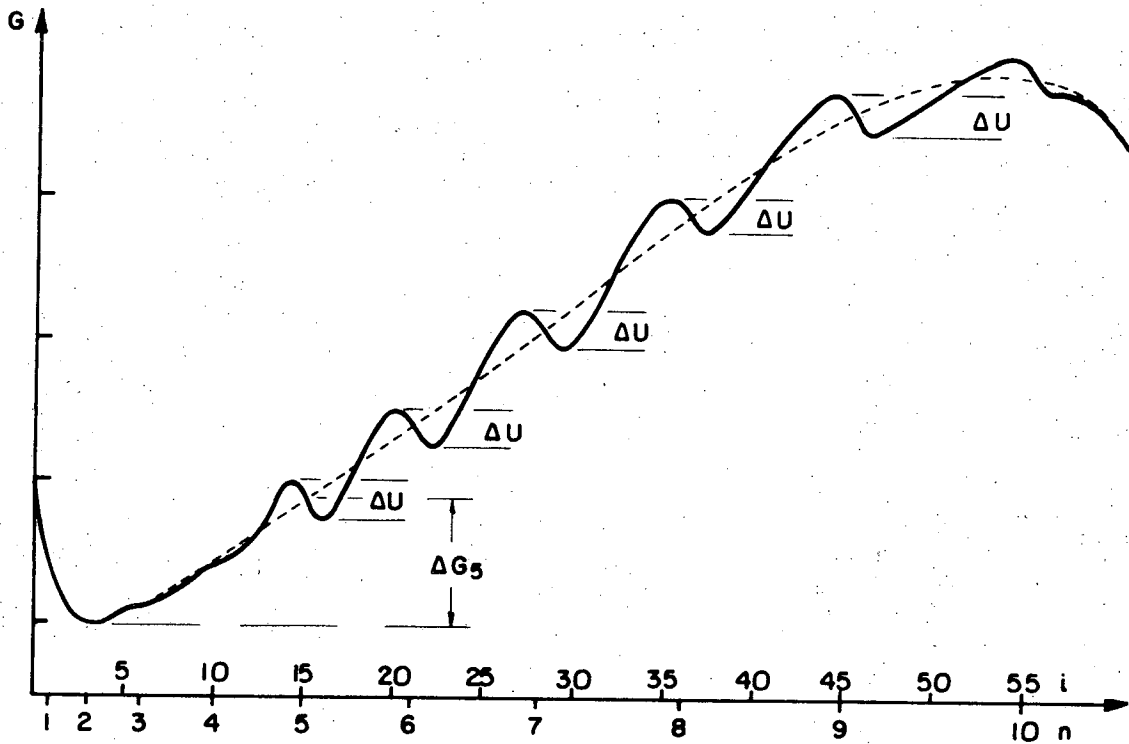
$$p_n^+ = A \cdot v \cdot \exp - (\Delta g_{n+1} + 1/2 \Delta U + U_D - \Delta) / kT \quad (A4-15)$$

$(1/2 \Delta U - \Delta \approx \Delta)$. This gives $p_n^+ < p_n^-$.

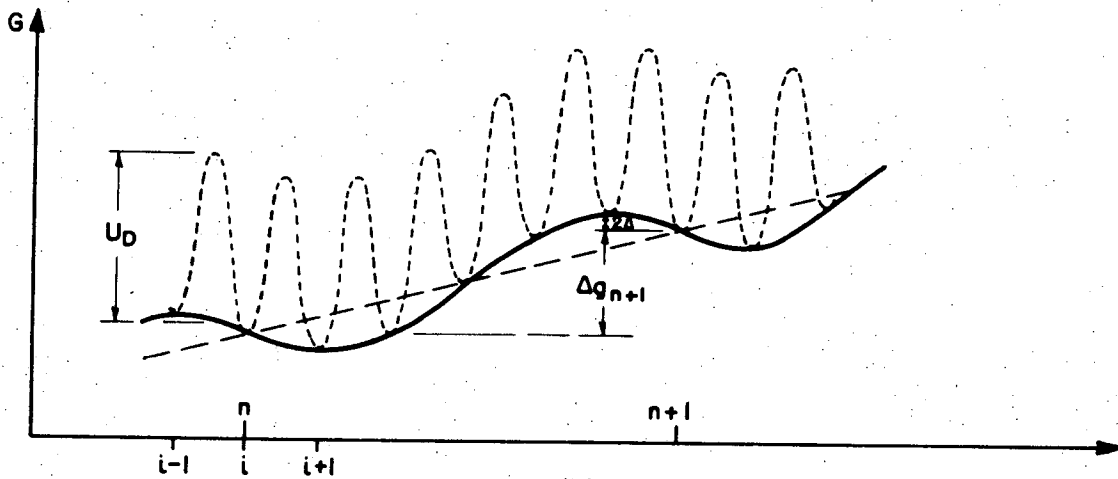


XBL 736-6248

Fig. A4-4. Variation of the free energy G of a Frank triangle with the formation of an unfaulted corner (cluster) as a function of the number of atoms n along the edge PQ . The dotted curve is for the 60° corner being the stable configuration, the oscillations due to the energy difference ΔU between reaction (I) and (II). The fully drawn curve represents the case with blunting by $i = 3$ atoms being the stable configuration, without taking ΔU into consideration.



(a)



(b)

XBL 735-6097

Fig. A4-5. (a) Variation of the free energy G of a faulted Frank triangle with the formation of an unfaulted corner as function of the number of atoms i in the corner or the number of atoms n along the complete row PQ of the corner. ΔU is the energy difference between the reactions (I) and (II) or $\Delta U = G_{i=1/2n(n+1)-1} - G_{i=1/2n(n+1)+1}$.

(b) Detail of the curve shown in (a) with the energy of self-diffusion superimposed (U_D). Also shown are the energy-corrections ΔU and Δ , $\Delta \approx 1/4\Delta U$. $i = n/2(n+1)$.

Using $i = 1/2n(n + 1)$, it is $p_i^- \ll p_i^+$ by a factor of about a 100 that leads to Escaig's argument of neglecting p_i^- and subsequently p_n^- . By only using p_i^+ 's we get the picture; Fig. A4-5b, and the following expressions: the net flux from $i - 1$ to i is $J(i - 1) = J_{i-1 \rightarrow i} = J_{i-1}^+ - J_i^- = J_{i-1}^+$;

$$J(i - 1) = c_{i-1} \cdot A \cdot v \cdot \exp - (U_D - \Delta)/kT \quad (\text{A4-16})$$

with $p_{i-1}^+ = A \cdot v \cdot \exp - (U_D - \Delta)/kT$, neglecting $p_i^- = A \cdot v \cdot \exp - (U_D + \Delta)/kT$ and thus J_i^- . Taking $p_{i=15}^-$ as the first negligible probability yields $J^* = J_{i=14}^+$;

$$J^* = c_{i=14} \cdot A \cdot v \cdot \exp - (U_D - \Delta)/kT \quad (\text{A4-17})$$

Assuming equilibrium up to $i = 14$;

$$J^* = c_{i=3} \cdot A \cdot v \cdot \exp - (G_{i=14} - G_{i=3} + U_D - \Delta)/kT$$

equal to Eq. (A4-13) with $G_{i=14} - G_{i=3} = \Delta G_5 + 1/2\Delta U$ and $c_{i=14} = c_{i=3} \cdot \exp - (G_{i=14} - G_{i=3})/kT$. Neglecting p_n^- gives the following steady state conditions;

$$J_{i=14}^+ = J_{i=15}^+ - J_{i=16}^- = \dots = J_{i=19}^+ - J_{i=20}^- = J_{i=20}^+ = J_{i=21}^+ - J_{i=22}^- = \dots$$

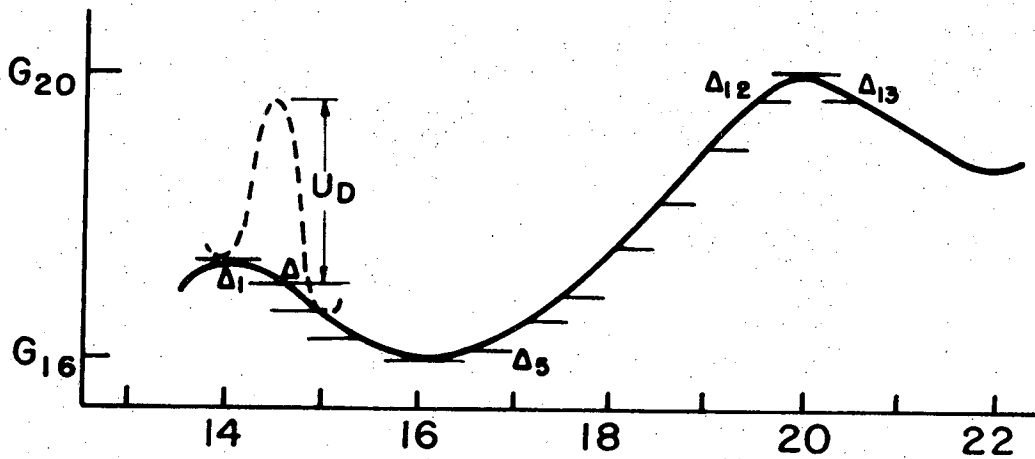
This set can be solved with respect to the c_i 's, giving;

$$c_{i=16} \approx c_{i=14} \left\{ \begin{aligned} &\exp \Delta/kT + \exp(G_{i=17} - G_{i=16} + \Delta)/kT \\ &+ \exp(G_{i=18} - G_{i=16} + \Delta')/kT + \exp(G_{i=19} - G_{i=16} + \Delta')/kT \\ &+ \exp(G_{i=20} - G_{i=16})/kT \end{aligned} \right\} \quad (\text{A4-18a})$$

and

$$c_{i=15} \approx c_{i=14} \left\{ 1 + \exp(G_{i=16} - G_{i=15} + \Delta')/kT + \exp(G_{i=17} - G_{i=15} + \Delta')/kT \right. \\ \left. + \exp(G_{i=18} - G_{i=15} + \Delta')/kT + \exp(G_{i=19} - G_{i=15} + \Delta')/kT \right. \\ \left. + \exp(G_{i=20} - G_{i=15})/kT \right\} \quad (A4-18b)$$

Here we have $-\Delta_1 + \Delta_5, -\Delta_1 + \Delta_7, -\Delta_1 + \Delta_9, -\Delta_1 + \Delta_{11} \approx \Delta' \approx 2\Delta \approx 1/2\Delta U$, and $-\Delta_1 + \Delta_3$ and $-\Delta_1 + \Delta_{13} \approx 0$ (see Fig. A4-6). As all the terms are positive as are most of the exponentials, we find $c_{i=15} \gg c_{i=14}$, and as $G_{i=16} < G_{i=15}$ we see that $c_{i=16} > c_{i=15}$. With further increase of i , c_i will decrease until the next step is reached; $i = 20$ where $c_{i=20} \approx c_{i=14}$.



XBL 735-6104

Fig. A4-6. Detail of the energy curve for the faulted Frank triangle with an unfaulted corner for the steps between $i = 14$ and $i = 22$. Also shown are the energy corrections Δ to the energy of self-diffusion U_D .

Even though $p_{i=15}^- \ll p_{i=14}^+$, we find by using Escaig's argument further on, that $c_{i=15} \gg c_{i=14}$. The resultant fluxes; $J_{i=14}^+ = c_{i=14} \cdot p_{i=14}^+$ and $J_{i=15}^- = c_{i=15} \cdot p_{i=15}^-$, will thus probably be of the same order of magnitude and it would be meaningless to neglect $p_{i=15}^-$ and $J_{i=15}^-$ as Escaig does.

APPENDIX 5. ENERGIES FOR SFT COLLAPSE MECHANISMS

The total energy of piecewise straight configuration made up of dislocation segments L_i with Burgers vector \bar{b}_i and sense \bar{s}_i is given by

$$W = \sum_i W_{s_i} + \sum_{i < j} W_{ij} \quad (\text{A5-1})$$

where W_{s_i} is the self-energy of the dislocation segment, and W_{ij} is the interaction energy between the segments i and j . W_{s_i} is given by

$$W_{s_i} = \frac{\mu}{4\pi} \left[(\bar{b}_i \cdot \bar{s}_i)^2 + \frac{(\bar{b}_i \times \bar{s}_i)^2}{1 - \nu} \right] L \ln \frac{L}{e\rho} \quad (\text{A5-2})$$

and the interaction energy for the coplanar case (Hirth and Lothe, 1968, p. 142) is given by

$$\begin{aligned} W_{ij} = & \frac{\mu}{4\pi} \{ (\bar{b}_i \cdot \bar{s}_i) (\bar{b}_j \cdot \bar{s}_j) - 2 [(\bar{b}_i \times \bar{b}_j) \cdot (\bar{s}_i \times \bar{s}_j)] \\ & + \frac{1}{1 - \nu} [\bar{b}_i \cdot (\bar{s}_i \times \bar{e}_3)] [\bar{b}_j \cdot (\bar{s}_j \times \bar{e}_3)] \} \times I(x_\alpha, y_\beta) \\ & + \frac{\mu}{4\pi(1 - \nu)} [(\bar{b}_i \cdot \bar{e}_3) (\bar{b}_j \cdot \bar{e}_3)] \times \{ R(x_\alpha, y_\beta) \\ & - \cos\theta [x_\alpha \ln t(x_\alpha, y_\beta) + y_\beta \ln t(x_\alpha, y_\beta)] \} \end{aligned} \quad (\text{A5-3})$$

Here

$$\bar{e}_3 = \frac{\bar{s}_i \times \bar{s}_j}{|\bar{s}_i \times \bar{s}_j|}$$

and

$$F(x_\alpha, y_\beta) = F(x_2, y_2) - F(x_1, y_2) - F(x_2, y_1) + F(x_1, y_1)$$

for $F = I, R, t, s$. $x_1 x_2$ being the dislocation segment L_i , and $y_1 y_2$ being the segment L_j . See Fig. A5-1. The integrals are

$$I(x, y) \times \ln \frac{R + y - x \cos \theta}{x} + y \ln \frac{R + x - y \cos \theta}{y}$$

$$R^2(x, y) = x^2 + y^2 - 2xy \cos \theta$$

$$s(x, y) = y \cos \theta - x + R$$

$$t(x, y) = x \cos \theta - y + R$$

For the case in Fig. A5-1 with both segments of size L we get

$$I(x_\alpha, y_\beta) = 2L \cdot \ln 3 = 2.2L$$

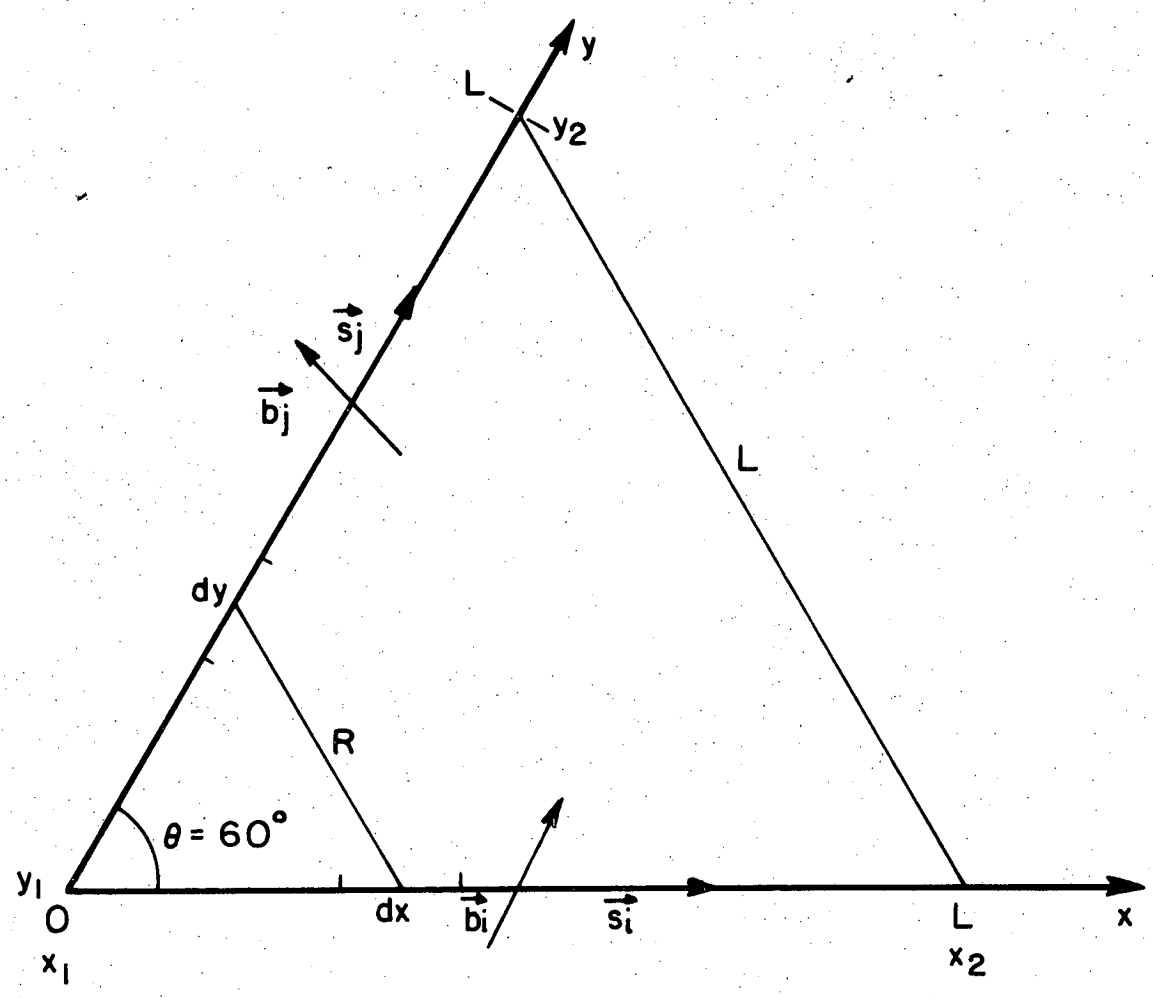
and

$$R(x_\alpha, y_\beta) - \cos \theta [x_\alpha \ln t(x_\alpha, y_\beta) + y_\beta \ln t(x_\alpha, y_\beta)] = L(\ln 3 - 1) = 0.1L$$

The energy of collapse of a SFT-corner, mechanism I, Fig. V-3, is given

$$\Delta W_I = W_{ST_c} - W_{SR_c} - 3/4 \cdot \sqrt{3} L^2 \cdot \gamma \quad (A5-4)$$

Here W_{ST_c} is the energy of the collapsed SFT corner consisting of a triangle of Shockleys (edges), W_{SR_c} is the energy of the removed corner consisting of three stair rods, and the last term represents the energy of the removed faulted area.



XBL 739-1903

Fig. A5-1. Corner configuration for intersecting dislocations i and j .

$$W_{ST_c} = \frac{\mu}{A\pi} \frac{a^2}{4} \frac{1}{1-\nu} \frac{1}{27} \{54 \ln \frac{L}{\rho} - 54 + 3 [(3\nu - 1)(2.2) - 16(0.1)]\} L$$

$$= A \cdot \{54 \ln L/\rho - 54.71\} L \quad (A5-5)$$

with $\nu = 0.354$, $\mu = 3.38 \cdot 10^{11}$ dynes/cm², $a = 4.0857\text{\AA}$, $\gamma = 18$ ergs/cm²
and $A = 4.018 \cdot 10^{-3}$ eV/Å.

$$W_{SR_c} = A \cdot 18 \{ \ln \frac{L}{\rho} - 18 - (1 - 3\nu)(2.2) - 4 \cdot (0.1) \} L$$

$$= A \{ 18 \ln \frac{L}{\rho} - 18.78 \} L \quad (A5-6)$$

$$\Delta W_I = A \{ 36 \ln \frac{L}{\rho} - 35.93 \} L - B \cdot L^2 \quad (A5-7)$$

$$B = 1.458 \cdot 10^{-3} \text{ eV/Å}^2.$$

The energy for unfauling of one face of the SFT from a corner is given (mechanism II)

$$\Delta W_{II} = W_{ST_{tc}} - W_{SR_t} - \frac{\sqrt{3}}{4} L^2 \cdot \gamma$$

where $W_{ST_{tc}}$ is the energy of the SFT corner with one unfaulted face enclosed by three Shockleys, W_{SR_t} is the energy of the two removed stair rods, both cases includes the interaction with the third stair rod, and the last term representing the removed faulted area.

$$W_{ST_{tc}} = A \cdot \{ 27(2 - \nu) (\ln \frac{L}{\rho} - 1) - (68 - 69\nu) \cdot (2.2) - 4(0.1) \} L$$

$$= A \{ 44.4 \ln \frac{L}{\rho} - 92.77 \} L \quad (A5-8)$$

$$W_{SR_t} = A \{ 12 \ln \frac{L}{\rho} - 12 - (1 - 3\nu)(2.2) - 4(0.1) \} L$$

$$= A \{ 12 \ln \frac{L}{\rho} - 12.78 \} L \quad (A5-9)$$

$$\Delta W_{II} = A \left\{ 32.44 \ln \frac{L}{\rho} - 79.99 \right\} L - C L^2 \quad (A5-10)$$

$$C = 0.486 \cdot 10^{-3} \text{ eV/\AA}^2.$$

Finally, the formation of an unfaulted Shockley triangle, mechanism III, is

$$\Delta W_{III} = W_{ST} - C L^2$$

$$\begin{aligned} W_{ST} &= A \left\{ 27(2 - \nu) \left(\ln \frac{L}{\rho} - 1 \right) - \frac{27}{2} (2 - \nu)(2.2) \right\} L \\ &= A \left\{ 44.44 \ln \frac{L}{\rho} - 93.32 \right\} L \end{aligned} \quad (A5-11)$$

$$\Delta W_{III} = A \left\{ 44.44 \ln \frac{L}{\rho} - 93.32 \right\} L - C L^2 \quad (A5-12)$$

In our cases we can neglect the interactions with the other segments with $\theta = 120^\circ$.

REFERENCES

- Aaronson, H. I., Laird, C. and Kinsman, K. R. (1970); "Mechanisms of Diffusional Growth of Precipitate Crystals" in Phase Transformations (Am. Soc. Metals, Cleveland, Ohio) pp. 313-396.
- Brun, G. (1966); "Annealing of Faulted Loops in Gold", (M. S. Thesis), University of California, Berkeley, UCRL-17060.
- Chik, K.-P. (1966); "Electron Diffraction Contrast of Small Stacking Fault Tetrahedra with Applications to Quenched Gold", Phys. Stat. Sol. 16, pp. 685-696.
- Clarebrough, L. M., Segall, R. L. and Loretto, M. H. (1966); "Faulted Defects in Quenched Copper and Silver", Phil. Mag. 13, pp. 1285-1291.
- Clarebrough, L. M. and Morton, A. J. (1968); "Fault Climb during Growth of Frank Loops in Quenched Silver and Copper-Aluminum Alloys", International Conference on Vacancies and Interstitials in Metals, Julich, pp. 200-214.
- Cockayne, D. J. H., Ray, I. L. F. and Whelan, M. J. (1969); "Investigations of Dislocation Strain Fields using Weak Beams", Phil. Mag. 20, pp. 1265-1270.
- Cotterill, R. M. J. and Doyama, M. (1964); "Removal of Stacking-Fault Tetrahedra in Gold", Appl. Phys. Letters 4, pp. 26-28.
- de Jong, M. and Koehler, J. S. (1963); "Annealing of Pure Gold Quenched from above 800°C", Phys. Rev. 129, pp. 49-61.
- Ericson, T. (1966); "The Temperature and Concentration Dependence of the Stacking Fault Energy in the Co-Ni-System", Acta Met. 14, pp. 853-865.
- Escaig, B. (1970a); "Communication on the Thermally Activated Motion of Dislocations", Cryst. Latt. Defects 1, pp. 189-191.

- Escaig, B. (1970b); "The Climb of Frank Loops in F.C.C. Metals of Low Stacking Fault Energy. Part I. Nucleation of Climb; The Process of Tetrahedra Collapse", *Cryst. Latt. Defects* 1, pp. 211-222.
- Feder, J. (1964); "Theory of Homogeneous Nucleation in Expansion-Chamber Experiments", (Cand. Real. Thesis) University of Oslo.
- Feder, J., Russell, K. C., Lothe, J. and Pound, G. M. (1966); "Homogeneous Nucleation and Growth of Droplets in Vapours", *Adv. Phys.* 15, pp. 111-178.
- Fraser, H. L., Loretto, M. H. and Smallman, R. E. (1971); "Direct Observations of the Annealing of Stacking Fault Tetrahedra in Gold and Voids in Ni-Al", International Conference on HVEM, Stockholm, paper 7.
- Hirsch, P. B., Howie, A., Nicholson, R. B., Pashley, D. W. and Whelan, M. J. (1965); Electron Microscopy of Thin Crystals (Butterworth and Co., London).
- Hirth, J. P. and Pound, G. M. (1963); Condensation and Evaporation, Nucleation and Growth Kinetics, Progress in Materials Science Vol. 11, B. Chalmers, ed. (Pergamon Press, London).
- Hirth, J. P. and Lothe, J. (1968); Theory of Dislocations (McGraw-Hill Book Co., New York).
- Howie, A. and Whelan, M. J. (1962); "Diffraction contrast of electron microscope images of crystal lattice defects. III. Results and experimental confirmation of the dynamical theory of dislocation image contrast", *Proc. Roy. Soc. London* A267, pp. 206-230.
- Humble, P., Segall, R. L. and Head, A. K. (1967); "The Energy of Dissociated Triangular Frank Dislocation Loops in F.C.C. Metals", *Phil. Mag.* 15, pp. 281-296.

- Jain, K. C. and Siegel, R. W. (1972); "Temperature Dependence of the Vacancy Sink Efficiency of Stacking-Fault Tetrahedra in Quenched Gold", *Phil. Mag.* 25, pp. 105-115.
- Johnston, I. A., Dobson, P. S. and Smallman, R. E. (1968); "The Heterogeneous Nucleation of Tetrahedra in Quenched Gold", International Conference on Vacancies and Interstitials in Metals, Jülich, pp. 140-153.
- Johnston, I. A., Dobson, P. S. and Smallman, R. E. (1971); "The Role of Jog Nucleation and Propagation in the Annealing of Faulted Loops in Low Stacking Fault Energy Metals", *Cryst. Latt. Defects* 2, pp. 133-139.
- Jössang, T., Hirth, J. P. and Hartley, C. S. (1965); "Anisotropic Elasticity Solutions for Dislocation Barriers in Face-Centered Cubic Crystals", *J. Appl. Phys.* 36, pp. 2400-2406.
- Jössang, T. and Hirth, J. P. (1966); "The Energies of Stacking-Fault Tetrahedra in F.C.C. Metals", *Phil. Mag.* 13, pp. 657-670.
- Jössang, T. (1968); "On an Approximate Method for Energy Calculation of Dislocations and its Application to Dissociated Dislocation Configurations in Face Centered Cubic Metals", (Dr. Philos Thesis) University of Oslo.
- Jössang, T. (1962); Private Communication.
- Kimura, H., Kuhlmann-Wilsdorf, D. and Maddin, R. (1963); "The Growth Mechanism of Stacking-Fault Tetrahedra in Quenched Gold", *Appl. Phys. Lett.* 3, pp. 4-5.
- Kuhlmann-Wilsdorf, D., Kimura, H. and Maddin, R. (1964); "Comment on a Paper by Cotterill and Doyama", *J. Appl. Phys.* 35, pp. 2557-2558.

Kuhlmann-Wilsdorf, D. (1965); "The Growth and Annealing of Stacking Fault Tetrahedra", Acta Met. 13, pp. 257-270.

Loretto, M. H., Clarebrough, L. M. and Segall, R. L. (1965); "Stacking-Fault Tetrahedra in Deformed Face-Centered Cubic Metals", Phil. Mag. 11, pp. 459-465.

Meshii, M. and Kauffman, J. W. (1959); "Quenching Studies on Mechanical Properties of Pure Gold", Acta Met. 7, pp. 180-186.

Meshii, M. and Kauffman, J. W. (1960); "The Mechanism of Quench-Hardening and Its Recovery in Gold", Phil. Mag. 5, pp. 939-946.

Nicholson, R. B., Thomas, G. and Nutting, J. (1958); "A technique for obtaining thin foils of aluminum and aluminum alloys for transmission electron metallography", Brit. J. Appl. Phys. 9, pp. 23-27.

Rühle, M., Wilkens, M. and Essmann, U. (1965); "Zur Deutung der elektronenmikroskopischen Kontrasterscheinungen und Fehlstellenagglomeraten in neutronenbestrahltem Kupfer", Phys. Stat. Sol. 11, pp. 819-829.

Silcock, J. M. and Tunstall, W. J. (1964); "Partial Dislocations Associated with NbC Precipitation in Austenitic Stainless Steels", Phil. Mag. 10, pp. 361-389.

Silcox, J. and Hirsch, P. B. (1959); "Direct Observations of Defects in Quenched Gold", Phil. Mag. 4, 72-89.

Smallman, R. E., Westmacott, K. H. and Coiley, J. H. (1959-60); "Clustered Vacancy Defects in Some Face-Centered Cubic Metals and Alloys", J. Inst. Metals 88, pp. 127-133.

Smallman, R. E., Dobson, P. S. and Goodhew, P. J. (1968); "Faulted Loops and Stacking Fault Energies", Trans. Japan Inst. Metals 9, Suppl., pp. 562-568.

- Thomas, G. and Bell, W. L. (1967); "Identification of Prismatic Dislocation Defects by Electron Microscopy" in Lattice Defects and Their Interactions, (Gordon and Breach, New York), pp. 477-542.
- Washburn, J. and Yokota, M. J. (1969); "Climb of $1/3 \langle 111 \rangle$ Dislocations in Gold", Cryst. Latt. Defects 1, pp. 23-29.
- Yokota, M. J. and Washburn, J. (1967); "Annealing of Stacking-Fault Tetrahedra in Gold", Phil. Mag. 16, p. 459-466.
- Yokota, M. J. (1968); "Hardening and Recovery of Quenched Gold", (Ph. D. Thesis), University of California, Berkeley, UCRL-17785.

LEGAL NOTICE

This report was prepared as an account of work sponsored by the United States Government. Neither the United States nor the United States Atomic Energy Commission, nor any of their employees, nor any of their contractors, subcontractors, or their employees, makes any warranty, express or implied, or assumes any legal liability or responsibility for the accuracy, completeness or usefulness of any information, apparatus, product or process disclosed, or represents that its use would not infringe privately owned rights.

TECHNICAL INFORMATION DIVISION
LAWRENCE BERKELEY LABORATORY
UNIVERSITY OF CALIFORNIA
BERKELEY, CALIFORNIA 94720